Report on the Refinement and Optimization of the Algorithms and Codes, and the Initial Clinical Validation and Adaptation of the "Oncosimulator"

Project Number:	FP6-2005-IST-026996
Deliverable id:	D 8.3
Deliverable name:	Report on the refinement and optimization of the algorithms and codes, and the initial clinical validation and adaptation of the "Oncosimulator"
Submission Date:	15/09/2008

COVER AND CONTROL PAGE OF DOCUMENT	
Project Acronym:	ACGT
Project Full Name:	Advancing Clinico-Genomic Clinical Trials on Cancer: Open Grid Services for improving Medical Knowledge Discovery
Document id:	D 8.3
Document name:	Report on the refinement and optimization of the algorithms and codes, and the initial clinical validation and adaptation of the "Oncosimulator"
Document type (PU, INT, RE)	**RE**
Version:	Final
Submission date:	15/09/2008
Editor: Organisation: Email:	Georgios S. Stamatakos ICCS-NTUA gestam@central.ntua.gr

Document type PU = public, INT = internal, **RE** = restricted

ABSTRACT:

This deliverable outlines the initial version of the ACGT Oncosimulator i.e. an integrated software system simulating *in vivo* tumour response to therapeutic modalities within the clinical trials environment and aiming at supporting patient individualized optimization of cancer treatment. The document refers to both the basic science and the technology modules of the system whereas a description of the clinical requirements and the types of medical data provided and exploited is included. As deliverable D8.2 contains the foundations of the simulation component only an outline of the major improvements, refinements, extensions and numerical checks and explorations of the simulation model is included in this document. A relatively detailed description of the technology modules is presented. The latter mainly refer to image processing, the grid execution scenario, cluster execution and parallelization of the simulation code, interactive and virtual reality visualization, subjunctive interfaces and the Oncosimulator component collaboration diagram. A brief outline of a possible future extension of the system which would address the immune system reaction has also been incorporated. The favourable outcome of an initial step towards the clinical adaptation and validation of the Oncosimulator is presented and discussed.

KEYWORD LIST: *in silico* oncology, Oncosimulator, cancer modeling, tumour growth, clinical trials, ACGT, SIOP 2001/GPOH clinical trial, TOP trial, multilevel cancer modeling, nephroblastoma, Wilms tumour, breast cancer, individualized treatment optimization, cancer systems biology, grid, virtual reality, clusters, subjunctive interfaces, tumour segmentation

MODIFICATION CONTROL			
Version	Date	Status	Author
1.0	25/08/08	Draft	Georgios S. Stamatakos, ICCS-NTUA
2.0	13/09/08	Draft	Georgios S. Stamatakos, ICCS, incorporating the contributions of all involved partners
3.0	14/09/08	Draft	Dimitra Dionysiou, ICCS-NTUA
4.0	14/09/08	Draft	Georgios S. Stamatakos, ICCS-NTUA
5.0	07/10/08	Draft	Norbert Graf, USAAR
6.0	08/10/08	Draft	Alexander Hoppe, USAAR
7.0	17/10/08	Final	Georgios S. Stamatakos, ICCS-NTUA

List of Contributors

- N. Graf, USAAR
- C. Desmedt, IJB
- E. Kolokotroni, ICCS-NTUA
- E. Georgiadi, ICCS-NTUA
- S. Giatili, ICCS-NTUA
- D. Dionysiou, ICCS-NTUA
- M. Erdt, FHG
- J. Jacques, INRIA
- J. Puckacki, PSNC
- R. Belleman, UvA
- P. Melis, UvA
- A. Lunzer, UHok
- A. d' Onofrio, IEO

CONTENTS.....5

1 Executive Summary

The present deliverable outlines the initial version of the ACGT Oncosimulator i.e. an integrated software system simulating *in vivo* tumour response to therapeutic modalities within the clinical trials environment and aiming at supporting patient individualized optimization of cancer treatment. The document refers to both the basic science and the technology modules of the system whereas a description of the clinical requirements and the types of medical data provided and exploited is included. As deliverable D8.2 contains the foundations of the simulation component only an outline of the major improvements, refinements, extensions and numerical checks and explorations of the simulation model has been incorporated into this document. Of particular interest are the novel tumour initialization technique, the study of its convergence and the numerical study of the sensitivity of the model to several critical parameters or parameter combinations. A relatively detailed description of the technology modules is presented. The latter refer mainly to image processing, the Oncosimulator grid execution scenario, the cluster execution and parallelization of the simulation code, interactive and virtual reality visualization, the subjunctive interfaces of the Oncosimulator and the Oncosimulator component collaboration diagram which actually provides the technological basis for the system integration. A brief outline of a possible future extension of the system which would address the immune system reaction has also been incorporated in the document. The outcome of an initial step towards the clinical adaptation and validation of the system is presented and discussed. Use of anonymized real data before and after chemotherapeutic treatment for the case of the SIOP 2001/GPOH nephroblastoma and TOP breast cancer clinical trials constitute the basis of the clinical adaptation and validation process. Functioning of the initial Oncosimulator platform, including both basic science and technology modules, was demonstrated during the Eindhoven ACGT annual review (May 27-28, 2008). By using real medical data concerning nephroblastoma and breast cancer in conjunction with plausible values for the model parameters (based on available literature and/or logic) a reasonable prediction of the actual tumour volume shrinkage has been made possible. Obviously as more and more sets of medical data are exploited the reliability of the model "tuning" is expected to increase. It should be pointed out that the large number of inherent biological boundary conditions (e.g. monotonic increase of all tumour cell category/state populations for an imaginable freely and smoothly growing tumour) dramatically limits the number of possible solutions (i.e. sets of parameter values that are able to predict real tumour shrinkage following treatment). This is particularly important since such limitations drastically facilitate the approach to the solution best representing clinical reality for each given medical data case. The successful performance of the initial combined Oncosimulator platform has been a particularly encouraging step towards the clinical translation of the system, being the first of its kind worldwide.

2 Introduction

Purpose of this document

The aim of this document is to report on the improvements of the algorithms and codes constituting the ACGT Oncosimulator (both its basic science and its technology aspects) that have taken place since the last ACGT review that took place in Brussels in December 2007. Furthermore, the document aims at providing a report on the initial clinical adaptation and validation steps of the combined system.

Contents of the document

As deliverable D8.2 contains the foundations of the simulation component only an outline of the major improvements, refinements, extensions and numerical checks and explorations of the simulation model is included in this document. A relatively detailed description of the technology modules is presented. The technology modules refer to the image processing of the medical data, the Oncosimulator grid execution scenario, the cluster execution and parallelization of the simulation code, interactive and virtual reality visualization, the subjunctive interfaces for the Oncosimulator and the Oncosimulator component collaboration diagram. A brief outline of a possible future extension of the system which would address the immune system reaction has also been included. The positive outcome of the initial step towards the clinical adaptation and validation of the system is presented and discussed in chapter 12.

3 Structure of the Deliverable

The deliverable begins with the *clinical positioning* of the Oncosimulator since the whole system is clearly *clinically driven* and *clinically oriented*. Within this context the clinical expectations of *in silico oncology*, an emerging scientific, technological and medical domain directly linked to the Oncosimulator development, are delineated in Chapter 4. Chapter 5 is devoted to the progress concerning the simulation module of the Oncosimulator. A novel algorithm concerning the *in vivo* tumour initialization, the convergence of the initialization method, the exploration of the model's sensitivity and the provision of theoretically possible solutions predicting the actual tumour shrinkage following treatment as observed in the actual clinical trial data constitute the main themes of this chapter. Chapter 6 is devoted to the image processing techniques and tools used in order to segment, interpolate and three dimensionally reconstruct the imaging data. Chapter 7 concerns the Oncosimulator grid execution scenario. Chapter 8 deals with the cluster execution and the parallelization of the simulation code. Chapter 9 refers to the interactive and virtual reality visualization of both the real and the predicted imaging data. Chapter 10 presents a system of subjunctive interfaces specially designed and implemented for the Oncosimulator. A component collaboration diagram concerning mainly the execution, exploitation and exploration of the simulation code is presented in chapter 11. Chapter 12 includes comments on the initial steps towards the clinical adaptation and validation of the Oncosimulator. Chapter 13 provides an outline of a possible future extension of the Oncosimulator that would deal with the modeling of the immune reactions to the tumour and possibly to immunotherapies. Finally Chapter 14 presents the conclusions.

4 Clinical Expectations of *In Silico* Oncology – Provision of Medical Data

[Chapter Code: C]

Introduction

A *clinicogenomic trial* is one of the final stages of a long and careful cancer research process. The search for new treatments begins in the laboratory. Molecular biology helps to better understand carcinogenesis thus finding new targets able to interact with agents that reverse the process of cancer cell development and proliferation. In the future new methods and technologies in molecular biology will result in an exponential increase of information that can be handled by advances in high performance computing and informatics. It is of paramount importance to extract this information from clinical data so at to gain new knowledge useful for the development of better treatments for cancer patients. This approach is to be taken into account when dealing with i*n silico* oncology. With the help of *in silico oncology* it is expected that cancer progression and response to different treatments can be simulated. Such *in silico* experiments should help clinicians to find the best way of treating an individual patient by simulating different treatments in the computer before starting the optimal treatment in reality. WP8 is engaged in developing such simulation models, by fully exploiting the insight gained by molecular biology, radiobiology, pharmacology and other disciplines as well as the individual patient's data. The workpackage is driven by clinicians defining the expectations from the clinical point of view and also providing clinical data according to the defined scenarios.

Clinical aspects of *in silico* oncology

From a clinical point of view (USAAR) two preconditions are of utmost importance if a physician is to rely on the predictions of *in silico* simulations:

1. every *in silico* simulation has to be part of a clinicogenomic trial
2. every prediction of an *in silico* simulation has to be compared with reality in a learning process or loop

In the process of developing *in silico* methods we have defined the necessary and available data in a first step. These data include data from the tumour (molecular biology, pathology, imaging), from the patient (clinical data) and from the possible treatments (pharmacokinetics and pharmacodynamics of the drugs that will be used, radiobiological parameters in the case of radiotherapy, treatment scheme) (Table C1). The data to be provided for the nephroblastoma *in silico* scenario are given in Table C2.

Table C1. Necessary and available data for *in silico oncology* simulations

- *Data generated primarily by the patient and the tumour*
  - clinical data
  - molecular data
  - imaging data
  - pathological data
  - treatment data
- *Data extracted from literature, databanks etc.*
  - pharmacokinetics of drugs
  - pharmacodynamics of drugs-tumour types
  - radiobiological parameters (for the case of radiotherapy)
  - molecular data

Table C2. Data that are necessary for the *in silico* experiment in the case of nephroblastoma treated with chemotherapy

Clinical Data	Age Sex Weight Height Syndromes (WAGR, Denys-Drash, Beckwith-Wiedermann and others) Family history
Imaging Data	at baseline i.e. just before chemotherapy starts: CT (DICOM) and/or MRI (DICOM) and/or ultrasound (DICOM)] Three ellipsoidal axes of the tumour. Delineation of the necrotic, cystic, hemorrhagic and solid tumour regions on the tomograhic slices.
Molecular Data	Profiling of antibodies against tumour antigens (antigen scenario) ↓ Estimated cell type composition of the tumour ↓ Estimated tumour cell responsiveness to the drugs under consideration
Recommended Treatment Scheme(s) Data	

To render the simulation predictions as precise and realistic as possible it is crucial to collect as much information as possible from each different data category. The volume and content of data will be restricted by the availability of tumour material, imaging data and clinical data. Therefore scenarios in *in silico oncology* have always to be integrated in clinicogenomic trials where data management including data security and anonymisation or pseudonymisation of data as well as tumour banking are well established. In addition the trial has to pass ethical committees and has to fulfil all other GCP criteria to obtain approval by regulatory authorities.

The simulation prediction of each *in silico* method has always to be compared with the reality (Fig.C1.).

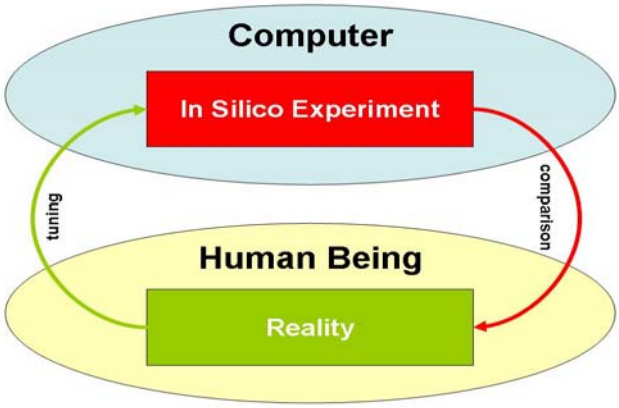

Fig.C1. Comparison between *in silico oncology* experiments and reality

The feedback given by reality has to tune the *in silico* method so as to achieve better predictions. If treatment is based on predictions of *in silico* methods, this control loop has to be part of the method and be automated. In that way an *in silico* experiment should work as a learning system. Only if there are *no* or *minimal* deviations between prediction and reality the *in silico* method is to be allowed to be used in the clinical setting. The clinician is the one who has to define what can be accepted as a minimal deviation between prediction and reality. This definition should always be included in the biometrics part of a clinicogenomic trial protocol. One has to be aware that a physician is treating *patients*. For the safety of patients a stopping rule has to be defined if clinical decisions are based on *in silico* experiments. Before an *in silico simulation* can be accepted as a routine method for treatment stratification a prospective and randomized trial has to show that patients treated according to the result of the *in silico simulation* experiment do better than the group of patients that are treated regardless of the *in silico simulation* experiment.

Clinical questions to be addressed by *in silico* oncology

For a clinician the following six questions should be addressed and answered precisely by *in silico simulation* experiments:

1. What is the natural local tumour growth over time in size and shape?
2. When and whereto is a tumour metastasizing?
3. Can the response of the local tumour and the metastases to a given treatment be predicted in size and shape over time?
4. What is the best treatment schedule for a patient regarding drugs, surgery, irradiation and their combination, dosage, time schedule and duration?
5. Is it possible to predict severe adverse events (SAE) of a treatment and to propose an alternative treatment to avoid them without deteriorating the outcome?
6. Is it possible to predict a cancer before occurring and to recommend a treatment that will prevent the occurrence or a recurrence of a cancer in an individual patient?

From the clinical point of view these questions are addressed and discussed extensively. ACGT is primarily addressing questions 3 and 4. In the nephroblastoma scenario question 3 is analyzed, whereas in the TOP trial it is question 4. If dealing with tumour response it is of utmost importance to keep in mind that most patients with cancer respond to therapy but not all of these are cured. Even objective clinical responses to a given treatment do not translate into substantial improvements in overall survival. The reason for this phenomenon can be explained by the fact that therapies successfully eliminating the vast majority of cancer cells may be ineffective against rare, biological distinct *cancer stem cells*. Therefore new methods for assessing treatment efficacy have to be developed as traditional response criteria such as the RECIST criteria measure tumour bulk and do not reflect changes in the rare *cancer stem cells*. If *in silico* experiments are of more help for a clinician than getting a prediction of changes in tumour volume and shape the response of treatment to the small fraction of cancer stem cells would be *of utmost importance*. From a clinical point of view cancer stem cells have to be taken into account in developing *in silico* models for tumour response. It might be time to eliminate traditional measures of clinical response as trial end points and to evaluate activity on *rare cancer stem cells*. It seems obvious that treatments effective against the gross majority of cancer cells with limited mitotic potential are ineffective for rare cancer stem cells. This implies a change of treatment after a patient is in clinical remission following the destruction or removal of the bulky tumour burden. Data on *cancer stem cells* for each tumour have to be obtained by molecular biologists. Clinicians have to provide researchers with tumour material. This again underlies the importance of enrolling patients into clinicogenomic trials when *in silico* experiments are done and conclusive results are awaited.

Functioning of the Oncosimulator *after* and *during* its clinical validation: the nephroblastoma paradigm

In the case of nephroblastoma the preoperative chemotherapy is simulated and compared with the *in vivo* response to chemotherapy (Fig.C2). Following the patient in the clinical institution the collection of the relevant clinical, imaging, molecular and pharmacokinetic data takes place (Table C2), These data are used by the Oncosimulator. The most important prediction of the Oncosimulator for the clinician is the amount of shrinkage of the given tumour in % of the initial volume. Provided that an eventually favorable clinical validation of the Oncosimulator will have been accomplished in the future, one of the following two situations will arise based on the Oncosimulator prediction:

1. Prediction of reduction of tumour volume by more than 10 %.
   - In this case the clinician would judge that preoperative chemotherapy would be beneficial to the patient.
2. Prediction of reduction of tumour volume by less than 10 % or no reduction of the tumour or even increase in tumour volume.
   - In this case the clinician would judge that preoperative chemotherapy would not be beneficial to the patient.

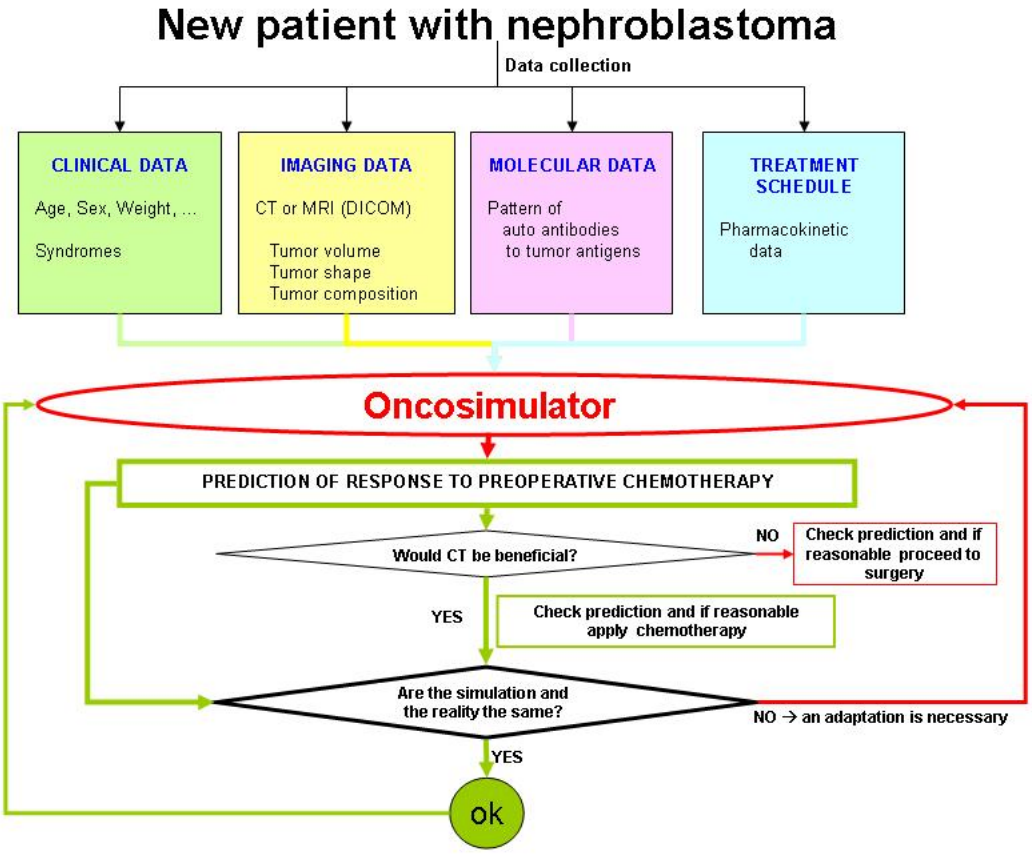

Fig.C2. Flow diagram of an *in silico simulation* experiment in the case of nephroblastoma.

However, before completion of the clinical validation process the patient will always receive preoperative chemotherapy independent of the above judgement. The actual chemotherapy administration schedule is then registered. At the end of the preoperative treatment the reduction of the tumour size in reality is compared with the predicted reduction by the *in silico* experiment. A "perfect correlation" between the Oncosimulator and the *in vivo* situation for the nephroblastoma case is defined by getting the same result of more or less than 10 % tumour volume reduction by both methods in all patients and by predicting the correct histological subtype. If there is no "perfect correlation" the Oncosimulator will be further tuned in a feedback loop as a learning system. Tumour volume response and histological outcome have to be evaluated independently. For the clinical situation the prediction of the correct tumour volume reduction before starting treatment is most important. This will help to choose the best treatment for an individual patient in advance (Table C3.). Before applying the prediction of the *in silico experiment* in the clinical setting a prospective trial has to prove the correctness of the predictions in all cases.

Table C3. Correlation of the tumour volume reduction between the *in vivo* situation and the *in silico* experiment

		In vivo	
		< 10 %	*> 10 %*
Oncosimulator	*< 10 %*	*good correlation / no preoperative chemotherapy is indicated*	*bad correlation / Oncosimulator has to be improved*
	> 10 %	*bad correlation / Oncosimulator has to be improved*	*good correlation / preoperative chemotherapy is indicated*

The question "What is the best treatment for a given tumour in an individual patient?" leads to a high level of individualization. To attain this goal it is of utmost importance that the result of the *in silico* experiment is available in a short timeframe after diagnosis. This implies that all data that are necessary for running the *in silico* experiment have to be available in a short timely manner. This is especially important for molecular biologists, radiologists and clinicians, who have to produce reliable data very fast. The *in silico* experiments itself should not be time consuming experiments.

The medical data collection and preprocessing procedure

Within the ACGT framework an advanced multilevel simulation model of clinical tumour growth and response to chemotherapy adapted to the case of nephroblastoma has been developed. More specifically a branch of the SIOP 2001 / GPOH clinical trial has been simulated as will be described in Chapter 5. Extensive use of pseudonymized actual SIOP 2001 / GPOH clinical trial data is expected to considerably refine the parameter value assignment. In order to simulate a realistic treatment scenario chemotherapy is assumed to start 4 days after the pretreatment imaging data are collected. Simulation continues up to 3 days after the last chemotherapy administration. This also represents a real SIOP 2001 / GPOH case.

One challenge is the provision of DICOM data and also sufficient knowledge about the segmentation of the tumour. The segmentation itself has to be done by the clinicians. A tool

for this process has been developed by FhG and evaluated by clinicians (USAAR) working in WP 2. Initial datasets of imaging studies of nephroblastoma have been provided for the *in silico* experiments and segmentation of the tumour has been done (Fig. C3).

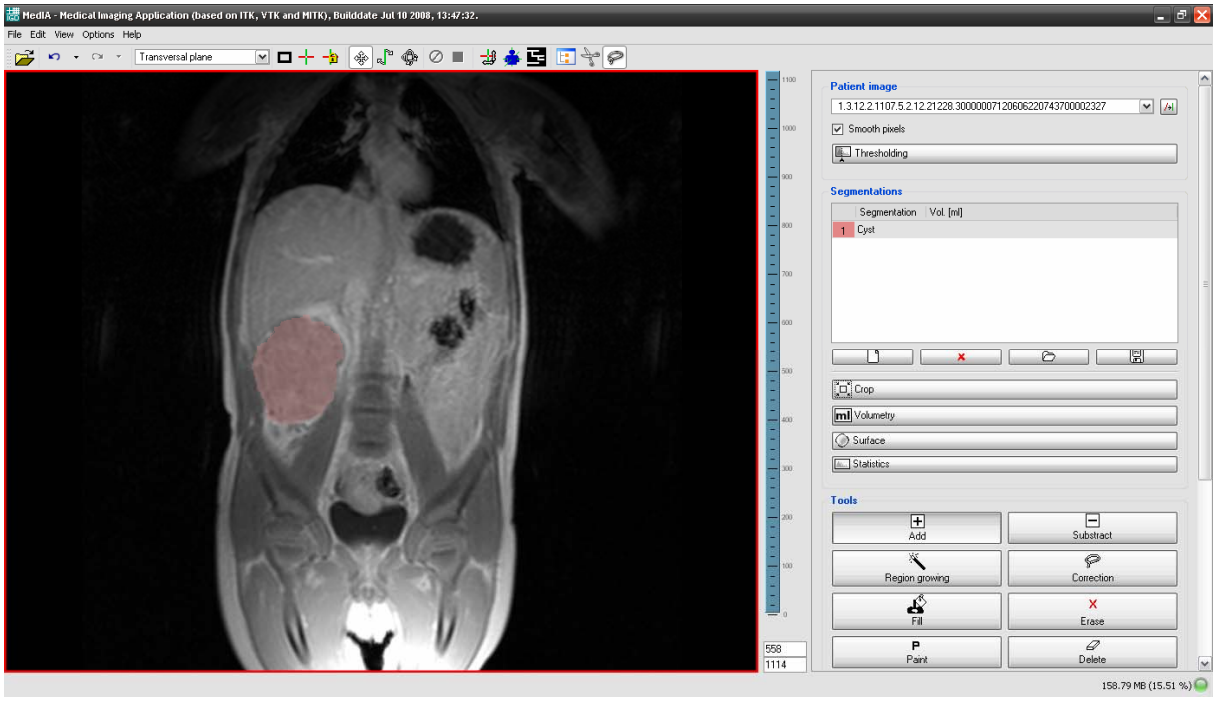

Fig. C3. Segmentation of a nephroblastoma tumour done by a clinician using the segmentation tool provided by FHG. (see Chapter 6)

Nephroblastoma is normally treated with chemotherapy and surgery. Vincristine is widely used in combination with dactinomycin and depending on the risk stratification in addition with doxorubicin. There are two different treatment approaches: one requiring chemotherapy to take place prior to surgery and the other one dictating the use of chemotherapeutic agents after the removal of the neoplasm. The simulation algorithms developed so far address the cases of preoperative chemotherapy with a combination of actinomycin-D and vincristine for unilateral stage I - III nephroblastoma tumors treated according to the SIOP 2001/GPOH clinical trial. These two or three drug combinations are the most widely adopted clinical treatment modalities for nephroblastoma. The combined chemotherapy simulation models is validated and optimized using pseudonymized data from the SIOP 2001/GPOH nephroblastoma clinical trial. The model presented has been shown to be able to reproduce important aspects of the clinical reality and practice and generally produce quite reasonable predictions. Nevertheless, in order to enter routine clinical practice as a decision support tool, an exhaustive validation, adaptation and optimization procedure has to take place. Furthermore, molecular methods of extraction of the crucial histological constitution of the tumour will be tested and integrated into the model. Following completion of this testing procedure the simulation model is expected to support clinicians' decisions concerning various candidate cancer treatment schemes and thus facilitating individualized treatment optimization, help suggest new therapeutic strategies based on *in silico* experiments and help train or inform doctors, life scientists, researchers or interested patients by demonstrations of the likely tumor response to different therapeutic schemes.

Regarding *breast cancer* the current trend in the treatment of localized disease is the combination of neoadjuvant chemotherapy (preoperative therapy given as initial treatment) and surgery with adjuvant therapy. The preoperative systematic therapy contributes to the shrinkage of the tumour and the surgery required area, even the avoidance of mastectomy in some cases. The chemotherapy agent and the therapeutic scheme chosen are based on the experience from clinical practice. However, due to the heterogeneity of the disease, the effectiveness and the benefits of the adopted therapy vary from individual to individual.
The chemotherapeutically treated breast cancer tumour, considered in the present work is mimicking a branch of the clinical study known as *Trial of Principle* (TOP). This study aims to evaluate the topoisomerase II alpha gene amplification and protein overexpression as markers predicting the efficacy of epirubicin in the primary treatment of breast cancer patients. The trial addresses non-metastatic, early breast cancer patients with ER-negative tumors of size >2cm as defined by ultrasound. The patients are treated with four cycles of single-agent epirubicin (100mg/m2, q3weeks) as neoadjuvant treatment, followed by surgery and adjuvant chemotherapy.

The data provided by clinicians for the *in silico* experiments include:

- imaging data before and after treatement [MRI data for a nephroblastoma case and ultrasound based largest dimensions of breast cancer tumours]
- histopathological data concerning the excat types of tumour
- molecular data which will be used in a subsequent stage in order to perturb the survival probabilities of each tumour cell foloowing its exposition to each drug under consideration

Our goal is to end up with a reliable simulation system able to assist clinicians with personalized optimization of cancer treatment. Optimization is expected to be achieved through performing *in silico* (on the computer) patient individualized treatment experiments. The clinically validated model might also serve as a valuable tool for researchers, professionals or patients.

In the future clinical data will be provided using ObTiMA. Pharmacogenetic data are collected from literature. Initial results of the first *in silico* experiments in nephroblastoma and breast cancer have been published (C1, C2, C3). For the parameter values considered in those papers the model was shown to behave at least in qualitative agreement with clinical reality. Quantitative clinical adaptation in conjunction with the exploitation of serum molecular data (the "antigen scenario") reflecting the tumour's histology as well as an extensive validation of the model are in progress.

Data types regarding the breast cancer trial

The following tables provide the pseudonymized breast cancer data (CRFs and biological data) provided by IJB and concrning the TOP trial. More specifically this section presents the parameters included in each file provided and their description and value range (wherever applicable). The parameters for which no value has been provided by IJB for any patient are in red. The data used for the breast cancer model validation appear in green (file 'CRF data TOP April2007-ASES.csv'). Parameters related to the pseudo-anonymisation procedure are omitted. Most of the data provided have not yet been exploited although exploitation of some of them has been planned to take place in the next stages of the Oncosimulator clinical adaptation and validation. The strategy of "distilling" the *molecular information* into the *cell survival probabilities* during and following treatment via the use of "digital" molecular circuits as described in D8.2 will serve as the basis to achieve this.

File: 'biological data TOP April2007.csv'

Parameters:

Name
ID
er
erscore (0-8)
pgr
pgrscore (0-8)
Neu.IHC
Neu.FISH ratio_local
Ki.67(%)
grade
CK5/6 (%)
CK5.6.int (0-3)
neu.fish ratio_central
topo.fish ratio_central
topo.IHC (%)
topo.IHC.int (0-3)
er_OP erscore_OP (0-8)
pgr_OP
pgrscore_OP (0-8)
Neu.IHC_OP
Neu.FISH ratio_local_OP
Ki.67 (%)_OP
grade_OP
topo.IHC (%)_OP
topo.IHC.int(0-3)_OP

File: 'CRF data TOP April2007-AE.csv'

Description: Toxicity

Parameters:

Name	Description	Value
AE_BEG_DATE	Adverse event start date or ongoing	
AE_END_DATE	Adverse event stop date or ongoing	
AE_TXEN	Adverse event	Allergy, Nausea, Vomiting, Cough, Arrhythmia etc
MT_REL	Relation to study medication	Yes or No
SER_YN	Serious?	Yes or No
NONE	None Cycle Number	Yes or No or NA
AE_GRADE	Adverse event grade	1-4
AE_CONT	Adverse event continuing	Continuing or empty cell
AE_ONG	Adverse event ongoing	Ongoing or empty cell

File: 'CRF data TOP April2007-ASES.csv'

Description: Tumor Assessment: Baseline Evaluation and Post-Epirubicin Evaluation

Parameters:

Name	Description	Value
ASSES_RSLT	Assessment measurement result (tumor size)	
ASSES_TYPE	Assessment Method	Clinical examination or Ultrasound
DIAG_YN	Lymph node involved	Yes or No
PROC_DATE	Assessment date	
PROC_TYPE	Tumor type	Primary, Primary tumor 2 if multifocal

		or multicentric lesions, Lymph node 1, Lymph node 2
ASSES_RSLT_UN	Assessment measurement units	mm
DIAG_INV_YN	Primary tumor 2 if multifocal or multicentric lesions	Yes, No or NA

File: 'CRF data TOP April2007-CANC.csv'

Description: Pre-treatment and residual tumor characteristics

Parameters:

Name	Description	Value
DIAG_BEG_DATE	Date of histologic diagnosis	
DIAG_SP	Description of Histopathologic type 3 'other'	
DIAG_SUB_TYPE1	Histopathologic type 1	ductal carcinoma invasive
DIAG_SUB_TYPE2	Histopathologic type 2	lobular carcinoma invasive
DIAG_SUB_TYPE3	Histopathologic type 3	other
DIAG_YN1	Occurance of Histopathologic type	Yes or No
DIAG_YN2	Occurance of Histopathologic type	Yes or No
DIAG_YN3	Occurance of Histopathologic type	Yes or No
GRADE	Histopathologic grade	not assessable, GI (well differentiated), GII (moderately differentiated), GIII (poorly differentiated)
LAB_RSLT1	Lab results for positive Estrogen receptor	
LAB_RSLT2	Lab results for positive Progesterone receptor	
LAB_RSLT_UN1	Lab results units for positive Estrogen receptor	% positive cells
LAB_RSLT_UN2	Lab results units for positive	% positive cells

	Progesterone receptor	
LYNOD_POS	LYNOD_POS	
RECP_STAT1	Estrogen receptor status	negative, positive or unknown
RECP_STAT2	Progesterone receptor status	negative, positive or unknown
LYNOD	LYNOD	
CARC_YN	In situ carcinoma	Yes or No
CARC_TYPE1	In situ carcinoma type 1:	lobural
CARC_TYPE2	In situ carcinoma type 2:	ductal
CARC_TYPE_YN1	Occurrence of In situ carcinoma type 1	Yes or No
CARC_TYPE_YN2	Occurrence of In situ carcinoma type 2	Yes or No
PT_CLIN	T classification (primary tumor)	T1, T2, T3 or T4
PN_CLIN	N classification (regional lymph node)	N0, N1, N2 or N3
PM	M classification (distant metastasis)	MX, M0 or M1
TUMOR_SIZE1	Size of the invasive component dimension 1	
TUMOR_SIZE2	Size of the invasive component dimension 2	
TUMOR_SIZE_UN	Size units	mm

PT_PATH	pT	pTx: primary tumor cannot be assessed pT0: No evidence of any primary tumor pTIS: Carcinoma in situ as sole remaining tumor: intraductal carcinoma or lobular carcinoma in situ or Paget disease of the nipple as all remaining tumor pT1: Invasive tumor of 2 cm or less in its greatest dimension pT2: Invasive tumor more than 2 cm but not more than 5 cm in its greatest dimension pT3: Invasive tumor more than 5 cm in its greatest dimension pT4: Invasive tumor of any size with direct extension to chest wall or skin
FOCAL_YN	Multifocal Tumor	Yes, No or NA
MARGIN	Surgical margins	Negative ($\geq$ 1 mm), Close (< 1 mm), *Involved*
PN_PATH	PN	pNx: regional lymph nodes cannot be assessed pN0: no regional lymph nodes metastasis pN1: metastasis to movable ipsilateral axillary node(s) pN2: metastasis to ipsilateral lymph node (s) that are fixed to one another or to other structures pN3: metastasis to ipsilateral internal mammary lymph node (s)
PCR_YN	pCR (pathological complete response (pT0 or pTIS and pN0)	Yes or No
CENTRIC_YN		
PT_SP		
PT0_YN		

PN0_YN		
PTIS_YN		
PCR	pathological complete response if Yes	pT0 , pTis, pN0

File: 'CRF data TOP April2007-CHST.csv'

Description:Primary Breast cancer

Parameters:

Name	Description	Value
SITE	Side of lesion	Left, Right
TRUCUT_DATE	Date of Trucut Biopsy	
TRUCUT_NO	Trucut Biopsy identification number	

File: 'CRF data TOP April2007-CMPL.csv'

Description: Primary treatment Completion

Parameters:

Name	Description	Value
CYCLE_NO	Total number of Epirubicin cycles given	
DOSE	Cumulative dose Epirubicin administered	
DOSE_UN	Dose units	mg/m^2
CMPL_REAS	End of Epirubicin treatment reason	1 Received maximum number of cycles as per protocol 2 Disease progression/relapse during active treatment 3 Death 4 Adverse event, 5 Consent withdrawn, 6 Lost to follow-up 7 Major protocol violation, 8 Other,

CMPL_RSP	Specific Epirubicin treatment end reason for cases 4-8 above	
DENSE_YN	Dose dense applied	Yes or No

File: 'CRF data TOP April2007-DEMO.csv'

Description: Registration checklist

Parameters:

Name	Description	Value
BIRTH_DATE	Date of Birth	
SUBJ_INIT	Patient initials	
INV_NAME	Responsible physician	
HOSP_NO	Patient Hospital Chart Number	

File: 'CRF data TOP April2007-DIAG.csv'

Parameters:

Name	Description	Value
DIAG_BEG_DATE	Start date of disease	
DIAG_TXEN	Disease	
DIAG_YN	Significant medical history	Yes/No
DIAG_CMPL	Significant medical history	

File: 'CRF data TOP April2007-ELIG.csv'

Description: Eligibility criteria

Parameters:

Name	Description	Value
ELI_CRIT	Inclusion and exclusion criteria	4.1.1 Inclusion criteria 1. Histologically-confirmed operable breast cancer (either operable, or locally Advanced or

		inflammatory) 2. Age ≤ 70 years 3. Female patient 4. Tumor size ≥ 2 cm at the ultrasound examination 5. ER-negative tumors, defined according to immunohistochemistry (i.e. < 10% of positive cells after immunostaining) 6. In case of multifocal or multicentric tumor: fixed and frozen samples obtained for each nodules and ER-negativity of each nodule confirmed 7. Fixed and frozen samples from the primary tumor, obtained before treatment with epirubicin, must be available for evaluation of biological markers (topo II α gene, p-53 gene, cDNA microarrays) 8. Written informed consent before study registration 9. Performance status ≤ 1 (ECOG Scale) 10. ANC ≥ 1500/mm3, platelets ≥ 100.000/mm3, Hb ≥ 10g/dl Tot. bilirubin and serum creatinine ≤ 1 N, GOT/GPT ≤ 1.5 N, AP ≤ 2 .5 N 11. Normal LVEF by Echocardiography or MUGA scan 12. Negative pregnancy test for all women of childbearing potential. 4.1.2 Exclusion criteria 1. Metastatic breast cancer 2. Serious medical conditions like : a) congestive heart failure or unstable angina pectoris, previous history of myocardial infarction within 1 year from study entry, uncontrolled arrhytmias b) history of significant neurologic or psychiatric disorders c) Active uncontrolled infection d) Active peptic ulcer, unstable diabetes mellitus 3. Concomitant contralateral invasive breast cancer 4. Concurrent treatment with hormonal replacement treatment 5. Concurrent treatment with any other anti-cancer therapy 6. Previous treatment with anthracyclines for breast cancer
ELI_YN	Criteria applied	Yes or No

File: 'CRF data TOP April2007-FU.csv'

Description: Follow up (every 4 months during the 2 first years of follow up and every 6 months after, up to 5 years of follow up)

Parameters:

Name	Description	Value
DCMDATE	Follow up date	
FU_YN	Are there any changes since previous assessment	Yes or No
FU_SP	Specify in case of yes	1 Breast Cancer Relapse 2 Second Primary Malignancy 3 Death
SPM_TYPE	Site of second primary malignancy	1 Controlateral breast 2 Other
SPM_SP	Specify in case of 'other'	
SPM_DATE	Date of second primary malignancy	
DEATH_DATE	Date of Death	
DEATH_TYPE	Cause of Death	1 Progression of disease 2 Adverse event; 3 Other
DEATH_SP	Specify in case of 2 and 3 above	

File: 'CRF data TOP April2007-FURES.csv'

Description: Relapse

Parameters:

Name	Description	Value
RECR_DATE	Date of recurrence	
RES_STAT	Recurrence type	1. Local recurrence 2. Regional recurrence 3. Distant recurrence
SITE	Recurrence site	

File: 'CRF data TOP April2007-MTD.csv'

Description: Administration of Epirubicin

Parameters:

Name	Description	Value
DCMDATE	Date of administration of Epirubicin	
DOSE	Total dose administered	
DOSE_UN	Dose units	mg
MOD_RSP	Reason for treatment dose delay in case of 'other'	
MT_MOD_YN	Was treatment dose delayed during study?	Yes or No
MT_TK_YN	Was treatment dose reduced during this cycle?	Yes or No
MT_TK_TYPE	Reason for treatment dose reduction	1. hematological toxicity 2. infection 3. non-hematological toxicity 4. other
MT_TK_RSP	Reason for treatment dose reduction in case of 'other'	
MT_MOD_TYPE	Reason for treatment dose delay	5. hematological toxicity 6. infection 7. non-hematological toxicity 8. other
GCSF_YN	If dose dense, was GCSF given according to the protocol during cycle?	Yes, No, or NA
GCSF_BEG_DATE	Date of dose dense administration	
GCSF_DOSE	Total dose administered in case of dose dense	
GCSF_DOSE_UN	Dense dose units	mg

File: 'CRF data TOP April2007-RND.csv'

Description: Patient inclusion

Parameters:

Name	Description	Value
INV_SIGN	Translational Research Unit signature	Present or not present
NPRTP_RSP	Reason for non-eligible patients	
OBS_COM1		
OBS_COM2		
OBS_COM3		
PRTP_YN	Is Patient eligible?	Yes or No
RND_DATE	Date of Inclusion	

File: 'CRF data TOP April2007-TR.csv'

Description: Post-Surgery Treatments

Parameters:

Name	Description	Value
CYCLE_NO	Total number of cycles given	
DOSE	Cumulative dose administered	
DOSE_UN	Dose units	mg/m^2
TR_BEG_DATE	Breast Cancer Surgery date	
TR_TXEN	Breast Cancer Surgery type And Post-Surgery specific Treatments	1. Lumpectomy 2. Quadrantectomy 3. Mastectomy 4. Axillary Node Dissection 5. Other 6. Radiotherapy 7. Hormonal Treatment with Tamoxifen 8. Hormonal Treatment with Aromatase inhibitor 9. Hormonal Treatment with LHRH analog 10. Hormonal Treatment with other

		11. Adjuvant Chemotherapy with Docetaxel 12. Adjuvant Chemotherapy with Other 13. Adjuvant Herceptin 14. Other Adjuvant Treatments
TR_YN	Application of Post-Surgery specific Treatments (Adjuvant Herceptin or Other Adjuvant Treatments)	Yes or No
TR_TXEN_YN	Application of Breast Cancer Surgery type And Post-Surgery specific Treatments	Yes or No
TRIAL_YN	Application of adjuvant treatment in context of HERA or other trial?	Yes or No
TRIAL_SP	Trial specified	
CRF_NO	HERA CRF number	
REGIMEN	Regimen	

References

C1. G.S.Stamatakos, D.D.Dionysiou, N.M.Graf, N.A.Sofra, C.Desmedt, A.Hoppe, N.Uzunoglu, M.Tsiknakis , The Oncosimulator: a multilevel, clinically oriented simulation system of tumor growth and organism response to therapeutic schemes. Towards the clinical evaluation of in silico oncology , Proceedings of the 29th Annual International Conference of the IEEE EMBS, Cite Internationale, August 23-26, SuB07.1: 6628-6631 , Lyon, France , 2007

C2. E. Ch. Georgiadi, G. S. Stamatakos, N. M. Graf, E. A. Kolokotroni, D. D. Dionysiou, A. Hoppe, N. K. Uzunoglu, "Multilevel Cancer Modeling in the Clinical Environment: Simulating the Behavior of Wilms Tumor in the Context of the SIOP 2001/GPOH Clinical Trial and the ACGT Project"accepted to be published as an 8 page full paper in Proceedings of the 8th IEEE International Conference on Bioinformatics and Bioengineering, Athens, Greece, 8-10 October 2008

C3. E. A. Kolokotroni, G. S. Stamatakos, D. Dionysiou, E. Ch. Georgiadi, C. Desmedt, N Graf, "Translating Multiscale Cancer Models into Clinical Trials: Simulating Breast Cancer Tumor Dynamics within the Framework of the "Trial of Principle" Clinical Trial and the ACGT Project," accepted to be published as an 8 page full paper in Proceedings of the 8th IEEE International Conference on Bioinformatics and Bioengineering, Athens, Greece, 8-10 October 2008

5 The Simulation Module

[Chapter code: S]

This chapter deals with the description of the parameters of the Oncosimulator simulation model, a novel numerical technique to *construct* the composition and dynamics of the baseline imageable tumour, a study of the convergence of this technique, a sensitivity analysis of the simulation model and finally the provision of two sets of parameter values that can predict tumour shrinkage following chemotherapeutic treatment for two actual clinical cases: one for a nephroblastoma case and another one for a breast cancer case. The simulation module follows the "top-down" tumour modeling approch and has been developed by the *In Silico* Oncology Group, ICCS-NTUA.

Table S0 shows the externally accessible parameters of the Oncosimulator simulation module for the paradigm of nephroblastoma treated with vincristine and dactinomycin (SIOP 2001/GPOH clinical trial). The case of breast cancer treated with epirubicin (TOP trial) is fairly analogous.

Table S0. EXTERNALLY ACCESSIBLE PARAMETERS OF THE ONCOSIMULATOR SIMULATION MODULE [MAY 2008 REVIEW VERSION]

REMARKS

If a parameter is "extern" [or is of matrix type] it is defined within the function cell_bucket::define_parameters(int layer) of the simulation code used during the Eindhoven 2008 ACGT review.

Some of the parameters that were changed during the Eindhoven 2008 ACGT review demonstration are shown in bold typeface and are underlined.

Not all parameters represent quantities that are to be adapted to clinical data. Some parameters offer the possibility to exlude a part of the code from execution (e.g. mesh reconstruction), to define the density of the discretization mesh or to perform other practical manipulations

Time values that are to be assigned by the user sould be given in multiples of 1 h

Although in the current version of the code there are two different macroscopic metabolic tumour layers i.e. the *proliferative* and the *necrotic* layer, the parameters which may distinguish between them have been set to the same value in order to simulate a macroscopically homogeneous tumour as the one considered during the Eindhoven 2008 review.

The values assigned to the parameters in this list might be used as default values if the user does not assign any value(s) to any parameter(s). This could be done *only* as a starting point towards the model's exploration.

The values of the parameters below represent their assumed *mean values* throughout the tumour or tumour layer to which they correspond. Furthermore, rates of cell category transitions imply their *mean values* over the time considered.

CELL STATE DURATIONS				
PARAMETER	DEFINED AT	TENTATIVE RANGE OF VALUES	NAME	DESCRIPTION / COMMENTS [TOA APPEAR ON CLICKING THE MOUSE]
const double cell_cycle_duration=23.0	constants.h	0.0 - 100.0	Cell cycle duration (h)	Cell cycle duration (not including G0 phase) *in hours*. The durations of each cell cycle phase is automatically calculated based on the cell cycle duration and on B.Katzung , "Basic and Clinical Pharmacology," Lange, New York, 2001, p. 926
stem_max_g0_time=96	constants.h	0.0 – 200.0	G0 phase duration (h) for stem cells	Maximum G0 phase duration before stem cell enters necrosis or re-enters G1 *in hours*.
limp_max_g0_time=96	constants.h	0.0 – 200.0	G0 phase duration (h) for limp cells	Maximum G0 phase duration before limp cell enters necrosis or re-enters G1 *in hours*.
extern int necrosis_time[2]			Time before necrosis products are eliminated (h)	Time (*in hours*) during which necrosis products occupy space in various layers of the tumour before their disappearance
necrosis_time[0]=20	cell_bucket:: define_parameters (int layer)	0.0 – 100.0	Time of necrotic cells in necrotic layer (h)	Time (*in hours*) during which necrosis products occupy space in the necrotic layer of the tumour before their disappearance
necrosis_time[1]=20	cell_bucket::	0.0 – 100.0	Time of necrotic cells in	Time (*in hours*) during

	define_parameters (int layer)		proliferative layer (h)	which necrosis products occupy space in the proliferative layer of the tumour before their disappearance
extern int apoptosis_time[2]	cell_bucket.cpp		Time before apoptosis products are eliminated (h)	Time (*in hours*) during which apoptosis products occupy space in various layers of the tumour before their disappearance (TABLE)
apoptosis_time[0]=6	cell_bucket:: define_parameters (int layer)	0.0 – 25.0	Time of apoptotic cells in necrotic layer (h)	Time (*in hours*) during which apoptosis products occupy space in the necrotic layer of the the tumour before their disappearance
apoptosis_time[1]=6	cell_bucket:: define_parameters (int layer)	0.0 – 25.0	Time of apoptotic cells in proliferating layer (h)	Time (in hours) during which apoptosis products occupy space in the proliferative layer of the tumour before their disappearance

CELL STATE/CATEGORY TRANSITION RATES

PARAMETER	DEFINED AT	TENTATIVE RANGE OF VALUES	NAME	DESCRIPTION / COMMENTS [TOA APPEAR ON CLICKING THE MOUSE]
const double apoptosis_rate=0.001	constants.h	0.0 – 1.0	Spontaneous apoptosis rate [*fraction of cell number per hour*]	Spontaneous apoptosis rate [*fraction of cell number per hour*] corresponding to transition to apoptosis from any of the G1, S, G2, M, G0 phases of the stem and progenitor cells
const double diff_apoptosis_rate=0.05	constants.h	0.0 – 1.0	Spontaneous senescence apoptosis rate [*fraction of cell number per hour*]	Spontaneous [senescence] apoptosis rate [*fraction of cell number per hour*] corresponding to transition to apoptosis from the differentiated cell state

const double diff_nec_rate=0.001	constants.h	0.0 – 1.0	Necrosis rate for differentiated cells [*fraction of cell number per hour*]	Rate ro enter necrosis for differentiated cells [*fraction of cell number per hour*]
stem_g0_to_g1_percent =0.01	constants.h	0.0 – 1.0	Fraction of dormant cancer stem cells re-entering the G1 phase per hour	Fraction of dormant cancer stem re-entering the G1 phase per hour
limp_g0_to_g1_percent =0.01	constants.h	0.0 – 1.0	Fraction of dormant cancer progenitor cells rentering the G1 phase per hour	Fraction of dormant cancer progenitor re-entering the G1 phase per hour
extern double sleep_percent[2]			Fraction of cells in a given layer that will enter G0 following a mitosis	Fraction of cells in a given layer that will enter G0 following a mitosis (TABLE)
sleep_percent[0] =0.28	cell_bucket:: define_parameters (int layer)	0.0 – 1.0	Fraction of cells in the necrotic layer that will enter G0 following mitosis	Fraction of cells in the necrotic layer that will enter G0 following mitosis
sleep_percent[1] =0.28	cell_bucket:: define_parameters (int layer)	0.0 – 1.0	Fraction of cells in the proliferative layer that will enter G0 following a mitosis	Fraction of cells in the proliferative layer that will enter G0 following a mitosis
extern double sym_percent[2]			Fraction of stem cells that divide symmetrically	Fraction of stem cells that divide symmetrically i.e. giving birth to two stem cells in a given tumour layer (TABLE). The rest of the stem cell will divide asymmetrically i.e. each stem cell will give birth to a stem and to a progenitor (limp) cell
sym_percent[0]=0.45	cell_bucket:: define_parameters (int layer)	0.0 – 1.0	Fraction of the stem cells in the necrotic tumour layer that divide symmetrically.	Fraction of the stem cells in the necrotic tumour layer that divide symmetrically i.e. they give birth to two stem cells. The rest of the stem cells will divide asymmetrically i.e. they will give birth to one one stem cell and one limited mitotic potential cell
sym_percent[1] =0.45	cell_bucket:: define_parameters	0.0 – 1.0	Fraction of the stem cells in the proliferative tumour layer that divide	Fraction of the stem cells cells in the proliferative tumour layer that divide

	(int layer)		symmetrically	symmetrically i.e. they give birth to two stem cells. The rest of the stem cells will divide asymmetrically i.e. they will give birth to one one stem cell and one limited mitotic potential (progenitor) cell

MISCELLANEOUS PARAMETERS

PARAMETER	DEFINED AT	TENTATIVE RANGE OF VALUES	NAME	DESCRIPTION / COMMENTS [TOA APPEAR ON CLICKING THE MOUSE]
const int no_limp_classes=7	constants.h	1 - 10	Limited mitotic potential (progenitor) cell stages	Number of limited mitotic potential (progenitor) cell stages before differentiation occurs = number of progenitor cell mitoses before differentiation occurs
const int x_dim=51	constants.h	30 - 96	Number of geometrical cells along the x axis	Number of geometrical cells along the x axis (x axis quantization)
const int y_dim=52	constants.h	30 - 96	Number of geometrical cells along the y axis	Number of geometrical cells along the y axis (y axis quantization)
const int z_dim=61	constants.h	30 - 96	Number of geometrical cells along the z axis	Number of geometrical cells along the z axis (z axis quantization)
const int number_biological_cells =8*10^6	constants.h	8*[900.000 – 1.100.000]	Number of cells contained within a geometrical cell of the mesh	Number of cells contained within a geometrical cell of the mesh. Traditionally a geometrical cell of 1 mm^3 is assumed to contain 10^6 biological cells
const double margin_percent=0.1	constants.h	0.0 – 0.5	Acceptable over-loading or under-loading of each geometrical cell	Acceptable over-loading or under-loading of each geometrical cell of the mesh as a fraction of the Number of Biological Cells (NBC) normally occupying a geometrical

				cell
const double color_criterion=0.98	constants.h	0.9-0.999	Minimum percentage of cells that should be dead in order to "paint" the geometrical cell necrotic	Colour criterion: minimum percentage of cells that should be dead in order to "paint" the geometrical cell necrotic [i.e. to assign the geometrical cell the colour 255 (white) in the current version of the code]
extern double distance_factor[2];			Factor adapting cell killing probability to each tumour layer	Factor adapting cell killing probability as estimated by pharmacodynamics to each tumour layer (TABLE)
distance_factor[0]=1.0	cell_bucket:: define_parameters (int layer)	0.0 – 1.0	Factor adapting cell killing probability to the necrotic layer	Factor adapting cell killing probability as estimated by pharmacodynamics to the necrotic layer
distance_factor[1]=1.0	cell_bucket:: define_parameters (int layer)	0.0 – 1.0	Factor adapting cell killing probability to the proliferative layer	Factor adapting cell killing probability as estimated by pharmacodynamics to the proliferative layer
const int drug=3	constants.h	"1", "2", "3"	Which drug or drug combination is to be simulated?	Which drug or drug combination is to be simulated? :"1" vincristine, "2" dactinomycin, "3" vincristine and dactinomycin
const int mode=2	constants.h	"1", "2"	What tumour course is to be simulated?	What tumour course is to be simulated? "1"free growth only, "2" treatment response [possibly inluding free growth]
const int reconstruction=1	constants.h	"0", "1"	Will geometric reconstruction be included in the simulations?	Will geometric reconstruction be included in the simulations? "1" yes, "0" no.

VINCRISTINE (vcr) DRUG ADMINISTRATION AND EFFECT

PARAMETER	DEFINED AT	TENTATIVE RANGE OF VALUES	NAME	DESCRIPTION / COMMENTS [TOA APPEAR ON CLICKING THE MOUSE]

const int vcr_adm_interval=168	constants.h	0 - 400	Interval between two subsequent administrations of vincristine (h)	Interval (*in hours*) between two subsequent administrations of vincristine
const int vcr_start_time=96	constants.h	0 -300	Time point of the first drug administration since initialization (h)	Time point after initialization *(in hours)* when the first drug administration takes place
const int vcr_no_sessions=4	constants.h	0- 10	Number of consecutive vincristine sessions to be simulated	Number of consecutive vincristine sessions to be simulated
const float stem_vcr_cell_kill_ratio =0.30f	constants.h	0.0f – 1.0f	Cell kill ratio of stem cells for a specific vincristine dose	Cell kill ratio of stem cells for vincristine dose 1.5 mg/m^2 [based on literature data] or another value of cell kill ratio between 0.0 and 1.0 that is known to correspond to a certain dose of vincristine.The cell kill ratio may be perturbed based on the molecular information available (e.g. via the use of molecular networks)
const float limp_vcr_cell_kill_ratio= 0.30f	constants.h	0.0f – 1.0f	Cell kill ratio of limp cells for a specific vincristine dose	Cell kill ratio of limp cells for vincristine dose 1.5 mg/m^2 [based on literature data] or another value of cell kill ratio between 0.0 and 1.0 that is known to correspond to a certain dose of vincristine.The cell kill ratio may be perturbed based on the molecular information available (e.g. via the use of molecular networks)

ACTINOMYCIN-D (act) DRUG ADMINISTRATION AND EFFECT

PARAMETER	DEFINED AT	TENTATIVE RANGE OF VALUES	NAME	DESCRIPTION / COMMENTS [TOA APPEAR ON CLICKING THE MOUSE]

const int act_adm_interval=336	constants.h	0 - 400	Interval between two subsequent administrations of actinomycin-D (h)	Interval (*in hours*) between two subsequent administrations of actinomycin-D
const int act_start_time=96	constants.h	0 -300	Time point of the first drug administration since initialization (h)	Time point after initialization *(in hours)* when the first drug administration takes place
const int act_no_sessions=2	constants.h	0 - 10	Number of consecutive actinomycin-D sessions to be simulated	Number of consecutive actinomycin-D sessions to be simulated
const float stem_act_cell_kill_ratio =0.20f	constants.h	0.0f – 1.0f	Cell kill ratio of stem cells for a specific vincristine dose	Cell kill ratio of stem cells for actinomycin-D dose= 45.0 ug/kg [based on literature data] or another value of cell kill between 0.0 and 1.0 that is known to correspond to a certain dose of vincristine. The cell kill ratio may be perturbed based on the molecular information available (e.g. via the use of molecular networks)
const float limp_act_cell_kill_ratio= 0.20f	constants.h	0.0f -1.0f	Cell kill ratio of limp cells for a specific vincristine dose	Cell kill ratio of l cells for actinomycin-D dose= 45.0 ug/kg [based on literature data] or another value of cell kill between 0.0 and 1.0 that is known to correspond to a certain dose of vincristine. The cell kill ratio may be perturbed based on the molecular information available (e.g. via the use of molecular networks)
TIME INTERVAL BETWEEN LAST TREATMENT AND POST-TREATMENT SCAN				
const int dt_posttreatment_scan= 72	constants.h	0-200	Time interval between last treatment and post-treatment scan (h)	How many hours after the last treatment session the post treatment scan is acquired

The *core output of the simulation code* is a number of matrices corresponding to the discretization mesh of the anatomic region of interest for a series of time points. Matrices contain all the necessary biological information to be used for the 3D metabolic, kinetic etc. reconstruction of the tumour at several time points or the production of several diagrams describing tumour dynamics and response to therapy as a function of space and/or time.

According to one branch of the the SIOP 2001/GPOH clinical trial combined administration of vincristine and dactinomycin takes place. In order to effectively simulate the tumour response to therapy the patient's pseudonymized imaging, molecular and clinical data are exploited. Particular emphasis is put on the effect of stem/clonogenic, progenitor and differentiated tumour cells on the overall tumour dynamics. The necessity to match the cell category/state transition rates to the cell category/state relative populations for free growth of an already large solid tumour at the start of the simulation has been addressed and clarified in deliverable D8.2. A novel technique has been recently suggested and successfully applied by ICCS-NTUA in order to ensure satisfaction of this condition and therefore a reasonable initialization of an *in vivo* tumour. In the following convergence issues are addressed and a sensitivity analysis is presented. Furthermore, a set of parameter values that is able to predict the actual tumour shrinkage following chemotherapeutic treatment and at the same time to satisfy a large number of biological boundary conditions is provided. This serves as the starting point for the clinical adaptation and optimization of the simulation module.

Tumour initialization - Convergence

As has been pointed out in deliverable D8.2 the initial distribution of cells to the cell categories and states (e.g. stem/clonogenic cells, progenitor cells, proliferating cells, dormant cells etc.) in conjunction with the cell category/state transition probabilities has a great impact on the tumour development. The concept of a nomogram adapting cell category/state transition rates to cell category/state relative populations has been introduced in deliverable D8.2.

The construction of the initial tumour cell category/state constitution and dynamics can be achieved by starting with a small number of stem/clonogenic cells and applying to each one of them the cell category/state transition probabilities that are assumed to hold true for a sufficiently small time interval about the treatment baseline. It is well known that only stem/clonogenic cells are responsible for the tumour sustenance and its further growth over long time intervals. All other tumour cells will die and be subsequently eliminated. As the virtual time is advancing all cell categories and states are populated and the relative populations of each category/state tend to reach *equilibrium*. If the relative cell category/state populations that will initialize the virtual *in vivo* tumour for given cell category/state transition rates correspond to that equilibrium a perfect match of the relative populations with the rates will be achieved and therefore the simulation of free growth of the tumour after the treatment baseline will not exhibit any peculiar course. For a relatively short time it is expected to follow a grossly exponential growth which in fact approximates a segment of the Gompertzian curve [S1, S2, S3] Obviously the cell category/state transition rates are considered approximately constant only for the same time interval and reflect the *means* of the actual cell category/state transition rates over the interval. It is pointed out that use of the means of several tumour dynamics parameters over a substantial time interval is quite customary in radiobiology [S4]. In case that there is macroscopic inhomogeneity of the tumour (distinct imageable necrotic and proliferative regions) different cell/category/state transition rates apply to the different regions. The challenge now is to successfully locate the point beyond

which equilibrium has been achieved and use the relative populations (or "fractions of populations") after that point for the correct initialization of the tumour.

In order to avoid the time consuming production and use of the nomograms mentioned above the following automatic method has been proposed, refined and implemented so as to obtain the initial cell category relative populations for given cell category/state transition probabilities. Part of the related work has already been published [S5, S6 and particularly S7, S8]. According to one variation of the method we consider 1000 geometrical cells of the tumour discretizing mesh. Each geometrical cell contains only 100 stem cells residing in the various cell cycle phases [G1, S, G2, M, G0]. Time initialization i.e. the time already spent in a phase by the cells residing in is achieved by means of a pseudo-random number generator. Different random numbers are assigned to different geometrical cells. The aim of this approach is to avoid artificial synchronization which would make the set of geometrical cells under consideration to behave as a single big geometrical cell.

Following introduction of the cell category/state transition probabilities (or equivalently rates) the system is left to evolve and produce all cell category/state populations. Execution continues until the relative populations of each cell category/state have been stabilized i.e. equilibrium has been achieved. The equilibrium condition applied is described by the following inequality:

$$\left| \frac{\sum_{time\ step\ i=n-N+1}^{n} \frac{cell\ category\ percentge\ at\ time\ step\ i}{N} - \sum_{time\ step\ j=(n-M)-N+1}^{n-M} \frac{cell\ category\ percentge\ at\ time\ step\ j}{N}}{\sum_{time\ step\ j=(n-M)-N+1}^{n-M} \frac{cell\ category\ percentge\ at\ time\ step\ j}{N}} \right| \leq \varepsilon$$

for k consecutive averages

In words the average value of N consecutive values of a given cell category/state relative population (or population percentage) is calculated every M time steps (hours). The relative difference of two average values corresponding to two consecutive steps is computed. If this relative difference is less than a given small number ε for a given number of k consecutive average values of the cell category/state relative population then *equilibrium* has been reached. This condition must hold true for all cell category/state relative populations.

In order to check the rationale of the equilibrium condition and determine the most effective values of the parameters M, N, ε, k a number of code executions have been performed. The conclusions regarding each parameter are given below.

5.1.1 Number of consecutive values of a given cell category/state relative population (N)

As explained above the equilibrium condition is to be applied to the average value of N consecutive values of a given cell category/state relative population (or population percentage)

$$\sum_{time\ step\ i=n-N+1}^{n} \frac{cell\ category\ percentge\ at\ time\ step\ i}{N}$$

A number of exploratory executions have been performed in order to determine the optimal value of N necessary for the convergence of the method. It appeared that the optimal value of N coincides with the cell cycle duration (in h). This is made clear in Fig. S1. Fig. S1 depicts the variation of the stem cell percentage over time. This relative population time course seems to follow a repeated pattern with period equal to the cell cycle duration (T_c) of the tumour under consideration. On the other hand the average value over $N=T_c$ values of stem cell relative populations follows a smooth course. Regarding the source of fluctuations, quantizations of the model certainly play a major role. However, the maximum fluctuation is about 1.5 % which is insignificant taking into account the uncertainties of the medical data to be used by the Oncosimulator.

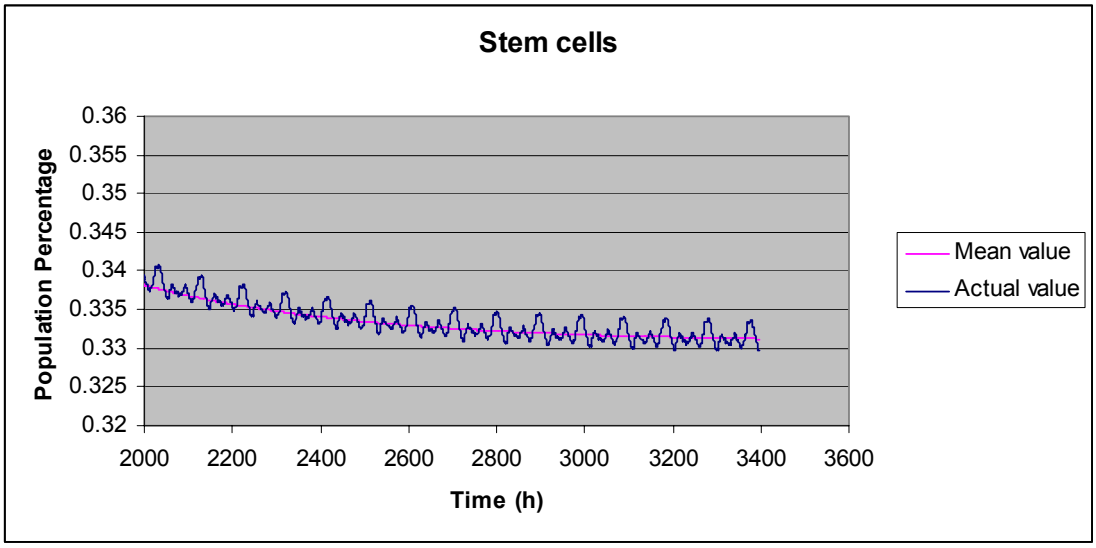

Fig. S1

Time interval M

The average value of N consecutive values of a given cell category/state relative population (or population percentage) is compared with its predecessor every M time steps (hours). Again it was shown that the most effective selection of M is the cell cycle value in h (Fig. S2). Fig. S2 depicts the relative variation of the average value of N consecutive values of the stem cell relative population over time. The curve is fairly smooth and tends to zero. On the contrary Fig. S3 depicts a case in which M has not been set to cell cycle and a small fluctuation of the relative variation over time (about 2%) is apparent. Although this fluctuation is not particularly pronounced it can be considered as an example of an imperfect selection of the value of M.

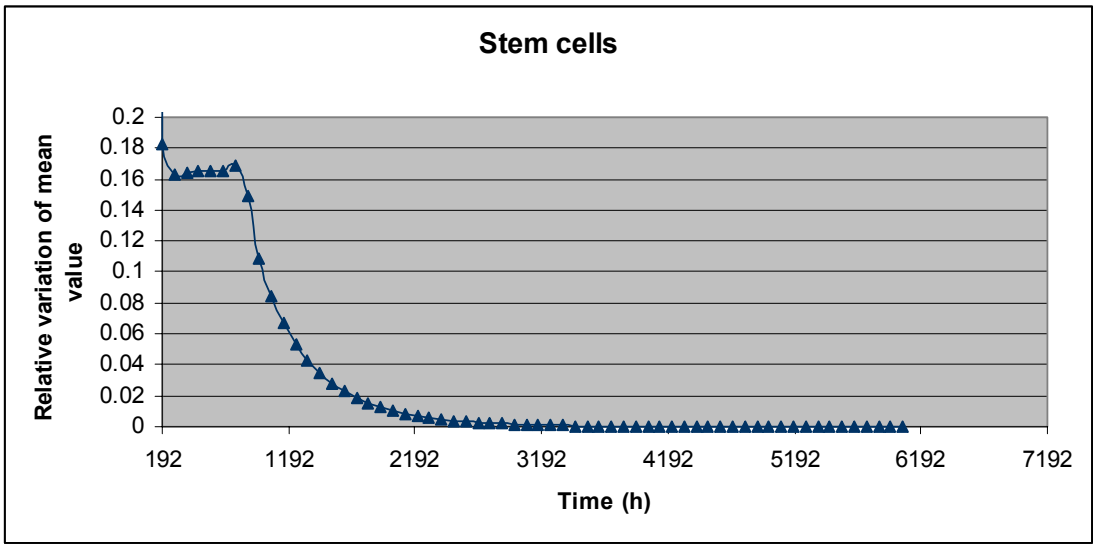

Fig. S2

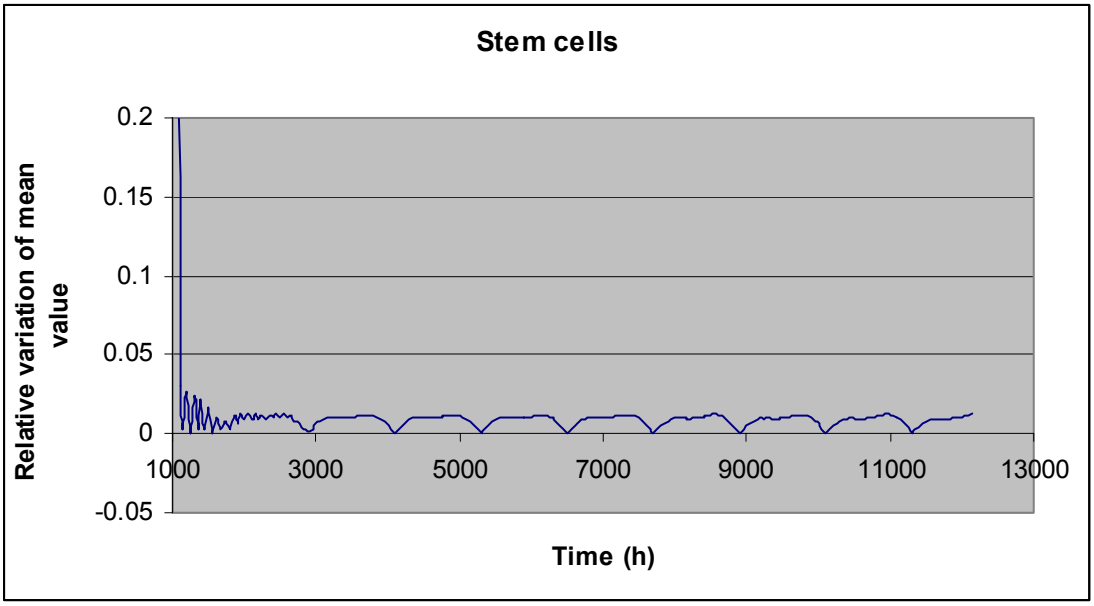

Fig. S3

5.1.3 Convergence limit ε

Ideally equilibrium has been reached when the relative variation of the average value of N consecutive values of a given cell category/state relative population over time has become zero i.e. when the average values remain constant over time. As for quantization reasons this may happen at infinity a value of ε=0.00001 has been adopted as it has been shown to be satisfactory for the tumour types explored so far (nephroblastoma and breast cancer).

5.1.4 Number of consecutive averages k

Satisfaction of the equilibrium condition for k=10 consecutive averages has proved to ensure convergence at least for the tumour types considered so far (nephroblastoma and breast cancer).

In order to demonstrate the efficiency of the method proposed and adopted we considered two extreme cases of tumour types i.e. a slowly and a rapidly evolving tumour as well as an intermediately progressing tumour. For the sensitivity analysis performed the values attributed to the code input parameters for each case study are given in Table S1. Table S1A provides the meanings of the parameter symbols used. Fig. S4 shows the simulation outcome of free tumour growth for each case. Fig. S5 depicts the time course of various cell category/state population percentages when the tumour is initialized only with stem cells for the three case studies. It is evident that if the growth rate is slow more time steps are required in order to reach equilibrium.

Table S1

Code Parameter	**Case Study A: Rapidly evolving tumor**	**Case Study B: Intermediate evolving tumor**	**Case Study C: Slowly evolving tumor**
T_c	23h	60h	96h
T_{G1}	$0.41(T_c - T_M)$		
T_S	$0.41(T_c - T_M)$		
T_{G2}	$0.18(T_c - T_M)$		
T_M	1h		
T_{G0}	96h		
T_N	20h		
T_A	6h		
N_{LIMP}	7		
R_A	0.0001	0.001	0.001
R_{NDiff}	0.001	0.001	0.001
R_{ADiff}	0.0001	0.001	0.001
P_{G0toG1}	0.01	0.01	0.0001
P_{sleep}	0.1	0.2	0.4
P_{sym}	0.9	0.6	0.835

Table S1A

Parameter symbol definition

T_c	Cell cycle duration
T_{G1}	Duration of Gap 1 phase
T_S	Duration of DNA synthesis phase
T_{G2}	Duration of Gap 2 phase
T_M	Duration of mitosis phase
T_{G0}	Duration of dormant phase
T_N	Time period needed for necrosis' products to disappear from the tumour
T_A	Time duration needed for apoptosis products to be removed from the tumour
N_{LIMP}	Number of mitoses performed by the progenitor cells before they become differentiated
R_A	Apoptosis rate of cancer cells
R_{NDiff}	Necrosis rate of differentiated cells
R_{ADiff}	Apoptosis rate of differentiated cells
P_{G0toG1}	Fraction of dormant cells that re-enter cell cycle
P_{MtoG0}	Fraction of cells that enter G0 phase following mitosis
P_{sym}	Fraction of stem cells that perform symmetric division

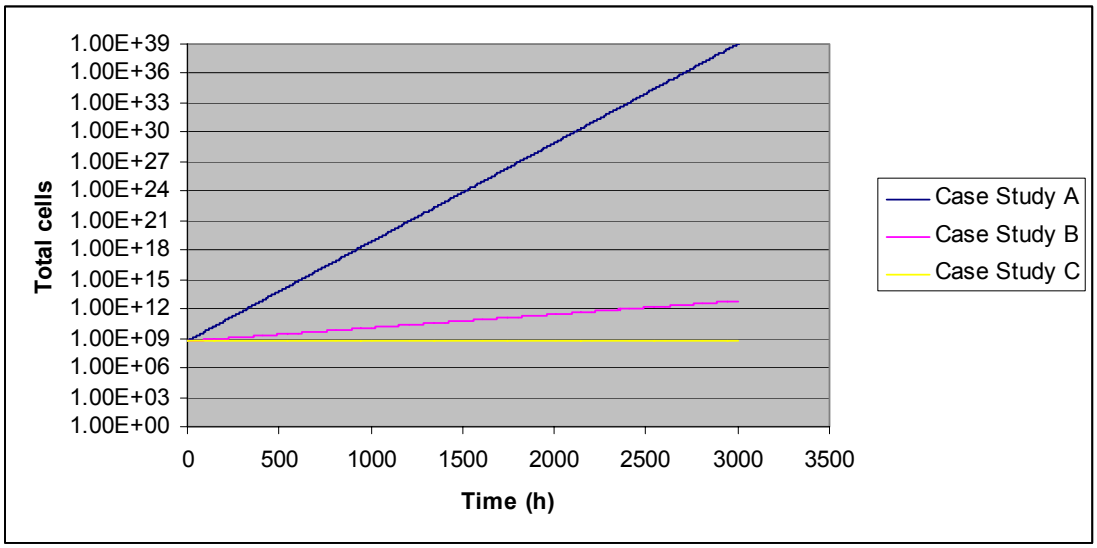
1.00E+39
1.00E+36
1.00E+33
1.00E+30
1.00E+27
1.00E+24
1.00E+21
1.00E+18
1.00E+15
1.00E+12
1.00E+09
1.00E+06
1.00E+03
1.00E+00
Total cells
0
500
1000
1500
2000
2500
3000
3500
Time (h)
Case Study A
Case Study B
Case Study C

Fig. S4

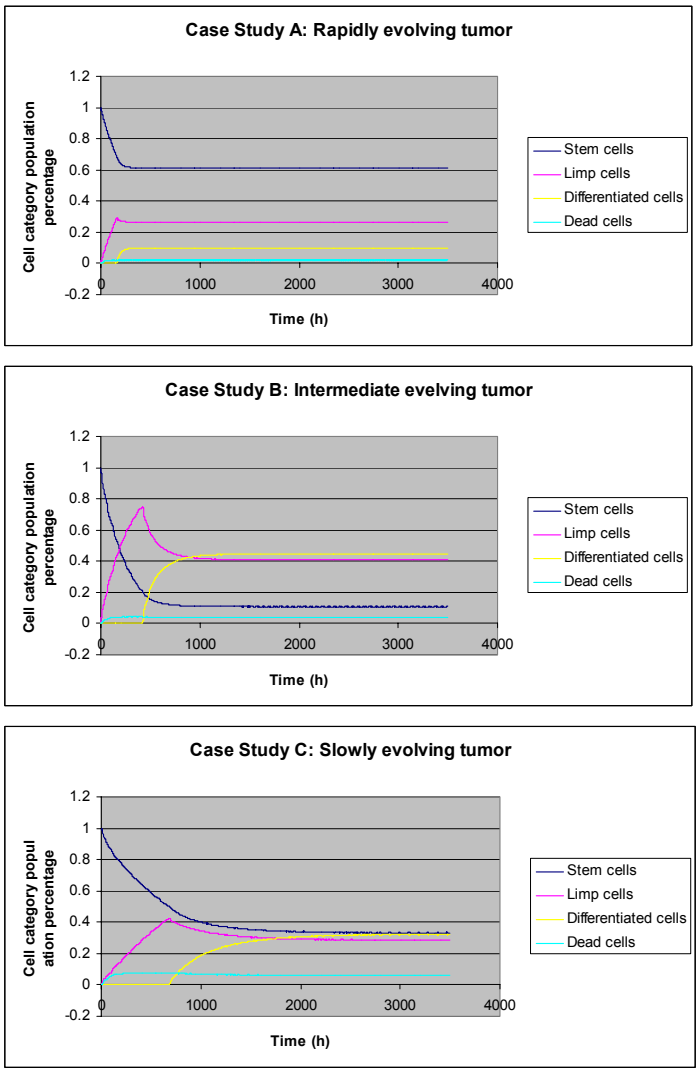

Fig. S5

For each case study the various cell category/state population percentages were calculated by the previously described method. Table S2 shows the results for various cell category/state population percentages. The last column on the right shows the time that the equilibrium condition is satisfied and therefore execution stops. Taking into account Fig. S5 it can be noted that the execution of the initialization process correctly stops earlier for the case A and later for the case C (Table S2).

Table S2

Case Study	Stem prolif fraction	Stem G0 fraction	Limp Prolif fraction	Limp G0 fraction	Diff fraction	Apoptotic fraction	Necrotic fraction	Stop Time
A	0.518237	0.0951152	0.2238641	0.04108716	0.100187	0.000429082	0.0210803	759
B	0.0820165	0.0262184	0.3090686	0.09880053	0.446598	0.0047246	0.0325732	2880
C	0.209745	0.132384	0.1734756	0.1094919	0.313331	0.00469234	0.056881	6048

Sensitivity Analysis

5.2.1 Condition for monotonic free tumour growth

Depending on the values assigned to the code input parameters we can simulate a non treated tumour that grows with time which is usually the desirable case or a tumour that diminishes with time and therefore cannot usually exist. The outcome strongly depends on the behavior of the stem proliferating cells. Since stem cells are the origin of the tumour in order to create a growing tumour the number of stem cells must increase with time. The following figure depicts the cytokinetic model of the stem proliferating cells.

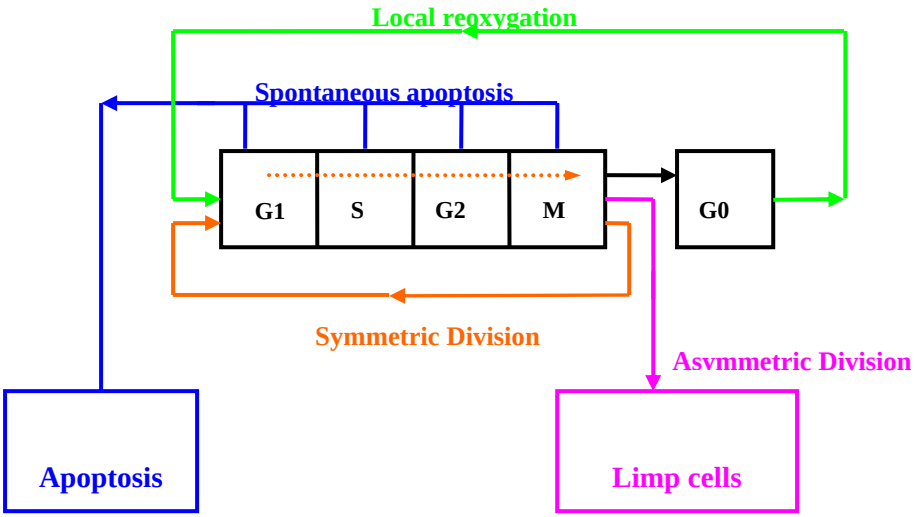

Fig. S6

Let us consider N stem cells residing at the G1 phase. At each execution step (every hour) a fraction of the stem cells will die due to apoptosis. This procedure is described by the parameter apoptosis rate (R_A). More specifically after the first hour a number of $N(1- R_A)$ cells will remain, after the second the stem population will be $N(1- R_A)^2$ etc. The number of stem cells that will eventually reach the mitosis phase and divide will be $N(1-R_A)^{T_C}$. From this population a fraction equal to P_{sym} will divide symmetrically giving rise to 2 stem cells, whereas the rest stem cells will give birth to 1 stem cell and 1 progenitor cell. After a few manipulations the number of stem cells after mitosis is calculated as $N(1-R_A)^{T_C}(1+P_{sym})$. The stem cells that will re-enter the cell cycle and not transit to dormant (G0 phase) will be $N(1-R_A)^{T_C}(1+P_{sym})(1-\mathrm{P_{sleep}})$. In order to have a growing tumour the number of stem cells after mitosis must be larger than the initial ones, i.e. the following inequality must hold

$$N(1-R_A)^{T_C}(1+P_{sym})(1-\mathrm{P_{sleep}}) \geq N \Rightarrow$$

$$(1-R_A)^{T_C}(1+P_{sym})(1-\mathrm{P_{sleep}}) \geq 1 \qquad \text{(S1)}$$

Equation (S1) enables us to compute the value range of one of the parameters, for example P_{sym} when specific values are attributed to the rest of the parameters. In the previous analysis the fraction of dormant cells that re-enter the cell cycle and expressed by P_{G0toG1} has not been taken into account. However, for small values of the latter (S1) is a very good approximation. It must be noted that the equality corresponds to a tumour that remains constant as a function of time. By increasing $\mathrm{P_{sym}}$ but keeping constant the rest of the parameters the tumour becomes more aggressive while its doubling time decreases. In the following we will explore the implication of condition (S1) to the range of values of each involved code parameter separately.

5.2.1.1 Apoptosis Rate R_A

Condition (S1) implies that

$$(1-R_A)^{T_C} \geq \frac{1}{(1+P_{sym})(1-\mathrm{P_{sleep}})} \Rightarrow$$

$$1-R_A \geq \frac{1}{(1+P_{sym})^{1/T_C}(1-\mathrm{P_{sleep}})^{1/T_C}} \Rightarrow$$

$$R_A \leq 1-\frac{1}{(1+P_{sym})^{1/T_C}(1-\mathrm{P_{sleep}})^{1/T_C}}$$

The equality corresponds to the upper limit of the apoptosis rate for specific values assigned to the cell cycle duration (T_C), symmetric division fraction (P_{sym}) and sleep fraction (P_{sleep}). We observe that that this upper limit increases when P_{sym} increases and P_{sleep} decreases. Therefore the maximum value of the rate upper limit of apoptosis is reached when all cells divide symmetrically and no cell enters the dormant phase i.e. P_{sym}=1 and P_{sleep}=0. Therefore,

$$R_A \le 1 - \frac{1}{2^{1/T_C}} \quad \text{(S2)}$$

Fig. S7 depicts the variation of this limit as a function of the cell cycle duration. The apoptosis rate can take values that are below the curve. We observe that the upper limit decreases as the cell cycle duration increases.

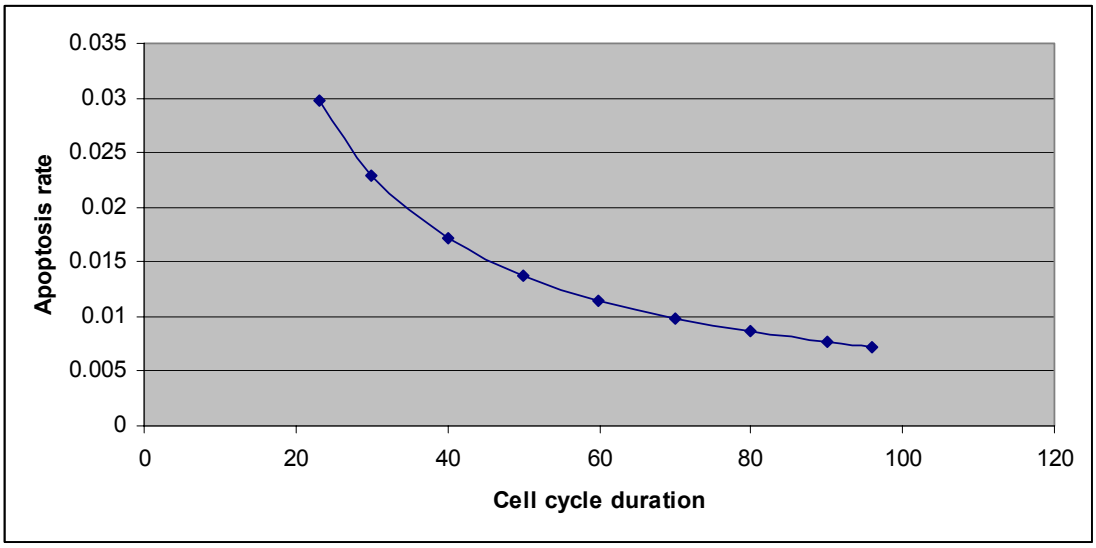

Fig. S7

5.2.2.2 Sleep Fraction P_{sleep}

As a first approximation the upper limit of the fraction of stem proliferating cells that enter the dormant phase after mitosis (P_{sleep}) is 0.5 since after mitosis at least half of the daughter stem cells must re-enter the cycle in order to ensure a steady population of stem proliferating cells. A refinement of this upper limit can be extracted from condition (S1). After the necessary calculations we obtain

$$P_{sleep} \le 1 - \frac{1}{(1+P_{sym})(1-R_A)^{T_C}}$$

If P_{sym}=1 i.e. all cells divide symmetrically the sleeping fraction takes its maximum value:

$$P_{sleep} \le 1 - \frac{1}{2(1-R_A)^{T_C}} \quad \text{(S3)}$$

For R_A=0, i.e. when no apoptosis occurs, the upper limit of P_{sleep}=0.5. For $R_A = 1 - \frac{1}{2^{1/T_C}}$, i.e. when apoptosis rate takes its maximum value P_{sleep}=0.

Fig. S8 depicts the variation of the upper limit of the sleeping fraction as a function of the apoptosis rate for three values of the cell cycle duration (T_c) (P_{sym} =1). The sleep fraction can take values under the relevant curve.

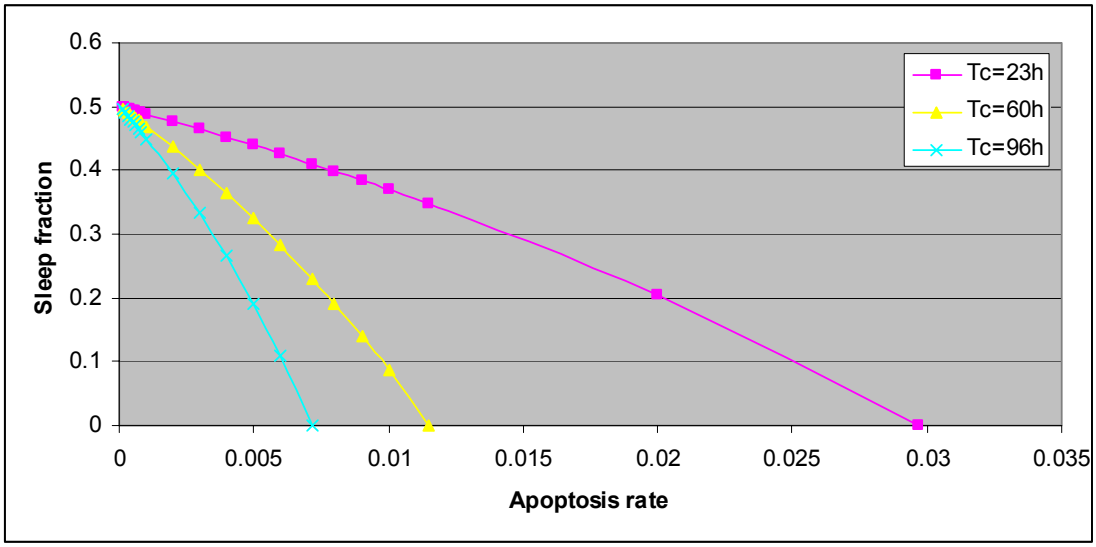

Fig. S8

5.2.2.3 Symmetric division fraction P_{sym}

The condition (S1) determines the lower limit for the symmetric division fraction:

$$P_{sym} \geq \frac{1}{(1-R_A)^{T_C}(1-\mathrm{P_{sleep}})} - 1 \quad \text{(S4)}$$

Fig. S9 depicts the variation of the lower limit of the symmetric division fraction as a function of the sleeping fraction for two values of the apoptosis rate (T_C=60h). The symmetric division fraction can take values above the relevant curve. The upper limit is obviously 1 in all cases.

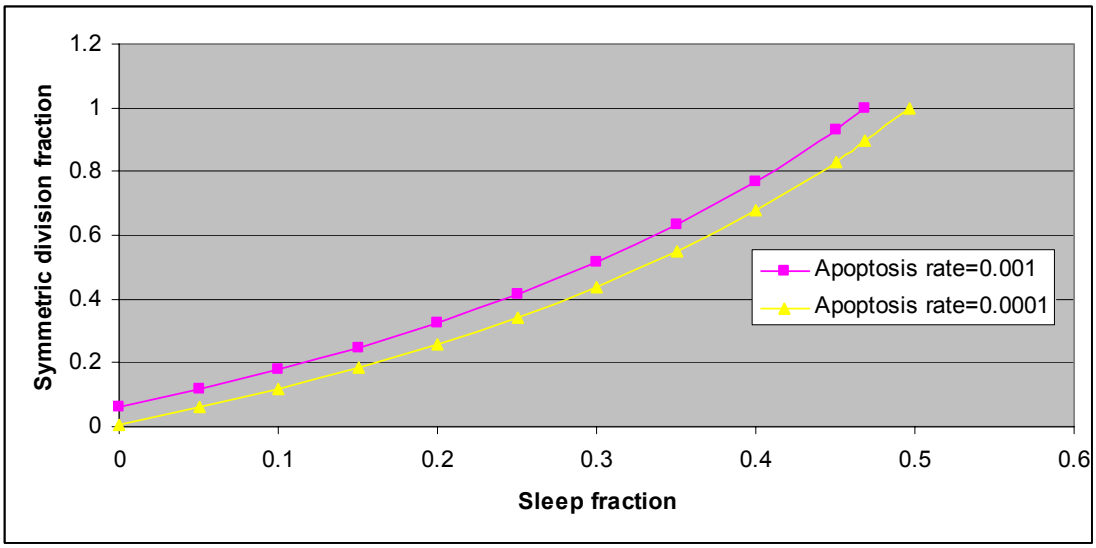

Fig. S9

Summarizing, inequalities (S1) to (S4) determine the value range of the parameters P_{sleep}, P_{sym} and R_A for a given cell cycle duration in order to have a monotonically growing tumour. The above observations are summarized in the Table S3

Table S3

	Min Value	**Max Value**
Apoptosis rate	0	$1-\frac{1}{2^{1/T_C}}$
Sleeping fraction	0	$1-\frac{1}{2(1-R_A)^{T_C}}$
Symmetric division fraction	$\frac{1}{(1-R_A)^{T_C}(1-\mathrm{P_{sleep}})}-1$	1
$(1-R_A)^{T_C}(1+P_{sym})(1-\mathrm{P_{sleep}})\geq 1$		

5.2.1 Doubling time

Different types of tumours with respect to the degree of aggressiveness can be simulated by attributing suitable values to the code input parameters. The purpose of this section is to explore the dependence of tumour growth rate on each code parameter. A macroscopically homogeneous tumour is considered, consisting of a single "proliferating" layer with no macroscopically distinct necrotic or other layer. This by no means implies that the growth fraction of the tumour [S4] is 1 or that the cell loss factor [S4] is 0. It actually implies that the microscopic necrotic regions which are primarily due to the imperfect neovascularization of the tumour are rather homogeneously distributed over the entire tumour. For a *sufficiently short time interval* tumour growth could be approximated by an exponential curve as shown in Fig. S10. In fact this exponential growth represents *only* a segment of the actual Gompertzian growth curve [S1, S2 and S3]. We observe that the temporal variation of the various cell category/state populations as a function of time for a limited time interval appears to be linear on a semi-logarithmic system of coordinates i.e. it exhibits an exponential behaviour. Therefore for a *short time interval* the population of the various cell categories evolves with time according to the equation:

$$N(t) = N_o e^{at}$$

Only for theoretical purposes the time interval considered in certain cases is deliberately extended beyond what would seem a short segment of the Gompertzian curve. It is noted that the "shortness' of the time interval is primarily determined by the actual volume doubling time of the tumour.

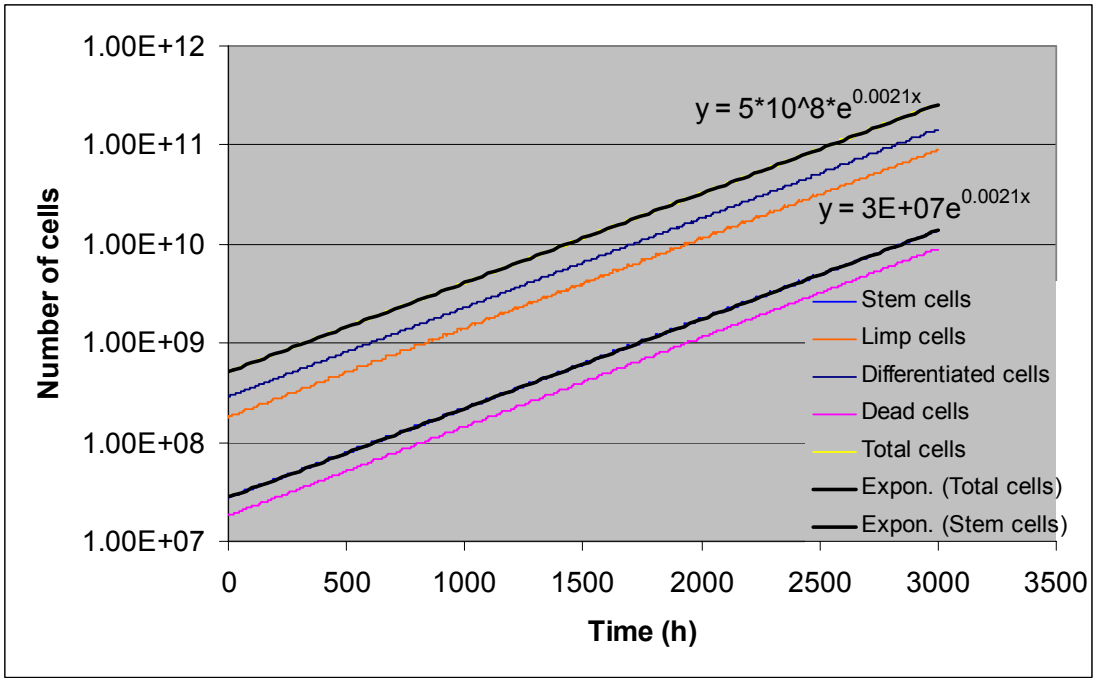

Fig. S10

The doubling time T_d is the most efficient parameter for expressing the growth rate of the tumour. Under the previous restrictions the following equation holds:

$$T_d = \frac{\ln 2}{a}$$

We observe that the curves corresponding to all cell category/state populations have the same slope in a semi-logarithmic graph. This implies that the exponent α and therefore the doubling time is the same for all cell category/state populations. The doubling time can be calculated based on the following equation:

$$T_d = \frac{\ln(2) * (t_2 - t_1)}{\ln\left(\frac{N_2}{N_1}\right)}$$

where N_1 and N_2 denote the cell category/state populations at times t_1 and t_2 respectively. The time period $\Delta t = t_2 - t_1$ has been choosen to be a multiple of the cell cycle duration ($10*T_c$) due to the periodicity of the relative cell category/state population fluctuation as explained previously.

It should be noted that the temporal variation of the cell population is not perfectly exponential but exhibits a repeated motif with a period equal to the cell cycle duration. Fig. S11 shows the temporal variation of the number of total tumour cells and an exponential fit. The same pattern characterises all cell categories. Again model quantizations are primarily responsible for these very slight deviations.

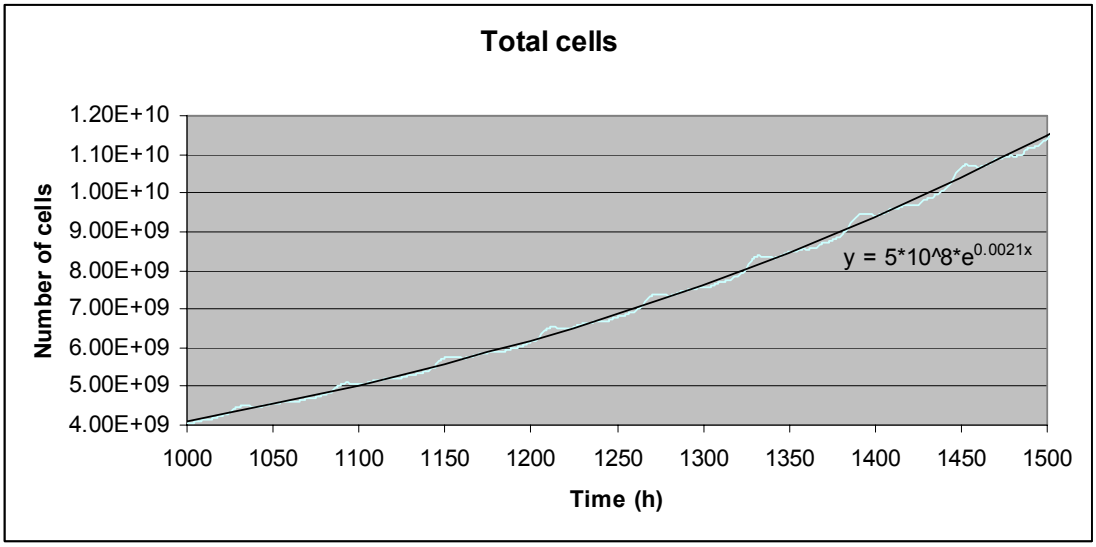

Fig. S11

Table S4 shows the values assigned to the code input parameters for the tumour considered *above*.

Table S4

Symbol	Description	Value
T_c	Cell cycle duration	60h
T_{G1}	Duration of Gap 1 phase	$0.41(T_c - T_M)$
T_S	Duration of DNA synthesis phase	$0.41(T_c - T_M)$
T_{G2}	Duration of Gap 2 phase	$0.18(T_c - T_M)$
T_M	Duration of mitosis phase	1h
T_{G0}	Duration of dormant phase	96h
T_N	Time period needed for necrosis' products to disappear from the tumour	20h
T_A	Time duration needed for apoptosis products to be removed from the tumour	6h
N_{LIMP}	Number of mitosis performed by progenitor cells before they become differentiated	7
R_A	Apoptosis rate of cancer cells	0.001
R_{NDiff}	Necrotic rate of differentiated cells	0.001
R_{ADiff}	Apoptosis rate of differentiated cells	0.001
P_{G0toG1}	Fraction of dormant cells that re-enter cell cycle	0.01
P_{sleep}	Fraction of cells that enter G0 phase following mitosis	0.2
P_{sym}	Fraction of stem cells that perform symmetric division	0.5

A number of exploratory executions have been performed in order to study the effect of certain code input parameter values on the tumour doubling time. Table S5 presents the model parameters concerning the cell category/state durations, the cell category/state transition rates and the range of certain values considered. The cell phase durations have been assumed constant throughout the executions. Similarly the following parameter values have also been assumed constant: duration of the mitosis phase (T_M), maximum duration of the dormant phase (T_{G0}), time interval needed for the necrotic products to disappear from the tumour (T_N), time interval needed for the apoptotic products to be eliminated from the tumour (T_A) and the number of mitoses performed by progenitor cells before they become differentiated (N_{LIMP}).

Table S5

Symbol	Description	Value
T_c	Cell cycle duration	23h-96h
T_{G1}	Duration of Gap 1 phase	$0.41(T_c - T_M)$
T_S	Duration of DNA synthesis phase	$0.41(T_c - T_M)$
T_{G2}	Duration of Gap 2 phase	$0.18(T_c - T_M)$
T_M	Duration of mitosis phase	1h
T_{G0}	Duration of dormant phase	96h
T_N	Time period needed for necrosis' products to disappear from the tumour	20h
T_A	Time duration needed for apoptosis products to be removed from the tumour	6h
N_{LIMP}	Number of mitosis performed by progenitor cells before they become differentiated	7
R_A	Apoptosis rate of cancer cells	0.0001-0.001
R_{NDiff}	Necrosis rate of differentiated cells	0.0001-0.001
R_{ADiff}	Apoptosis rate of differentiated cells	0.0001-0.001
P_{G0toG1}	Fraction of dormant cells that re-enter cell cycle	0.0001-0.01
P_{sleep}	Fraction of cells that enter G0 phase following mitosis	0.1-0.28
P_{sym}	Fraction of stem cells that perform symmetric division	0.4-0.8

5.2.1.1 Cell cycle duration

Nine code executions have been performed with variable cell cycle duration ranging from 23h-96h. The values of the rest of the code input parameters are shown in Table S5 and Table S6. The temporal variation of the total cell category/state populations as a function of time is depicted in Fig. S13. Fig. S12 shows the variation of the doubling time as a function of the cell cycle duration. We observe that an increase in the cell cycle duration leads to a tumour with a higher doubling time. The relation between these two parameters is not linear as shown in Fig. S12

Table S6

Execution	T_c	P_{sleep}	P_{sym}	P_{G0toG1}	R_A	R_{ADiff}	R_{NDiff}
A	23	0.2	0.5	0.01	0.001	0.001	0.001
B	30	0.2	0.5	0.01	0.001	0.001	0.001
C	40	0.2	0.5	0.01	0.001	0.001	0.001
D	50	0.2	0.5	0.01	0.001	0.001	0.001
E	60	0.2	0.5	0.01	0.001	0.001	0.001
F	70	0.2	0.5	0.01	0.001	0.001	0.001
G	80	0.2	0.5	0.01	0.001	0.001	0.001
H	90	0.2	0.5	0.01	0.001	0.001	0.001
I	96	0.2	0.5	0.01	0.001	0.001	0.001

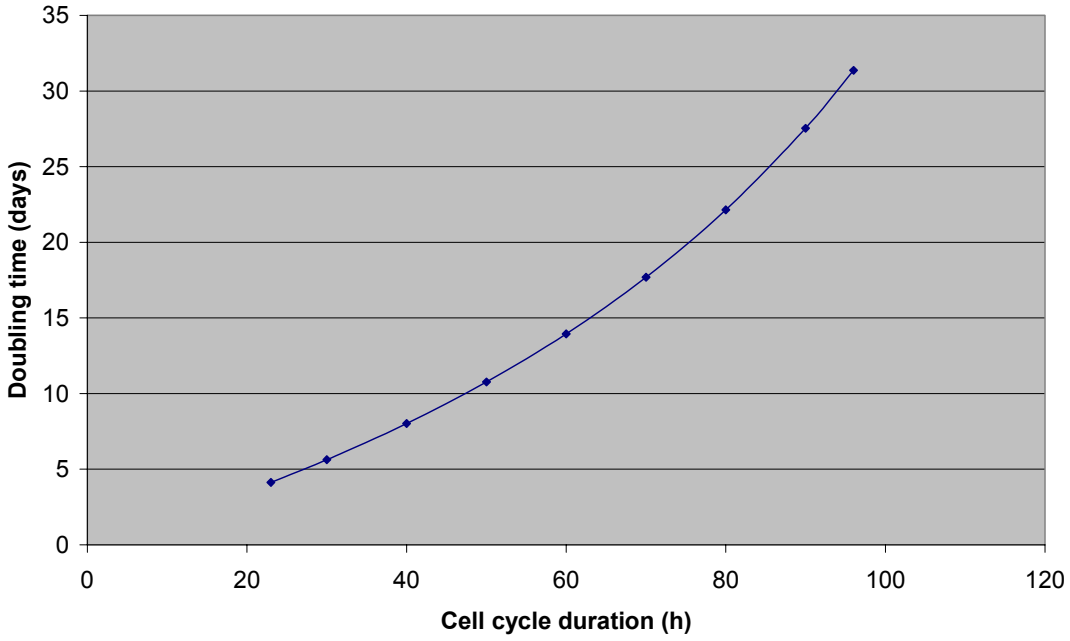
35
30
25
20
15
10
5
0
Doubling time (days)
0
20
40
60
80
100
120
Cell cycle duration (h)

Figure S12

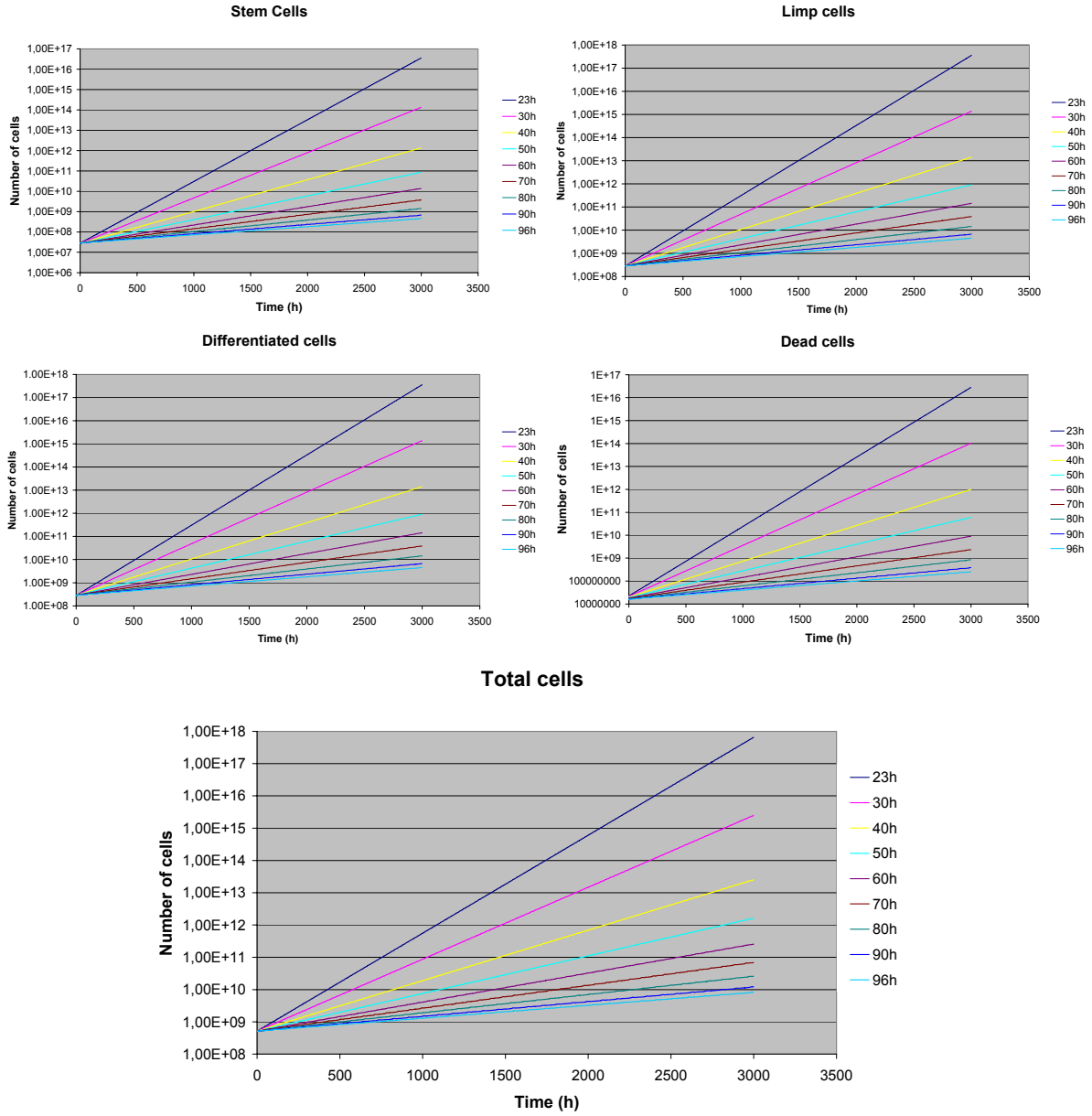
Stem Cells
Limp cells
Differentiated cells
Dead cells
Total cells
Number of cells
Time (h)
23h
30h
40h
50h
60h
70h
80h
90h
96h

Figure S13

5.2.1.2 Sleeping fraction

Ten code executions have been performed with varying sleeping fraction (fraction of cells that enter G0 phase after mitosis) from 0.1 to 0.28 (Table S7). The values of the rest of the code input parameters are provided in Table S5 and Table S7. The temporal variation of total cell category/state populations as a function of time is depicted in Fig. S15. Fig. S14 provides the variation of the doubling time as a function of the cell cycle duration. We observe that an increase in the sleeping fraction leads to a tumour with a higher doubling time. The relation between these two parameters is not linear as shown in Fig. S14.

Table S7

Execution	$\mathbf{T_c}$	$\mathbf{P_{sleep}}$	$\mathbf{P_{sym}}$	P_{G0toG1}	R_A	R_{ADiff}	R_{NDiff}
A	60	0.10	0.5	0.01	0.001	0.001	0.001
B	60	0.12	0.5	0.01	0.001	0.001	0.001
C	60	0.14	0.5	0.01	0.001	0.001	0.001
D	60	0.16	0.5	0.01	0.001	0.001	0.001
E	60	0.18	0.5	0.01	0.001	0.001	0.001
F	60	0.20	0.5	0.01	0.001	0.001	0.001
G	60	0.22	0.5	0.01	0.001	0.001	0.001
H	60	0.24	0.5	0.01	0.001	0.001	0.001
I	60	0.26	0.5	0.01	0.001	0.001	0.001
J	60	0.28	0.5	0.01	0.001	0.001	0.001

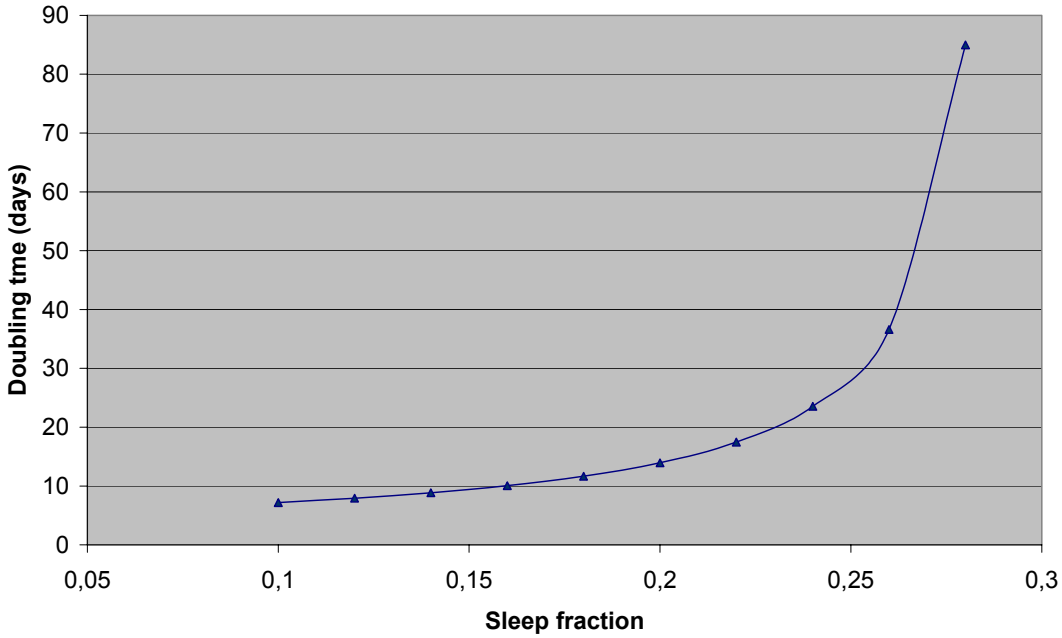
90
80
70
60
50
40
30
20
10
0
Doubling tme (days)
0,05
0,1
0,15
0,2
0,25
0,3
Sleep fraction

Fig. S14

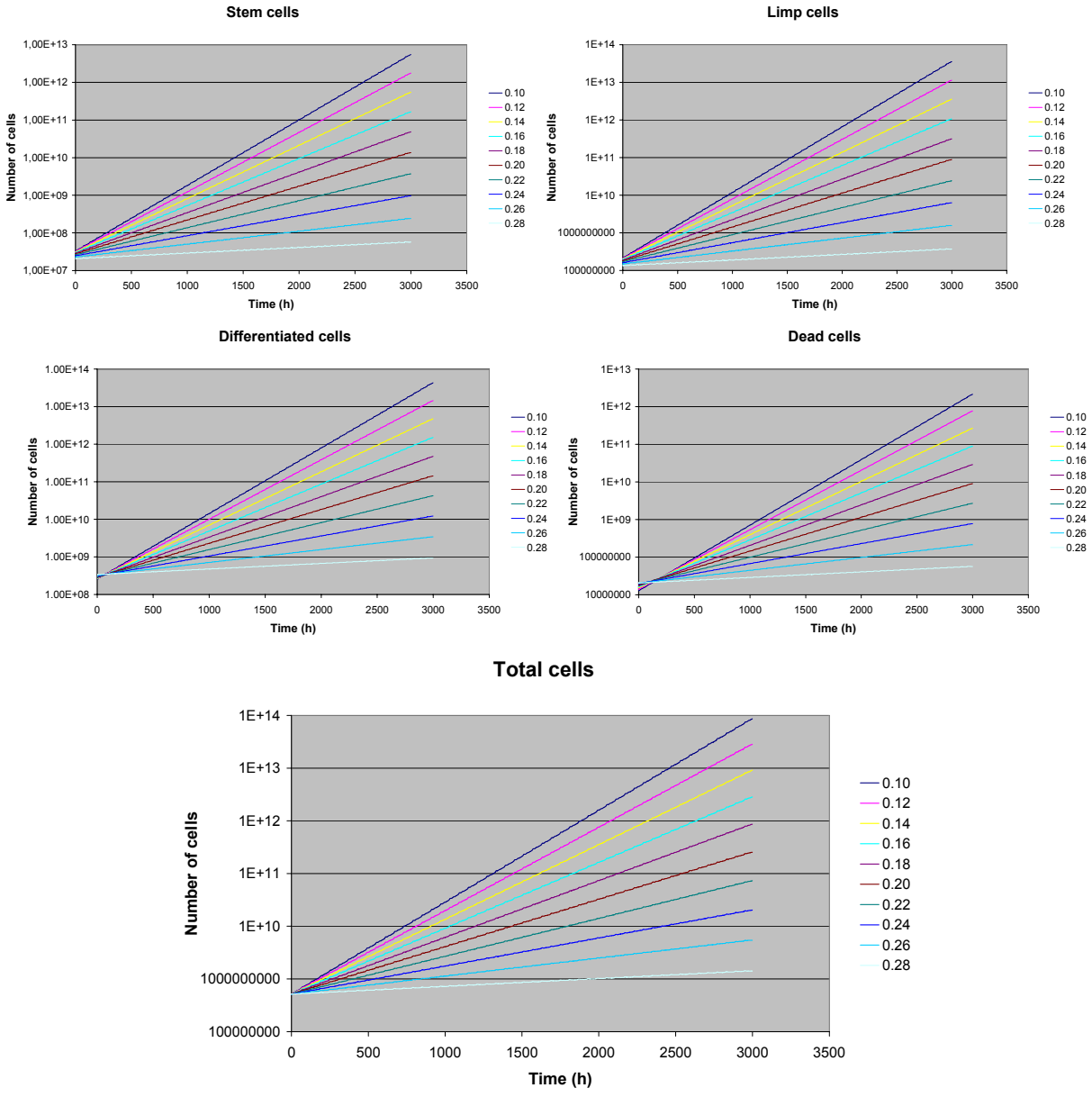

Total cells

Fig. S15

5.2.1.3 Symmetric division fraction

Nine code executions have been performed with variable symmetric division fraction (fraction of the stem cells that divide symmetrically i.e. each one giving birth to two stem cells) ranging from 0.4 to 0.8 (Table S8). The values of the rest of the code input parameters are included in Table S5 and Table S8. The temporal variation of the total cell category/state populations as a function of time is depicted in Fig. S17. Fig. S16 shows the variation of the doubling time as a function of the cell cycle duration. We observe that an increase in the symmetric division fraction leads to a tumour with smaller doubling time. The relation between these two parameters is not linear as shown in Fig. S16.

Table S8

Execution	T_c	P_{sleep}	P_{sym}	P_{G0toG1}	R_A	R_{ADiff}	R_{NDiff}
A	60	0.2	0.4	0.01	0.001	0.001	0.001
B	60	0.2	0.45	0.01	0.001	0.001	0.001
C	60	0.2	0.5	0.01	0.001	0.001	0.001
D	60	0.2	0.55	0.01	0.001	0.001	0.001
E	60	0.2	0.6	0.01	0.001	0.001	0.001
F	60	0.2	0.65	0.01	0.001	0.001	0.001
G	60	0.2	0.7	0.01	0.001	0.001	0.001
H	60	0.2	0.75	0.01	0.001	0.001	0.001
I	60	0.2	0.8	0.01	0.001	0.001	0.001

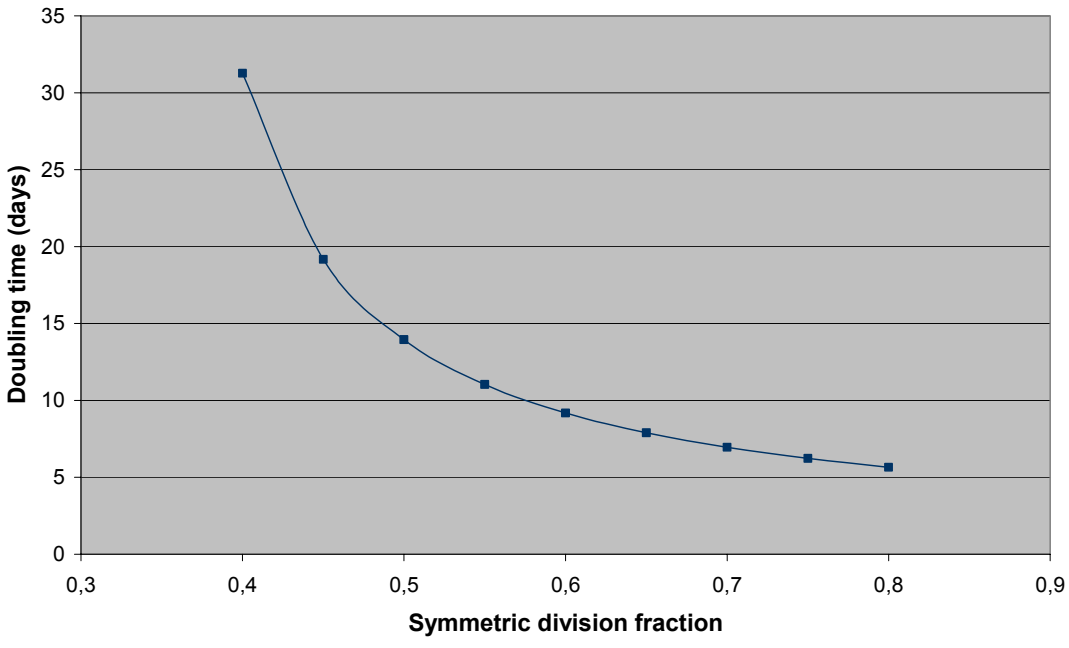

Fig. S16

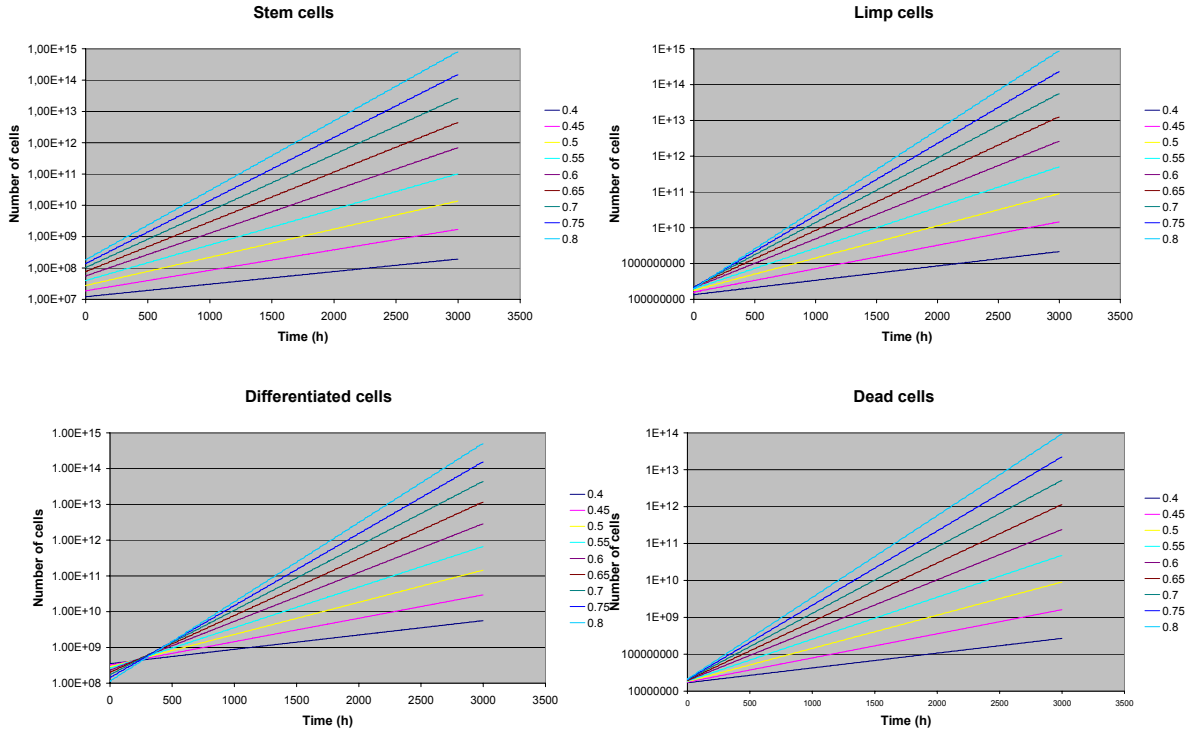

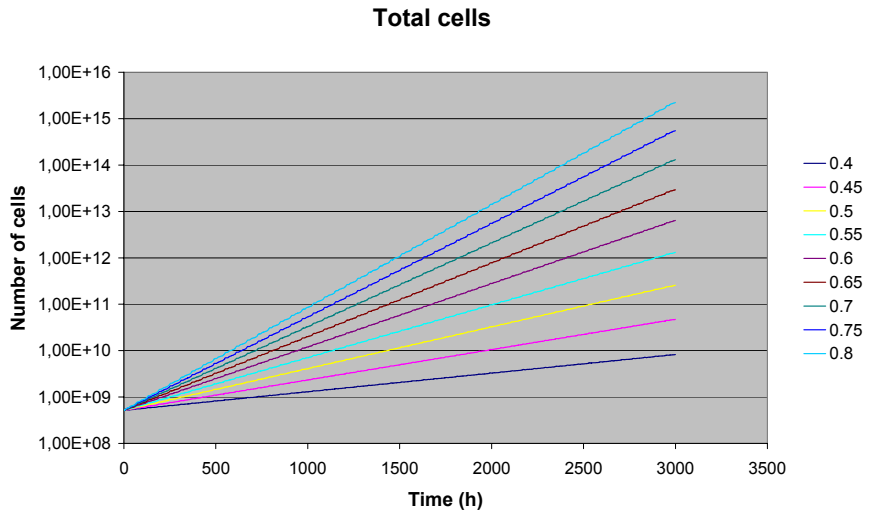

Fig. S17

5.2.1.4 G0 to G1 fraction

Ten executions have been performed with variable G0 to G1 fraction ranging from 0.0001 to 0.01 (Table S9). The values of the rest of the code input parameters are presented in Table S5 and Table S9. The temporal variation of the total cell category/state populations is depicted in Fig. S19. Fig. S18 shows the variation of the doubling time as a function of the cell cycle duration. We observe that an increase in G0 to G1 fraction leads to a tumour with slightly smaller doubling time. The relation between these two parameters is linear as shown in Fig. S18.

Table S9

Execution	$\mathbf{T_c}$	$\mathbf{P_{sleep}}$	$\mathbf{P_{sym}}$	P_{G0toG1}	R_A	R_{ADiff}	R_{NDiff}
A	60	0.2	0.5	0.01	0.0001	0.0001	0.001
B	60	0.2	0.5	0.01	0.0002	0.0002	0.001
C	60	0.2	0.5	0.01	0.0003	0.0003	0.001
D	60	0.2	0.5	0.01	0.0004	0.0004	0.001
E	60	0.2	0.5	0.01	0.0005	0.0005	0.001
F	60	0.2	0.5	0.01	0.0006	0.0006	0.001
G	60	0.2	0.5	0.01	0.0007	0.0007	0.001
H	60	0.2	0.5	0.01	0.0008	0.0008	0.001
I	60	0.2	0.5	0.01	0.0009	0.0009	0.001
J	60	0.2	0.5	0.01	0.001	0.001	0.001

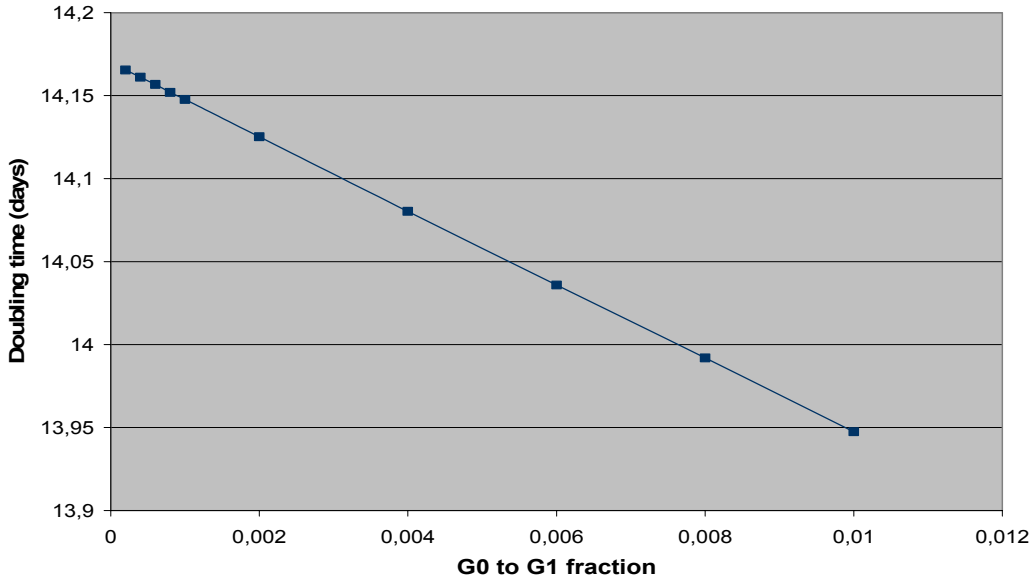

Fig. S18

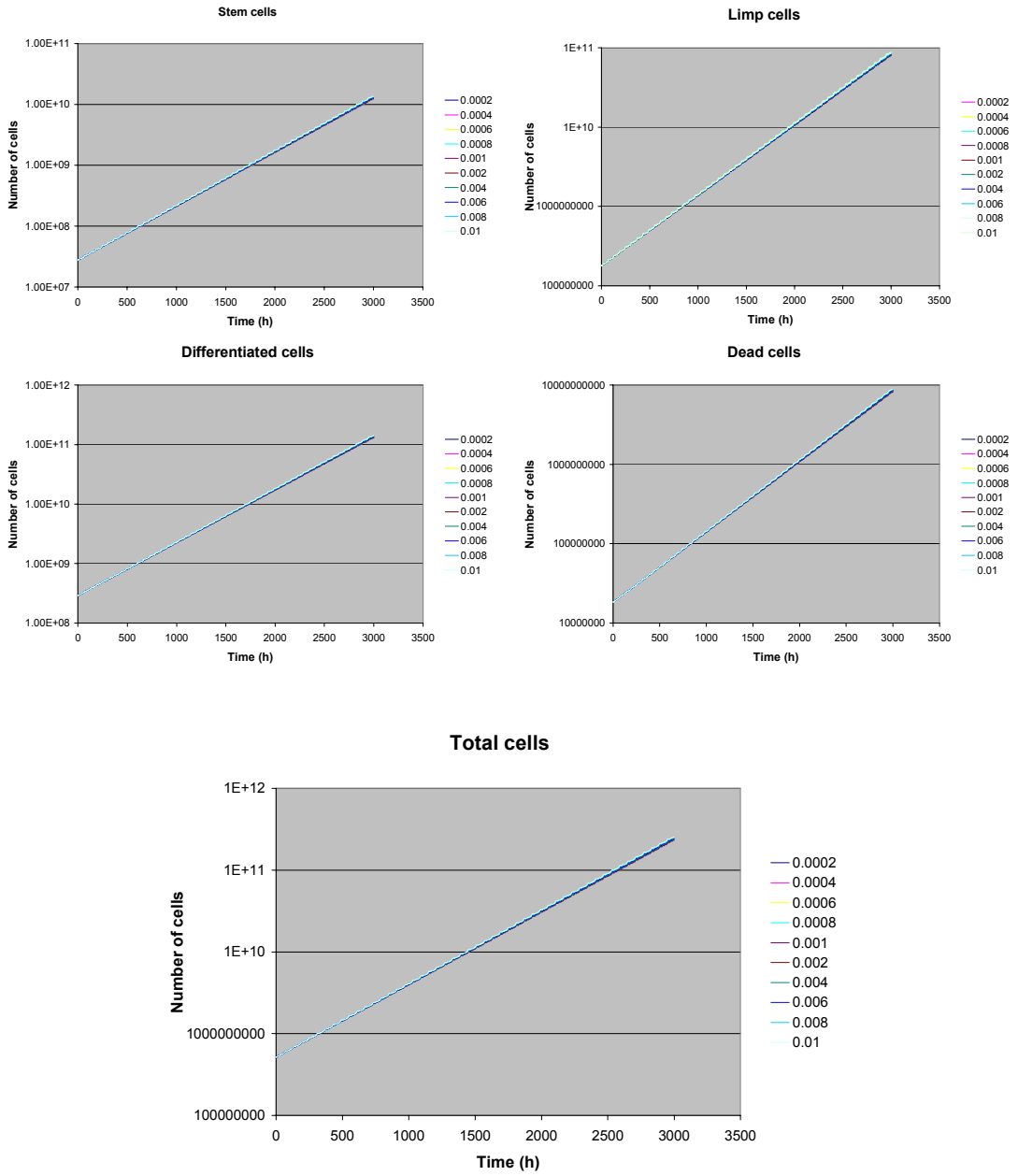
Stem cells
Number of cells
1.00E+11
1.00E+10
1.00E+09
1.00E+08
1.00E+07
0
500
1000
1500
2000
2500
3000
3500
Time (h)
0.0002
0.0004
0.0006
0.0008
0.001
0.002
0.004
0.006
0.008
0.01
Limp cells
Number of cells
1E+11
1E+10
1000000000
100000000
Time (h)
Differentiated cells
Number of cells
1.00E+12
1.00E+11
1.00E+10
1.00E+09
1.00E+08
Time (h)
Dead cells
Number of cells
10000000000
1000000000
100000000
10000000
Time (h)

Total cells
Number of cells
1E+12
1E+11
1E+10
1000000000
100000000
0
500
1000
1500
2000
2500
3000
3500
Time (h)
0.0002
0.0004
0.0006
0.0008
0.001
0.002
0.004
0.006
0.008
0.01

Fig. S19

5.2.2.5 Apoptosis Rate

Ten code executions have been performed with variable apoptosis rate for all types of cells (proliferating and differentiated) ranging from 0.0001 to 0.001 (Table S10). The values of the rest of the code input parameters are included in Table S5 and Table S10. The temporal variation of the total cell populations is depicted in Fig. S20A. Fig. 20 depicts the variation of the doubling time as a function of the cell cycle duration. We observe that an increase in the apoptosis rate leads to a tumour with elevated doubling time. The relation between these two parameters is not linear as shown in Fig. S20.

Table S10

Execution	**T_c**	**P_{sleep}**	**P_{sym}**	P_{G0toG1}	R_A	R_{ADiff}	R_{NDiff}
A	60	0.2	0.5	0.01	0.0001	0.0001	0.001
B	60	0.2	0.5	0.01	0.0002	0.0002	0.001
C	60	0.2	0.5	0.01	0.0003	0.0003	0.001
D	60	0.2	0.5	0.01	0.0004	0.0004	0.001
E	60	0.2	0.5	0.01	0.0005	0.0005	0.001
F	60	0.2	0.5	0.01	0.0006	0.0006	0.001
G	60	0.2	0.5	0.01	0.0007	0.0007	0.001
H	60	0.2	0.5	0.01	0.0008	0.0008	0.001
I	60	0.2	0.5	0.01	0.0009	0.0009	0.001
J	60	0.2	0.5	0.01	0.001	0.001	0.001

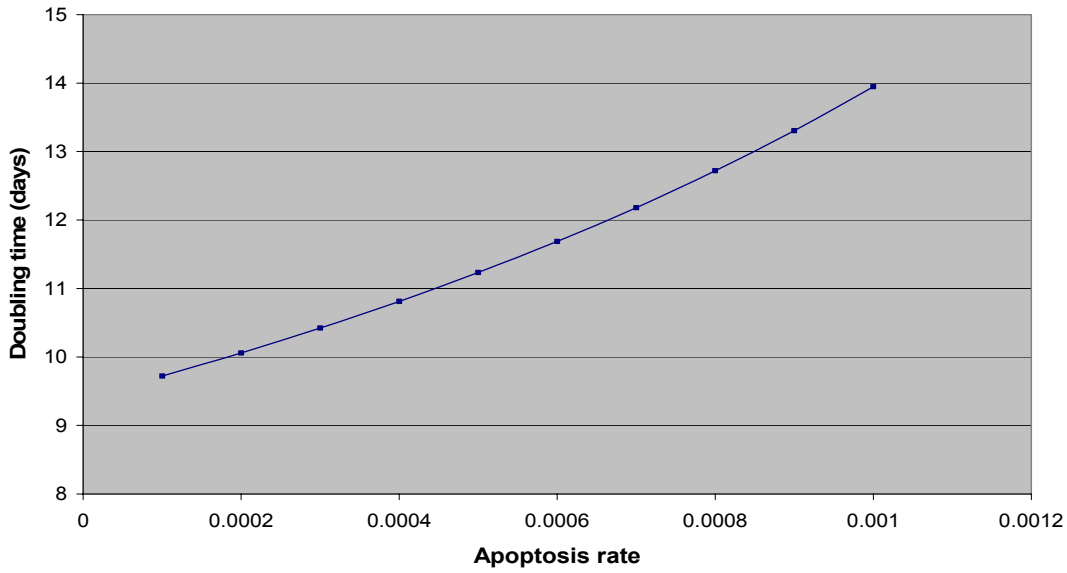

Fig. S20

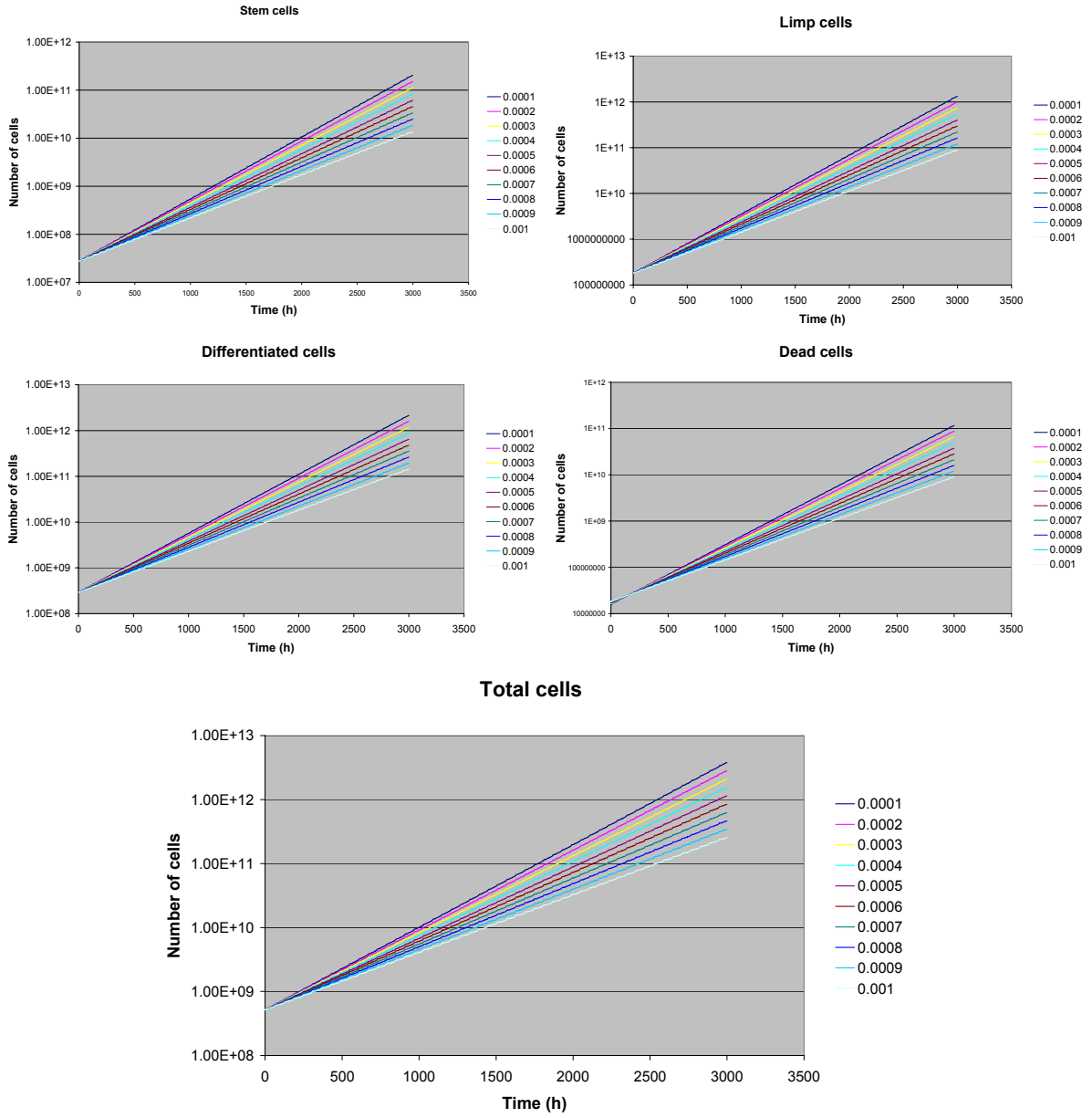
Stem cells
Number of cells
Time (h)
Limp cells
Number of cells
Time (h)
Differentiated cells
Number of cells
Time (h)
Dead cells
Number of cells
Time (h)
Total cells
Number of cells
Time (h)
0.0001
0.0002
0.0003
0.0004
0.0005
0.0006
0.0007
0.0008
0.0009
0.001

Fig. S20A

5.2.2.6 Necrosis rate of differentiated cells

Ten code executions have been performed with varying necrosis rate of differentiated cells ranging from 0.0001 to 0.001 (Table S11). The values of the rest of the code input parameters are shown in Table S5 and Table S11. The total cell category/state populations as a function of time are depicted in Fig. S22. Fig. S21 depicts the doubling time as a function of the cell cycle duration. We observe that the necrosis rate of the differentiated cells does not affect the doubling time in the value range considered.

Table S11

Execution	$\mathbf{T_c}$	$\mathbf{P_{sleep}}$	$\mathbf{P_{sym}}$	P_{G0toG1}	R_A	R_{ADiff}	R_{NDiff}
A	60	0.2	0.5	0.01	0.001	0.001	0.0001
B	60	0.2	0.5	0.01	0.001	0.001	0.0002
C	60	0.2	0.5	0.01	0.001	0.001	0.0003
D	60	0.2	0.5	0.01	0.001	0.001	0.0004
E	60	0.2	0.5	0.01	0.001	0.001	0.0005
F	60	0.2	0.5	0.01	0.001	0.001	0.0006
G	60	0.2	0.5	0.01	0.001	0.001	0.0007
H	60	0.2	0.5	0.01	0.001	0.001	0.0008
I	60	0.2	0.5	0.01	0.001	0.001	0.0009
J	60	0.2	0.5	0.01	0.001	0.001	0.001

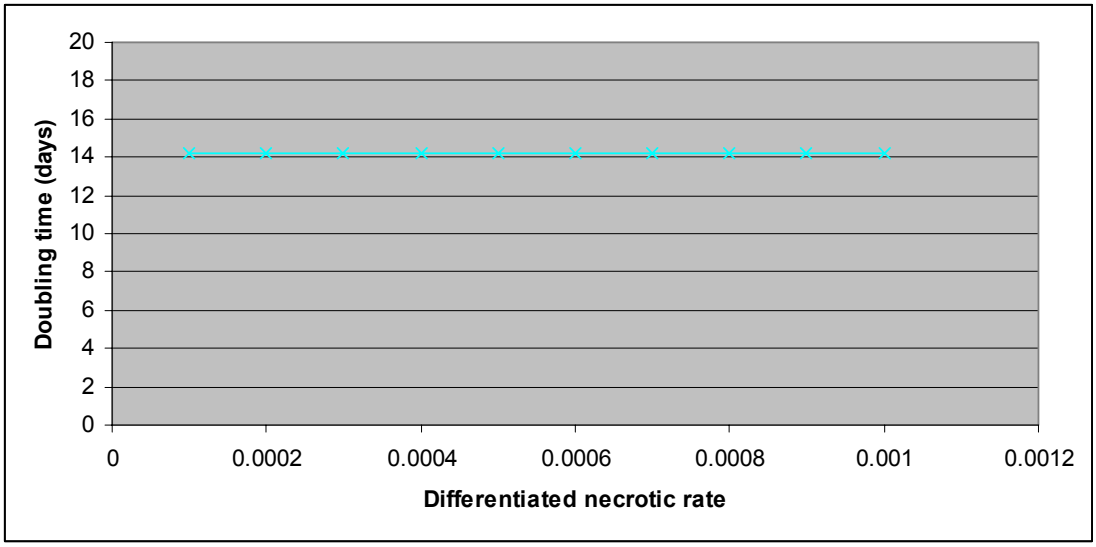

Fig. S21

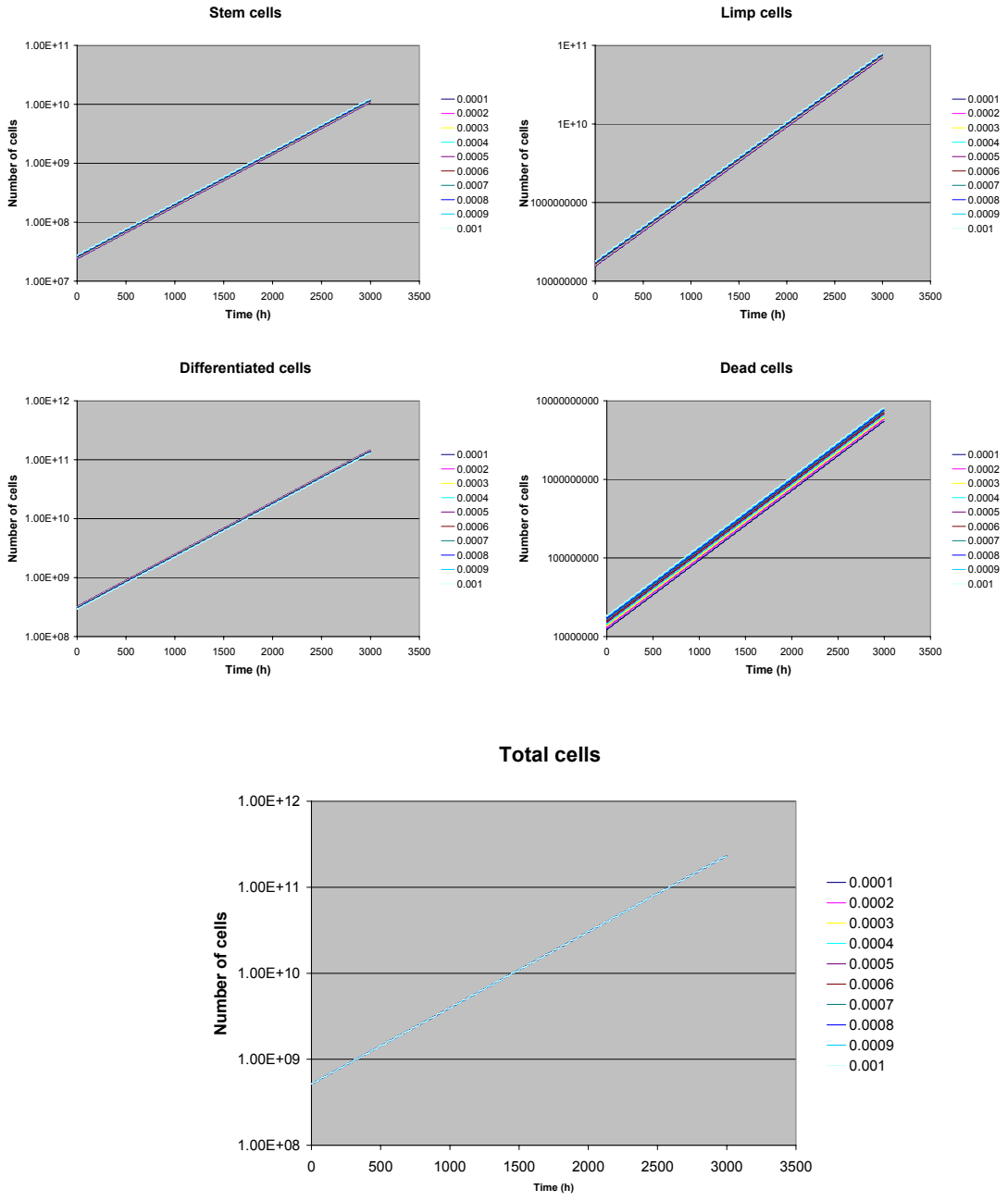
Stem cells
Number of cells
Time (h)
Limp cells
Number of cells
Time (h)
Differentiated cells
Number of cells
Time (h)
Dead cells
Number of cells
Time (h)
Total cells
Number of cells
Time (h)
0.0001
0.0002
0.0003
0.0004
0.0005
0.0006
0.0007
0.0008
0.0009
0.001

Fig. S22

5.2.3 The cell category/state transition rates – cell category/state relative populations nomogram

If we initialize the geometrical cells of the discretizing mesh with totally arbitrary values of the various tumour cell categories [dormant, stem cells, proliferating progenitor cells, etc], it is very likely to observe peculiar free growth behaviour i.e. an unexpected (abnormal) decrease of its volume, followed by a volume increase. In order to avoid such behaviour the concept of tumour cell division properties - tumor cell categories population nomogram has been introduced. Fig. S23 shows the outcome of two simulations performed with the same transition percentages and cell cycle durations (Table S12) but with different initial populations of the distinct cell types (stem, progenitor, differentiated and dead cells).

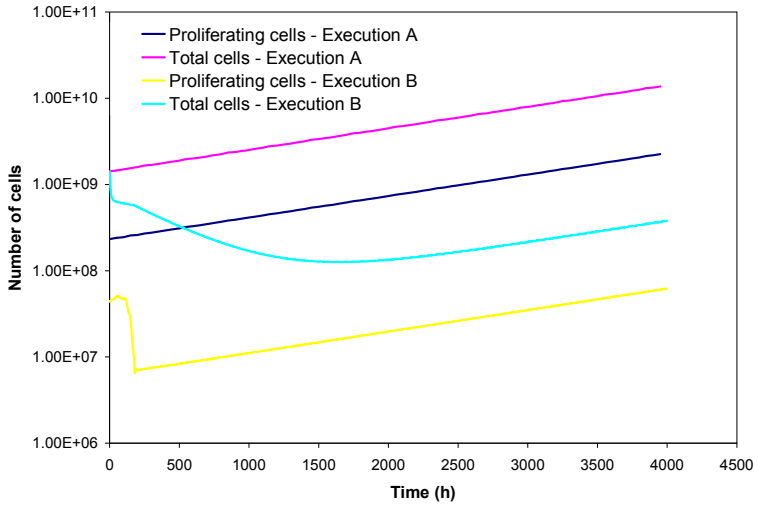

Fig. S23

Therefore, a number of exploratory simulation executions have been performed in order to determine the initial percentages of the various populations as they are regulated by different transition probabilities and cell cycle durations. The "few initial stem cell method" has been used to calculate the relative cell category/state populations. The effect of each code parameter on several cell category/state relative populations is examined below.

Table S12

Symbol	Description	Value
T_c	Cell cycle duration	60h
T_{G1}	Duration of Gap 1 phase	$0.41(T_c - T_M)$
T_S	Duration of DNA synthesis phase	$0.41(T_c - T_M)$
T_{G2}	Duration of Gap 2 phase	$0.18(T_c - T_M)$
T_M	Duration of mitosis phase	1h
T_{G0}	Duration of dormant phase	96h

T_N	Time period needed for necrosis' products to disappear from the tumour	20h
T_A	Time duration needed for apoptosis products to be removed from the tumour	6h
N_{LIMP}	Number of mitosis performed by progenitor cells before they become differentiated	3
R_A	Apoptosis rate of cancer cells	0.001
R_{NDiff}	Necrotic rate of differentiated cells	0.001
R_{ADiff}	Apoptosis rate of differentiated cells	0.001
P_{G0toG1}	Fraction of dormant cells that re-enter cell cycle	0.01
P_{sleep}	Fraction of cells that enter G0 phase following mitosis	0.1
P_{sym}	Fraction of stem cells that perform symmetric division	0.18

5.2.3.1 Sleeping fraction

A number of code executions have been performed with variable sleeping fraction ranging from 0 to 0.35 for values of the cell cycle duration i.e. 30h, 60h and 90h. The values of the code input parameters considered are included in Table S13. Fig. S24 presents the variation of the relative population of the various cell categories (fraction of the total cells) as a function of the sleeping fraction for variable cell cycle duration. The relevant values are given in Table S14. The yellow area in Table S14 corresponds to a combination of the model parameters that leads to a non self-conservative tumour i.e. a tumour that shrinks by itself and therefore usually cannot exist.

Table S13

Symbol	Description	Value
T_c	Cell cycle duration	30h, 60h, 90h
T_{G1}	Duration of Gap 1 phase	$0.41(T_c - T_M)$
T_S	Duration of DNA synthesis phase	$0.41(T_c - T_M)$
T_{G2}	Duration of Gap 2 phase	$0.18(T_c - T_M)$
T_M	Duration of mitosis phase	1h
T_{G0}	Duration of dormant phase	96h
T_N	Time period needed for necrosis' products to disappear from the tumour	20h
T_A	Time duration needed for apoptosis products to be	6h

	removed from the tumour	
N_{LIMP}	Number of mitosis performed by progenitor cells before they become differentiated	7
R_A	Apoptosis rate of cancer cells	0.001
R_{NDiff}	Necrotic rate of differentiated cells	0.001
R_{ADiff}	Apoptosis rate of differentiated cells	0.001
P_{G0toG1}	Fraction of dormant cells that re-enter cell cycle	0.01
P_{sleep}	Fraction of cells that enter G0 phase following mitosis	0-0.35
P_{sym}	Fraction of stem cells that perform symmetric division	0.7

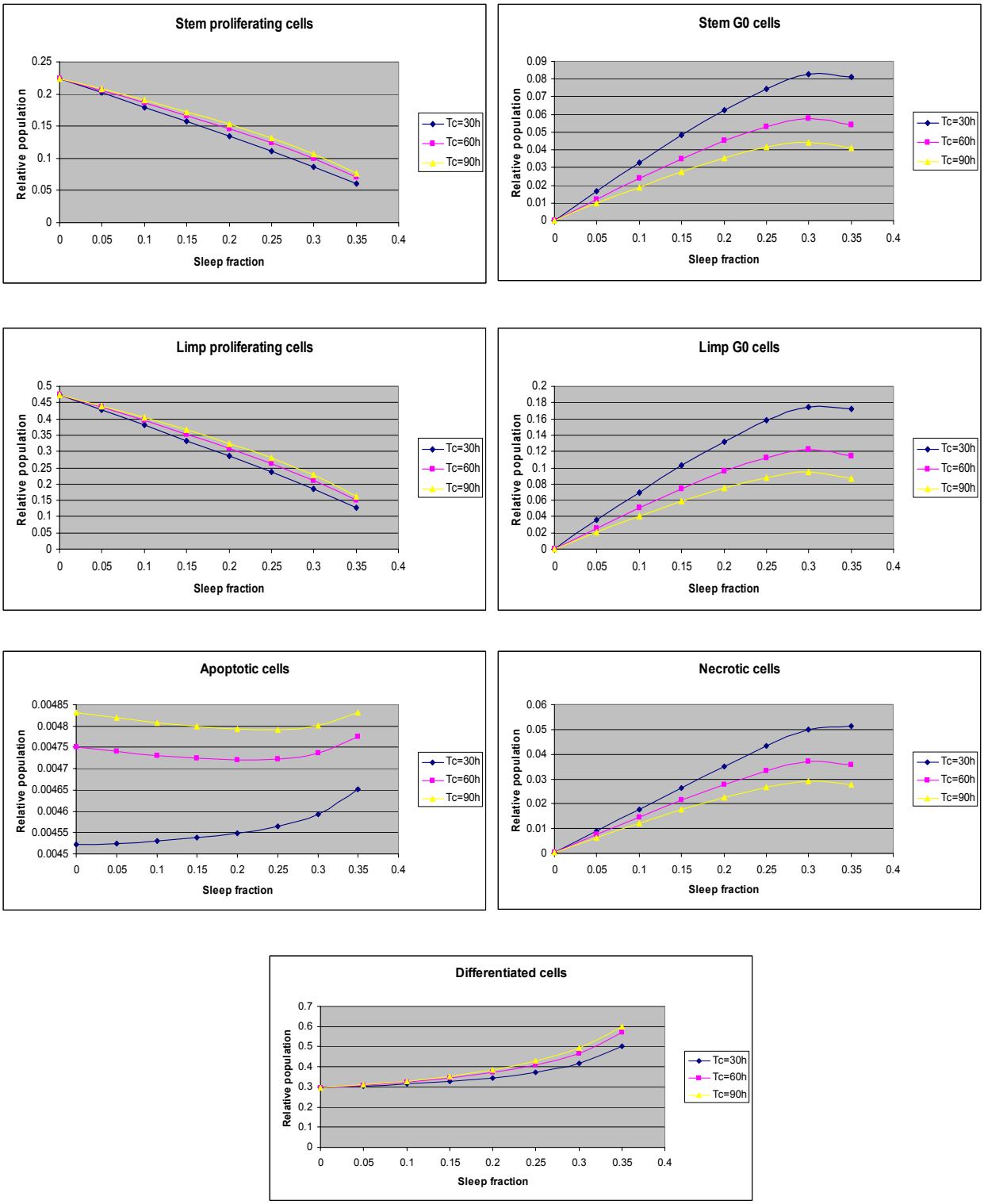
Stem proliferating cells
Relative population
Sleep fraction
Tc=30h
Tc=60h
Tc=90h
Stem G0 cells
Relative population
Sleep fraction
Tc=30h
Tc=60h
Tc=90h
Limp proliferating cells
Relative population
Sleep fraction
Tc=30h
Tc=60h
Tc=90h
Limp G0 cells
Relative population
Sleep fraction
Tc=30h
Tc=60h
Tc=90h
Apoptotic cells
Relative population
Sleep fraction
Tc=30h
Tc=60h
Tc=90h
Necrotic cells
Relative population
Sleep fraction
Tc=30h
Tc=60h
Tc=90h
Differentiated cells
Relative population
Sleep fraction
Tc=30h
Tc=60h
Tc=90h

Fig. S24

Table S14

Tc	P_{sleep}	Stem proliferating	Stem G0	Limp proliferating	Limp G0	Differentiated	Apoptotic	Necrotic
30	0	0.223669	0	0.4740375	0	0.297349	0.00452232	0.000422709
	0.05	0.201758	0.016746	0.4276003	0.03549105	0.304941	0.00452449	0.00893892
	0.1	0.179679	0.0329362	0.3808065	0.06980424	0.314619	0.00452969	0.0176256
	0.15	0.157379	0.04831	0.3335443	0.10238699	0.327436	0.00453748	0.0264069
	0.2	0.134747	0.0624399	0.2855783	0.1323335	0.345262	0.00454789	0.0350919
	0.25	0.111571	0.0744685	0.2364605	0.1578266	0.371846	0.00456464	0.0432636
	0.3	0.0873257	0.082519	0.1850758	0.1748889	0.415775	0.00459306	0.0498225
	0.35	0.0604405	0.0812109	0.1280961	0.1721163	0.502131	0.0046513	0.0513535
	0.4							
60	0	0.223977	0	0.4746913	0	0.296095	0.00475012	0.000485682
	0.05	0.205497	0.0122149	0.435526	0.02588786	0.308602	0.00474003	0.00753224
	0.1	0.186509	0.0239818	0.3952817	0.05082635	0.324132	0.00473103	0.014538
	0.15	0.166852	0.0350676	0.3536224	0.07432132	0.344041	0.00472366	0.0213718
	0.2	0.146287	0.0450293	0.310037	0.095434	0.370694	0.00472002	0.0277984
	0.25	0.124339	0.0530845	0.2635207	0.11250606	0.408487	0.00472232	0.033341
	0.3	0.100021	0.0575665	0.2119823	0.1220048	0.466741	0.0047362	0.0369483
	0.35	0.0708152	0.0542682	0.1500841	0.11501464	0.56918	0.00477571	0.0358623
	0.4							
90	0	0.224325	0	0.4754287	0	0.294905	0.00483165	0.000509904
	0.05	0.207911	0.00962613	0.4406424	0.02040138	0.310269	0.00481938	0.00633009
	0.1	0.190758	0.0188969	0.4042885	0.04004962	0.329137	0.00480821	0.0120617
	0.15	0.172651	0.027589	0.3659118	0.0584715	0.353	0.00479893	0.0175779
	0.2	0.153238	0.0353229	0.3247696	0.07486267	0.384361	0.00479285	0.0226531
	0.25	0.131897	0.0414081	0.2795398	0.08775916	0.427744	0.0047922	0.0268587
	0.3	0.107378	0.0444609	0.2275733	0.0942294	0.492255	0.00480152	0.0293025
	0.35	0.0767626	0.0411816	0.1626886	0.08727925	0.599429	0.00483201	0.0278272
	0.4							

5.2.3.2 Symmetric division fraction

A number of code executions have been performed with variable symmetric division fraction ranging from 0.3 to 1 for three values of the cell cycle duration 30h, 60h and 90h. The values of the code input parameters are included in Table S15. Fig. 25 depicts the variation of the relative populations of the various cell categories/states (fraction of total cells) as a function of the symmetric division fraction for variable cell cycle duration. Table S16 contains the corresponding parameter values.

Table S15

Symbol	Description	Value
T_c	Cell cycle duration	30h, 60h, 90h
T_{G1}	Duration of Gap 1 phase	$0.41(T_c - T_M)$
T_S	Duration of DNA synthesis phase	$0.41(T_c - T_M)$
T_{G2}	Duration of Gap 2 phase	$0.18(T_c - T_M)$
T_M	Duration of mitosis phase	1h
T_{G0}	Duration of dormant phase	96h
T_N	Time period needed for necrosis' products to disappear from the tumour	20h
T_A	Time duration needed for apoptosis products to be removed from the tumour	6h
N_{LIMP}	Number of mitosis performed by progenitor cells before they become differentiated	7
R_A	Apoptosis rate of cancer cells	0.001
R_{NDiff}	Necrotic rate of differentiated cells	0.0001
R_{ADiff}	Apoptosis rate of differentiated cells	0.001
P_{G0toG1}	Fraction of dormant cells that re-enter cell cycle	0.01
P_{sleep}	Fraction of cells that enter G0 phase following mitosis	0.2
P_{sym}	Fraction of stem cells that perform symmetric division	0.3-1

According to Table S16 and Figure S25 an increase in the parameter P_{sym} leads to an increase in the fraction of the stem cells in the tumour (which is reasonable as more stem cells are produced during mitoses) and a decrease in the differentiated cells as less cells follow the path to differentiation. On the other hand the fraction of progenitor (or limp i.e. Limited Mitotic Potential) cells exhibits an initial increase, reaches a maximum and then decreases with a small variation between the minimum and the maximum values. Limp cells derive from the asymmetric division of stem cells and their population depends on the product of two competitive factors: the number of stem cells and the asymmetric division fraction. The combination of these two factors leads to the observed behaviour of the limp

cell relative population (fraction) in the tumour as a function of the symmetric division fraction.

An increase of T_c leads to an increase of the stem and limp cell category populations as they live for a longer period and a decrease in the differentiated and dead cells.

Finally the yellow area in Table S16 corresponds to a combination of the model parameters that leads to a non self-conservative tumour i.e. a tumour that shrinks by itself and therefore cannot exist.

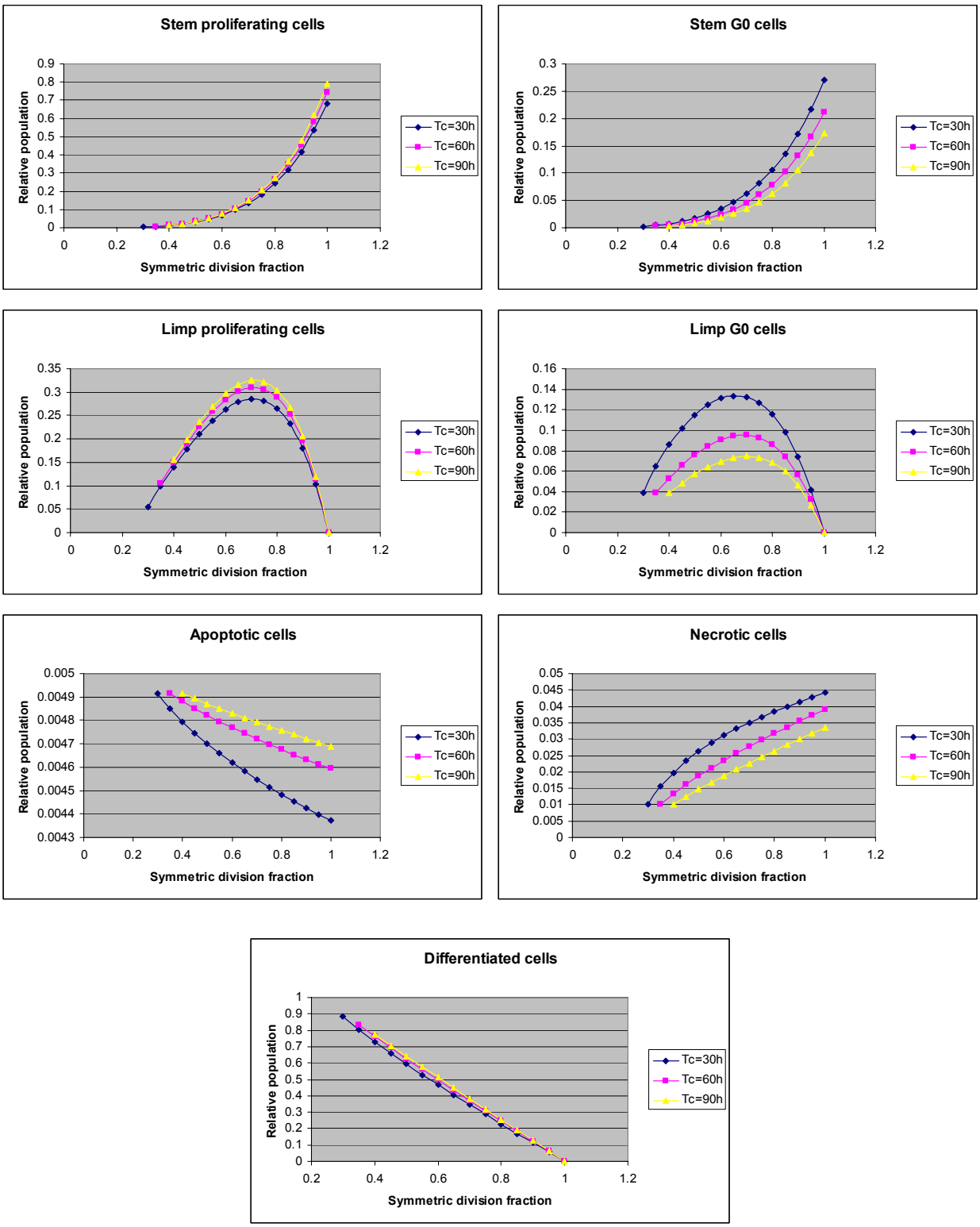
Stem proliferating cells
Relative population
Symmetric division fraction
Tc=30h
Tc=60h
Tc=90h
Stem G0 cells
Relative population
Symmetric division fraction
Tc=30h
Tc=60h
Tc=90h
Limp proliferating cells
Relative population
Symmetric division fraction
Tc=30h
Tc=60h
Tc=90h
Limp G0 cells
Relative population
Symmetric division fraction
Tc=30h
Tc=60h
Tc=90h
Apoptotic cells
Relative population
Symmetric division fraction
Tc=30h
Tc=60h
Tc=90h
Necrotic cells
Relative population
Symmetric division fraction
Tc=30h
Tc=60h
Tc=90h
Differentiated cells
Relative population
Symmetric division fraction
Tc=30h
Tc=60h
Tc=90h

Fig. S25

Table S16 Nomogram - Relative populations

Tc	P_{sym}	Stem proliferating	Stem G0	Limp proliferating	Limp G0	Differentiated	Apoptotic	Necrotic
30	0.3	0.00281668	0.00200672	0.05464051	0.03892814	0.886554	0.00491353	0.0101408
	0.35	0.00674112	0.00442644	0.09884467	0.06490462	0.804737	0.00485079	0.0154958
	0.4	0.0125455	0.00767981	0.13978981	0.08557346	0.729861	0.00479556	0.0197549
	0.45	0.0208627	0.0120143	0.17729215	0.10209815	0.659719	0.00474593	0.0232678
	0.5	0.0324795	0.017726	0.210842	0.11506911	0.592933	0.00470046	0.026249
	0.55	0.048365	0.0251656	0.2396527	0.1246976	0.52862	0.00465855	0.0288408
	0.6	0.0697011	0.0347542	0.2626596	0.13096664	0.466163	0.00461925	0.031136
	0.65	0.0979219	0.0469823	0.2785236	0.13363384	0.405151	0.00458266	0.033205
	0.7	0.134747	0.0624386	0.2855797	0.1323307	0.345263	0.00454797	0.0350927
	0.75	0.182227	0.0818143	0.2818146	0.1265257	0.286271	0.00451475	0.036832
	0.8	0.242809	0.105888	0.2648438	0.1154979	0.228017	0.0044838	0.0384609
	0.85	0.31935	0.135613	0.2318063	0.0984369	0.170352	0.00445385	0.0399877
	0.9	0.415219	0.172056	0.1793633	0.07432371	0.11318	0.00442512	0.0414321
	0.95	0.534347	0.216448	0.1036094	0.04196918	0.0564182	0.00439774	0.0428105
	1	0.681285	0.270212	0	0	0	0.00437144	0.0441314
60	0.3							
	0.35	0.00723017	0.00263772	0.10601559	0.03867672	0.830399	0.00491541	0.0101257
	0.4	0.0134448	0.00475025	0.14981053	0.05293039	0.760948	0.0048824	0.0132337
	0.45	0.0224024	0.00769028	0.19037688	0.06535234	0.693247	0.00485153	0.0160793
	0.5	0.0349639	0.0116939	0.2269697	0.07591169	0.626924	0.00482248	0.0187139
	0.55	0.0521916	0.0170482	0.258614	0.08447549	0.561699	0.00479499	0.0211765
	0.6	0.0753846	0.0240993	0.2840772	0.0908153	0.497358	0.00476884	0.0234966
	0.65	0.106118	0.0332622	0.3018358	0.09460917	0.433733	0.0047439	0.0256978
	0.7	0.146288	0.0450267	0.31004	0.09542849	0.370697	0.00472008	0.0277989
	0.75	0.198156	0.0599846	0.3064487	0.09276612	0.308134	0.00469703	0.0298129
	0.8	0.264407	0.078824	0.2884021	0.08597727	0.245962	0.00467483	0.0317527
	0.85	0.348225	0.102327	0.2527657	0.07427589	0.184122	0.00465363	0.0336309
	0.9	0.453309	0.131462	0.1958169	0.05678804	0.122542	0.00463282	0.0354501

	0.95	0.584057	0.167241	0.1132482	0.03242784	0.0611855	0.00461323	0.0372274
	1	0.745452	0.210997	0	0	0	0.00459382	0.0389569
90	0.3							
	0.35							
	0.4	0.0140016	0.00347796	0.15601543	0.03875371	0.772621	0.00491601	0.0102138
	0.45	0.0233095	0.00570105	0.19808504	0.04844771	0.707094	0.00489349	0.0124696
	0.5	0.0364018	0.00878008	0.236304	0.05699631	0.642009	0.00487184	0.0146366
	0.55	0.0544066	0.0129551	0.2695894	0.06419349	0.577276	0.00485107	0.0167282
	0.6	0.0787043	0.0185226	0.2965871	0.06980013	0.512799	0.004831	0.0187557
	0.65	0.110975	0.025835	0.3156503	0.07348372	0.448517	0.00481165	0.0207281
	0.7	0.153242	0.035317	0.3247769	0.07484984	0.384368	0.00479293	0.0226529
	0.75	0.207922	0.0474849	0.3215516	0.07343536	0.320295	0.00477467	0.0245367
	0.8	0.277891	0.0629425	0.3031101	0.06865463	0.256261	0.00475678	0.0263841
	0.85	0.366583	0.0823539	0.2660912	0.05977814	0.192254	0.00473963	0.0282001
	0.9	0.477952	0.106607	0.2064623	0.04605121	0.128216	0.00472271	0.0299887
	0.95	0.616751	0.136575	0.1195876	0.0264818	0.0641438	0.00470651	0.0317542
	1	0.788322	0.173492	0	0	0	0.0046902	0.0334958

5.2.3.3 G0 to G1 fraction

A number of executions have been performed with variable G0 to G1 fraction ranging from 0 to 0.01 for three values of the cell cycle duration i.e. 30h, 60h and 90h. The values of the code input parameters are presented in Table S17. Fig. S26 depicts the variation of the relative population of the various cell categories (fraction of the total cells) as a function of the G0 to G1 fraction for variable cell cycle duration. Table S18 contains the corresponding parameter values.

Table S17

Symbol	Description	Value
T_c	Cell cycle duration	30h, 60h, 90h
T_{G1}	Duration of Gap 1 phase	$0.41(T_c - T_M)$
T_S	Duration of DNA synthesis phase	$0.41(T_c - T_M)$
T_{G2}	Duration of Gap 2 phase	$0.18(T_c - T_M)$
T_M	Duration of mitosis phase	1h
T_{G0}	Duration of dormant phase	96h
T_N	Time period needed for necrosis' products to disappear from the tumour	20h
T_A	Time duration needed for apoptosis products to be removed from the tumour	6h
N_{LIMP}	Number of mitosis performed by progenitor cells before they become differentiated	7
R_A	Apoptosis rate of cancer cells	0.001
R_{NDiff}	Necrotic rate of differentiated cells	0.001
R_{ADiff}	Apoptosis rate of differentiated cells	0.001
P_{G0toG1}	Fraction of dormant cells that re-enter cell cycle	0-0.01
P_{sleep}	Fraction of cells that enter G0 phase following mitosis	0.2
P_{sym}	Fraction of stem cells that perform symmetric division	0.5

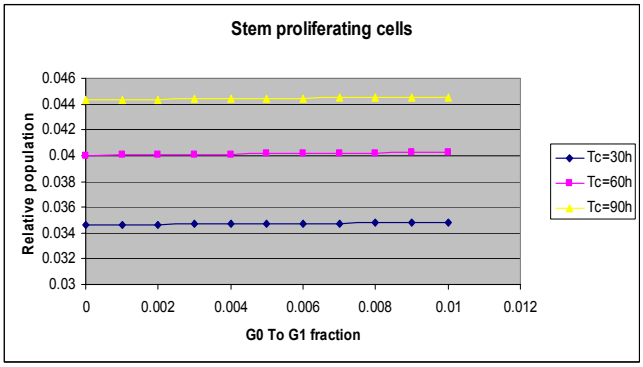
Stem proliferating cells
Relative population
0.046
0.044
0.042
0.04
0.038
0.036
0.034
0.032
0.03
0
0.002
0.004
0.006
0.008
0.01
0.012
G0 To G1 fraction
Tc=30h
Tc=60h
Tc=90h

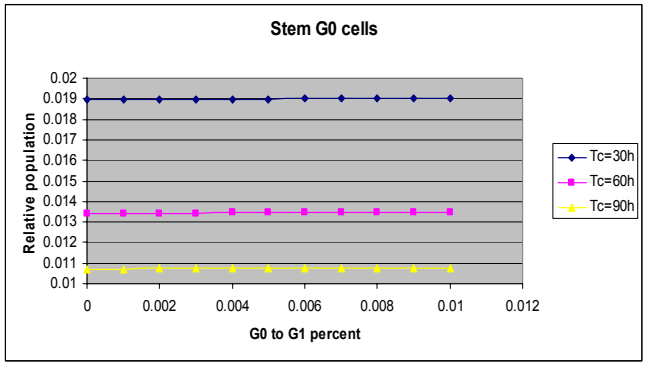
Stem G0 cells
Relative population
0.02
0.019
0.018
0.017
0.016
0.015
0.014
0.013
0.012
0.011
0.01
0
0.002
0.004
0.006
0.008
0.01
0.012
G0 to G1 percent
Tc=30h
Tc=60h
Tc=90h

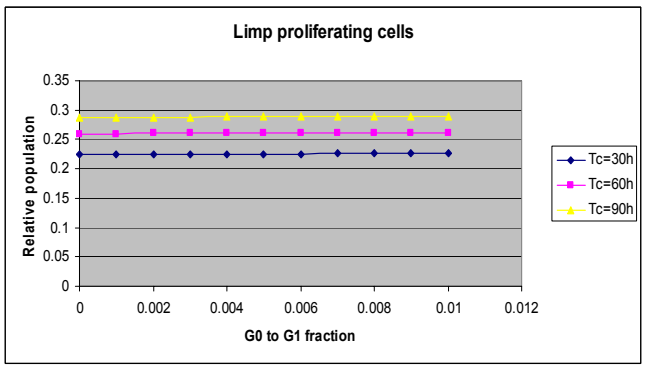
Limp proliferating cells
Relative population
0.35
0.3
0.25
0.2
0.15
0.1
0.05
0
0
0.002
0.004
0.006
0.008
0.01
0.012
G0 to G1 fraction
Tc=30h
Tc=60h
Tc=90h

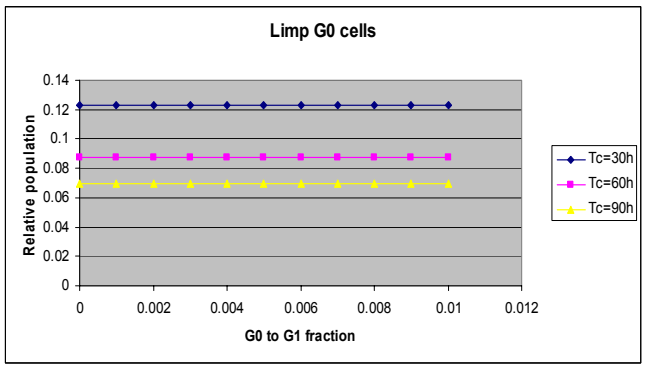
Limp G0 cells
Relative population
0.14
0.12
0.1
0.08
0.06
0.04
0.02
0
0
0.002
0.004
0.006
0.008
0.01
0.012
G0 to G1 fraction
Tc=30h
Tc=60h
Tc=90h

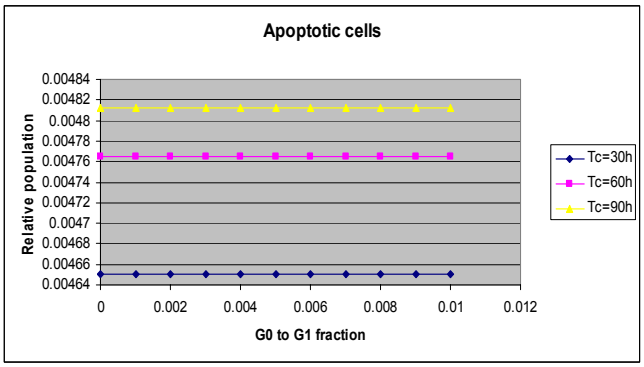
Apoptotic cells
Relative population
0.00484
0.00482
0.0048
0.00478
0.00476
0.00474
0.00472
0.0047
0.00468
0.00466
0.00464
0
0.002
0.004
0.006
0.008
0.01
0.012
G0 to G1 fraction
Tc=30h
Tc=60h
Tc=90h

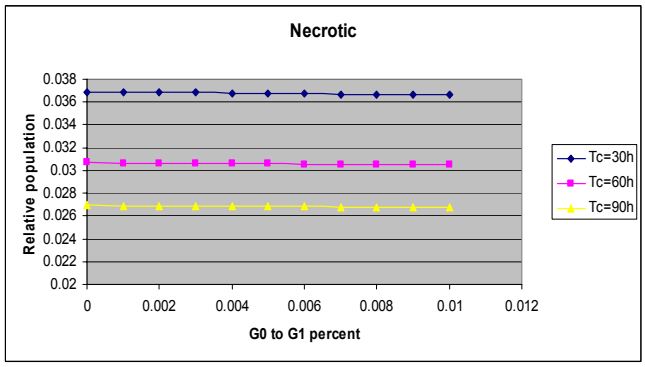
Necrotic
Relative population
0.038
0.036
0.034
0.032
0.03
0.028
0.026
0.024
0.022
0.02
0
0.002
0.004
0.006
0.008
0.01
0.012
G0 to G1 percent
Tc=30h
Tc=60h
Tc=90h

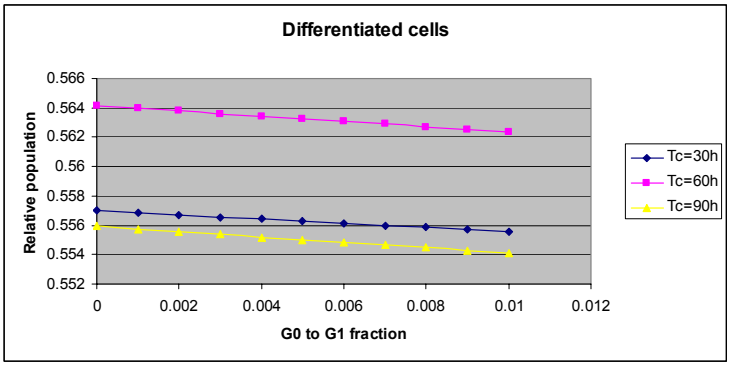
Differentiated cells
Relative population
0.566
0.564
0.562
0.56
0.558
0.556
0.554
0.552
0
0.002
0.004
0.006
0.008
0.01
0.012
G0 to G1 fraction
Tc=30h
Tc=60h
Tc=90h

Fig. S26

Table S18

Tc	P_{G0toG1}	Stem proliferating	Stem G0	Limp proliferating	Limp G0	Differentiated	Apoptotic	Necrotic
30	0	0.0346198	0.0189681	0.2247358	0.12313206	0.557	0.00465069	0.0368929
	0.001	0.0346392	0.0189721	0.2248621	0.12315819	0.556855	0.00465057	0.0368632
	0.002	0.0346588	0.0189756	0.2249892	0.12318114	0.55671	0.00465053	0.0368342
	0.003	0.0346789	0.0189779	0.2251195	0.123196	0.55657	0.00465066	0.0368071
	0.004	0.0346983	0.0189819	0.2252454	0.1232218	0.556425	0.00465053	0.0367773
	0.005	0.0347181	0.0189848	0.2253739	0.12324056	0.556283	0.00465059	0.0367493
	0.006	0.0347374	0.0189888	0.2254989	0.1232667	0.556138	0.00465046	0.0367196
	0.007	0.0347572	0.0189914	0.225628	0.1232836	0.555997	0.00465054	0.0366919
	0.008	0.034777	0.0189943	0.2257562	0.12330257	0.555856	0.00465057	0.0366635
	0.009	0.0347962	0.0189982	0.2258812	0.12332781	0.555712	0.00465047	0.036634
	0.01	0.0348161	0.0190007	0.2260101	0.12334382	0.555572	0.00465057	0.0366065
60	0	0.0400202	0.0134283	0.2597928	0.08717022	0.56414	0.00476465	0.0306839
	0.001	0.040043	0.0134325	0.2599407	0.08719747	0.563959	0.00476463	0.0306631
	0.002	0.0400663	0.0134356	0.2600921	0.08721788	0.563781	0.00476465	0.0306427
	0.003	0.0400895	0.013439	0.2602424	0.08723992	0.563602	0.00476464	0.0306222
	0.004	0.0401128	0.013442	0.260394	0.08725968	0.563425	0.00476467	0.0306018
	0.005	0.040136	0.0134453	0.2605445	0.087281	0.563247	0.0047647	0.0305814
	0.006	0.0401587	0.0134495	0.2606917	0.08730776	0.563067	0.00476466	0.0305604
	0.007	0.0401821	0.0134523	0.2608435	0.08732639	0.562891	0.00476467	0.0305399
	0.008	0.0402052	0.0134555	0.2609937	0.08734704	0.562714	0.00476469	0.0305195
	0.009	0.0402283	0.0134587	0.2611436	0.08736759	0.562538	0.00476472	0.0304992
	0.01	0.0402514	0.0134619	0.2612936	0.08738863	0.562361	0.00476472	0.0304785
90	0	0.044322	0.010718	0.2877178	0.06957609	0.555929	0.00481184	0.0269254
	0.001	0.0443463	0.0107201	0.2878757	0.06959017	0.555747	0.00481188	0.0269087
	0.002	0.0443697	0.0107236	0.2880279	0.06961253	0.555563	0.00481186	0.0268916
	0.003	0.0443929	0.0107273	0.2881786	0.06963661	0.555378	0.00481186	0.026875
	0.004	0.0444169	0.0107299	0.2883339	0.06965356	0.555196	0.00481188	0.0268582
	0.005	0.0444404	0.010733	0.2884869	0.06967397	0.555013	0.00481188	0.0268413

	0.006	0.0444644	0.0107355	0.2886426	0.06968999	0.554831	0.00481191	0.0268245
	0.007	0.0444884	0.0107379	0.2887984	0.0697053	0.55465	0.00481194	0.0268076
	0.008	0.0445122	0.0107406	0.2889527	0.06972297	0.554469	0.00481196	0.0267908
	0.009	0.0445353	0.0107443	0.2891025	0.06974696	0.554285	0.00481194	0.0267739
	0.01	0.0445594	0.0107463	0.2892593	0.06976019	0.554106	0.00481198	0.0267571

5.2.3.4 Apoptosis rate

A number of code executions have been performed with variable apoptosis rate ranging from 0 to 0.01 for three values of the cell cycle duration i.e. 30h, 60h and 90h. The values of the code input parameters are included in Table S19. Fig.S27 depicts the variation of the relative populations of the various cell categories/states (fraction of the total cells) as a function of the apoptosis rate for variable cell cycle duration. Table S20 included the corresponding model parameter values.

Table S19

Symbol	Description	Value
T_c	Cell cycle duration	30h, 60h, 90h
T_{G1}	Duration of Gap 1 phase	$0.41(T_c - T_M)$
T_S	Duration of DNA synthesis phase	$0.41(T_c - T_M)$
T_{G2}	Duration of Gap 2 phase	$0.18(T_c - T_M)$
T_M	Duration of mitosis phase	1h
T_{G0}	Duration of dormant phase	96h
T_N	Time period needed for necrosis' products to disappear from the tumour	20h
T_A	Time duration needed for apoptosis products to be removed from the tumour	6h
N_{LIMP}	Number of mitosis performed by progenitor cells before they become differentiated	7
R_A	Apoptosis rate of cancer cells	0-0.001
R_{NDiff}	Necrotic rate of differentiated cells	0.001
R_{ADiff}	Apoptosis rate of differentiated cells	0-0.001
P_{G0toG1}	Fraction of dormant cells that re-enter cell cycle	0.01
P_{sleep}	Fraction of cells that enter G0 phase following mitosis	0.2
P_{sym}	Fraction of stem cells that perform symmetric division	0.5

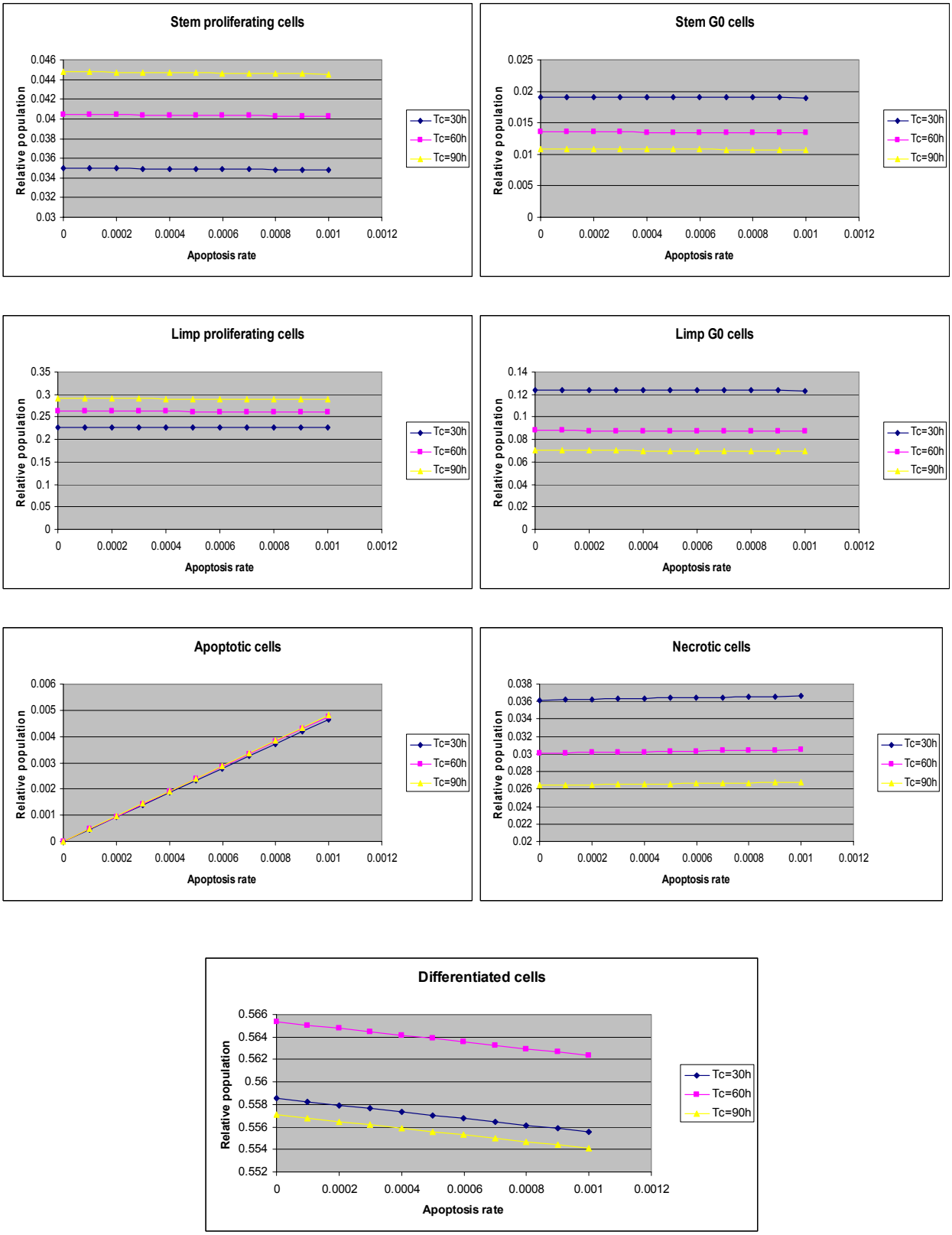
Stem proliferating cells
Relative population
Apoptosis rate
Tc=30h
Tc=60h
Tc=90h
Stem G0 cells
Limp proliferating cells
Limp G0 cells
Apoptotic cells
Necrotic cells
Differentiated cells

Fig. S27

Table S20

Tc	R_{apop}	Stem proliferating	Stem G0	Limp proliferating	Limp G0	Differentiated	Apoptotic	Necrotic
30	0	0.035001	0.019101	0.227209	0.123995	0.558517	0	0.036178
	0.0001	0.034982	0.019092	0.227086	0.123937	0.55822	0.000465	0.036218
	0.0002	0.034964	0.019081	0.226968	0.123868	0.557928	0.00093	0.036262
	0.0003	0.034945	0.019072	0.226848	0.123804	0.557633	0.001395	0.036304
	0.0004	0.034927	0.019061	0.226729	0.123737	0.55734	0.00186	0.036347
	0.0005	0.034909	0.019051	0.22661	0.123669	0.557046	0.002325	0.03639
	0.0006	0.03489	0.019041	0.22649	0.123606	0.556751	0.00279	0.036433
	0.0007	0.034871	0.019032	0.226368	0.123545	0.556454	0.003255	0.036475
	0.0008	0.034853	0.019021	0.22625	0.123476	0.556162	0.00372	0.036519
	0.0009	0.034834	0.019011	0.226129	0.123413	0.555866	0.004185	0.036562
	0.001	0.034816	0.019001	0.22601	0.123344	0.555572	0.004651	0.036607
60	0	0.040466	0.013534	0.262687	0.087858	0.565363	0	0.030092
	0.0001	0.040445	0.013527	0.262549	0.087808	0.565064	0.000476	0.03013
	0.0002	0.040424	0.013519	0.262413	0.087756	0.564767	0.000953	0.030169
	0.0003	0.040402	0.013513	0.26227	0.087717	0.564463	0.001429	0.030206
	0.0004	0.04038	0.013505	0.262131	0.087669	0.564164	0.001905	0.030245
	0.0005	0.040359	0.013498	0.261993	0.08762	0.563865	0.002382	0.030284
	0.0006	0.040337	0.013491	0.26185	0.08758	0.563562	0.002858	0.030322
	0.0007	0.040316	0.013484	0.26171	0.087533	0.563262	0.003335	0.030361
	0.0008	0.040294	0.013477	0.261572	0.087483	0.562962	0.003811	0.0304
	0.0009	0.040274	0.013468	0.261438	0.087428	0.562664	0.004288	0.03044
	0.001	0.040251	0.013462	0.261293	0.087389	0.562361	0.004765	0.030479
90	0	0.044797	0.010804	0.2908	0.070133	0.557058	0	0.026408
	0.0001	0.044773	0.010798	0.290646	0.070096	0.556763	0.000481	0.026442
	0.0002	0.04475	0.010792	0.290495	0.070054	0.55647	0.000962	0.026477
	0.0003	0.044726	0.010787	0.290338	0.070021	0.556174	0.001443	0.026512
	0.0004	0.044702	0.010781	0.290185	0.069984	0.555879	0.001924	0.026546
	0.0005	0.044678	0.010775	0.290031	0.069946	0.555584	0.002405	0.026581
	0.0006	0.044655	0.010769	0.289877	0.069909	0.555288	0.002886	0.026616

	0.0007	0.044631	0.010763	0.289726	0.069867	0.554994	0.003368	0.026651
	0.0008	0.044607	0.010759	0.289565	0.069839	0.554696	0.003849	0.026686
	0.0009	0.044583	0.010752	0.289414	0.069797	0.554402	0.004331	0.026722
	0.001	0.044559	0.010747	0.289258	0.069763	0.554105	0.004812	0.026757

5.2.3.5 Necrosis rate of differentiated cells

A number of code executions have been performed with a variable necrosis rate of the differentiated cells ranging from 0 to 0.001 for three values of the cell cycle duration i.e. 30h, 60h and 90h. The values of the code input parameters are reported in Table S21. Fig. S28 depicts the variation of the relative populations of the various cell categories/states (fraction of total cells) as a function of the necrosis rate of the differentiated cells for a variable cell cycle duration. Table S22 contains the corresponding parameter values.

Table S21

Symbol	Description	Value
T_c	Cell cycle duration	30h, 60h, 90h
T_{G1}	Duration of Gap 1 phase	$0.41(T_c - T_M)$
T_S	Duration of DNA synthesis phase	$0.41(T_c - T_M)$
T_{G2}	Duration of Gap 2 phase	$0.18(T_c - T_M)$
T_M	Duration of mitosis phase	1h
T_{G0}	Duration of dormant phase	96h
T_N	Time period needed for necrosis' products to disappear from the tumour	20h
T_A	Time duration needed for apoptosis products to be removed from the tumour	6h
N_{LIMP}	Number of mitosis performed by progenitor cells before they become differentiated	7
R_A	Apoptosis rate of cancer cells	0.001
R_{NDiff}	Necrotic rate of differentiated cells	0-0.001
R_{ADiff}	Apoptosis rate of differentiated cells	0.001
P_{G0toG1}	Fraction of dormant cells that re-enter cell cycle	0.01
P_{sleep}	Fraction of cells that enter G0 phase following mitosis	0.2
P_{sym}	Fraction of stem cells that perform symmetric division	0.5

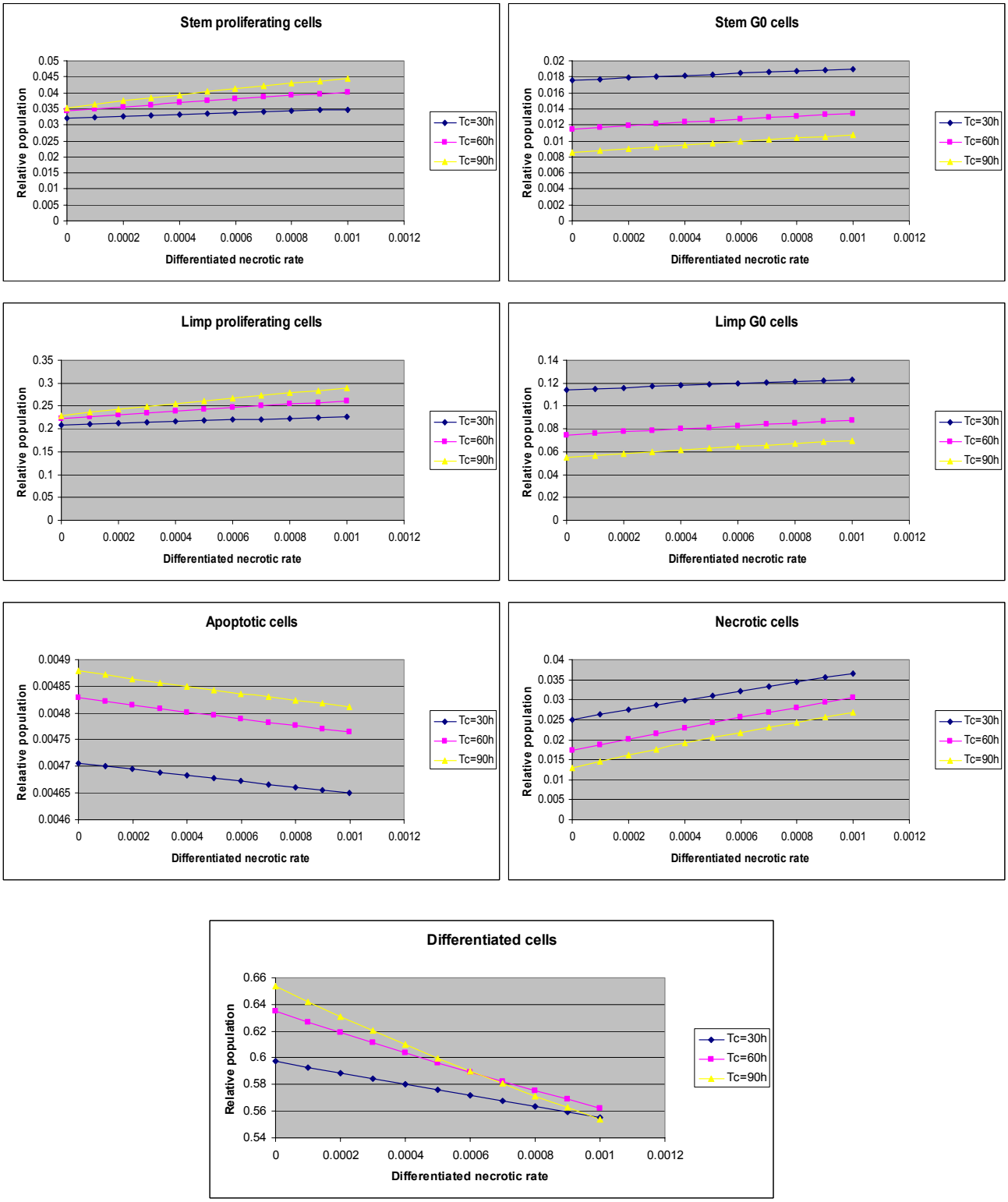
Stem proliferating cells
Relative population
Differentiated necrotic rate
Tc=30h
Tc=60h
Tc=90h
Stem G0 cells
Limp proliferating cells
Limp G0 cells
Apoptotic cells
Relaative population
Necrotic cells
Differentiated cells

Fig. S28

Table S22

Tc	R_{NDiff}	Stem proliferating	Stem G0	Limp proliferating	Limp G0	Differentiated	Apoptotic	Necrotic
30	0	0.0322	0.017574	0.20903	0.11408	0.597397	0.004706	0.025012
	0.0001	0.03248	0.017726	0.210843	0.115068	0.592934	0.004701	0.026249
	0.0002	0.032755	0.017876	0.212628	0.11604	0.588538	0.004695	0.027469
	0.0003	0.033026	0.018023	0.214388	0.116999	0.584206	0.004689	0.02867
	0.0004	0.033293	0.01817	0.216119	0.11795	0.579933	0.004683	0.029853
	0.0005	0.033556	0.018313	0.217829	0.118876	0.575729	0.004678	0.03102
	0.0006	0.033815	0.018454	0.219512	0.119798	0.57158	0.004672	0.032169
	0.0007	0.034071	0.018594	0.221171	0.120705	0.567491	0.004666	0.033302
	0.0008	0.034323	0.018732	0.222807	0.121596	0.563462	0.004661	0.034419
	0.0009	0.034571	0.018867	0.22442	0.122476	0.559489	0.004656	0.035521
	0.001	0.034816	0.019001	0.226009	0.123346	0.555571	0.004651	0.036606
60	0	0.034301	0.011472	0.222664	0.074471	0.635024	0.00483	0.017238
	0.0001	0.034964	0.011693	0.226971	0.075908	0.626927	0.004823	0.018714
	0.0002	0.035611	0.01191	0.231168	0.077314	0.619029	0.004815	0.020153
	0.0003	0.036242	0.01212	0.235263	0.07868	0.61133	0.004809	0.021556
	0.0004	0.036856	0.012327	0.239253	0.080022	0.603815	0.004802	0.022924
	0.0005	0.037457	0.012527	0.243152	0.081317	0.596491	0.004795	0.02426
	0.0006	0.038042	0.012724	0.246952	0.082596	0.589335	0.004789	0.025563
	0.0007	0.038614	0.012915	0.250664	0.083839	0.582351	0.004783	0.026836
	0.0008	0.039172	0.013102	0.254289	0.085051	0.575531	0.004776	0.028078
	0.0009	0.039718	0.013284	0.257833	0.086231	0.568871	0.004771	0.029292
	0.001	0.040251	0.013463	0.261289	0.087396	0.562358	0.004765	0.030478
90	0	0.035333	0.008522	0.229365	0.055323	0.653529	0.00488	0.013048
	0.0001	0.036402	0.00878	0.236304	0.056995	0.64201	0.004872	0.014637
	0.0002	0.037434	0.009029	0.243003	0.05861	0.63089	0.004864	0.01617
	0.0003	0.038431	0.009268	0.249476	0.060167	0.62015	0.004857	0.017651

	0.0004	0.039394	0.009501	0.255728	0.061678	0.609766	0.00485	0.019083
	0.0005	0.040326	0.009726	0.261778	0.063134	0.599727	0.004843	0.020467
	0.0006	0.041228	0.009942	0.267632	0.064542	0.590013	0.004836	0.021807
	0.0007	0.042101	0.010153	0.273298	0.065907	0.580608	0.00483	0.023103
	0.0008	0.042945	0.010358	0.278782	0.067238	0.571494	0.004824	0.024359
	0.0009	0.043765	0.010555	0.284102	0.068517	0.562666	0.004818	0.025577
	0.001	0.044559	0.010747	0.289257	0.069763	0.554105	0.004812	0.026757

5.3 A TOP trial breast cancer case simulation

5.3.1 The TOP trial data considered

The purpose of this section is to report on the initial step towards the clinical validation of the model using real TOP trial data. A set of trial data corresponding to the chemotherapeutic response of one patient with breast cancer that followed the TOP trial protocol has been randomly chosen. A number of exploratory simulations have been performed, by varying the values assigned to the input code parameters in order to find a parameter value set that most effectively fits the clinical data.

The patient selected had a tumour size of

- 17mm before therapy
- 12mm after therapy

Due to non availability of all desirable clinical details at this early phase of the clinical validation process specific assumptions had to be made regarding tumour shape and size and the exact days at which the imaging data was obtained. More specifically:

The data available (till the completion of the preparation of the present deliverable) include the maximum size of the tumour as measured by ultrasound. No MRI data have been provided as yet. Therefore a refined 3D reconstruction of the tumour cannot be made at this stage. Non availability of the three dimensions of the tumour and the exact tumour shape has led us to make the following assumption:

Assumption #1*: The tumour is a homogeneous sphere with a diameter of the given size each time*

Furthermore due to the unavailability of information concerning the exact days at which the tumour was measured both before and after therapy the following assumption has been made:

Assumption #2*: The maximum dimension of the tumour correspond to*

- *2 weeks before the first administration of epirubicin*
- *1 week after the last administration of epirubicin*

The above assumption has been based on the following feedback we received from the TOP trial responsible partner (IJB). TOP trial patients have all pre-treatment investigations including ultrasound examinations done within 4 weeks before the beginning of treatment whereas the post-treatment ultrasound examination is generally performed some weeks after the last treatment session or sometimes at the same time as the last treatment session. The assumed timings correspond approximately to the mean values of the above ranges.

5.3.2 Simulation results

One possible combination of the model input parameter values that successfully simulates the clinical situation i.e. predicts the actual tumour volume shrinkage and satisfies several biological boundary conditions is reported below.

5.3.2.1 Code input parameters

The values assigned to the transition rates, the cell cycle phase durations etc are presented in the following table.

Table S23

Symbol	Description	Value
T_c	Cell cycle duration	60h
T_{G1}	Duration of Gap 1 phase	$0.41(T_c - T_M)$
T_S	Duration of DNA synthesis phase	$0.41(T_c - T_M)$
T_{G2}	Duration of Gap 2 phase	$0.18(T_c - T_M)$
T_M	Duration of mitosis phase	1h
T_{G0}	Duration of dormant phase	96h
T_N	Time period needed for necrosis' products to disappear from the tumour	20h
T_A	Time duration needed for apoptosis products to be removed from the tumour	6h
N_{LIMP}	Number of mitosis performed by progenitor cells before they become differentiated	7
R_A	Apoptosis rate of cancer cells	0.001
R_{NDiff}	Necrotic rate of differentiated cells	0.001
R_{ADiff}	Apoptosis rate of differentiated cells	0.001

P_{G0toG1}	Fraction of dormant cells that re-enter cell cycle	0.01
P_{sleep}	Fraction of cells that enter G0 phase following mitosis	0.1
P_{sym}	Fraction of stem cells that perform symmetric division	0.185

Table S23A provides the parameter values assigned to the module dealing with epirubicin pharmacokinetics and pharmacodynamics

Table S23A.
Parameter values assigned to the model module dealing with epirubicin pharmacokinetics and pharmacodynamics

Symbol	Parameter	Value
D	Dose	100 mg/m^2
V_d	Volume of distribution	480.1L/m^2
k_{12}	Inter-compartmental transfer rate constant	0.1498
k_{21}	Inter-compartmental transfer rate constant	0.7231
k_{13}	Inter-compartmental transfer rate constant	0.1498
k_{31}	Inter-compartmental transfer rate constant	0.7231
k_{el}	Elimination rate constant	0.155h^{-1}
AUC	Area Under Curve	2/3*0.8877mg*h/ L≈ 0.592mg*h/L
SF	Survival fraction	≈ 0.65

5.3.2.2 Population initialization

The tumour is assumed to have a density of 10^6 cells/mm^3. This is the standard assumption made by radiobiologists. Since each cubic geometrical cell (GC) of the mesh occupied by the tumour has a dimension of 1mm x 1mm x 1mm it is initialized with 10^6 cells.

Each GC that belonging to the tumour consists of the following types of cells (percentages have been rounded):

- 0.4% STEM cells of which
  - 86% Proliferative (G1,S,G2,M according to cell cycle phase durations)
  - 14% G0
- 15% LIMP cells (**LIM**ited **P**roliferative Potential cells- up to 7 divisions)
  - 87% Proliferative
  - 13% G0
- 82,1% DIFF cells (**DIFF**erentiated cells)
- 2,5% DEAD cells of which
  - 80% necrotic and
  - 20% apoptotic

The above percentages have been calculated internally by a code function and correspond to the specific values of the code input parameters that are presented in Table S24.

Table S24

Type of cell		Percentage
STEM	Proliferating	0.339616%
	G0	0.0558006%
LIMP	Proliferating	12.830958%
	G0	2.108192%
DIFF		82.1715%
DEAD	Apoptotic	0.487232%
	Necrotic	2.00667%

5.3.2.3 Charts: Tumour volume and temporal variation of the cell category/state populations

Fig. S29-Fig. S33 show the simulated time course for several quantities of interest for the clinical case considered. In all cases fairly reasonable tumour dynamics behaviour can be easily noticed. However, the efforts for the identification of more plausible solutions which will satisfy further clinical requirements (e.g. tumour volume doubling time falling within the range corresponding to a particular tumour type etc.) will continue. It is expected that by being able to fit the model's parameters to a good number of medical data sets *invaluable* estimates for all model parameters will be produced. These will serve as the starting points for the Oncosimulator functioning. On the other hand such estimates are expected to shed light into

the process of understanding the natural phenomenon of cancer, particularly from the cancer stem cell point of view.

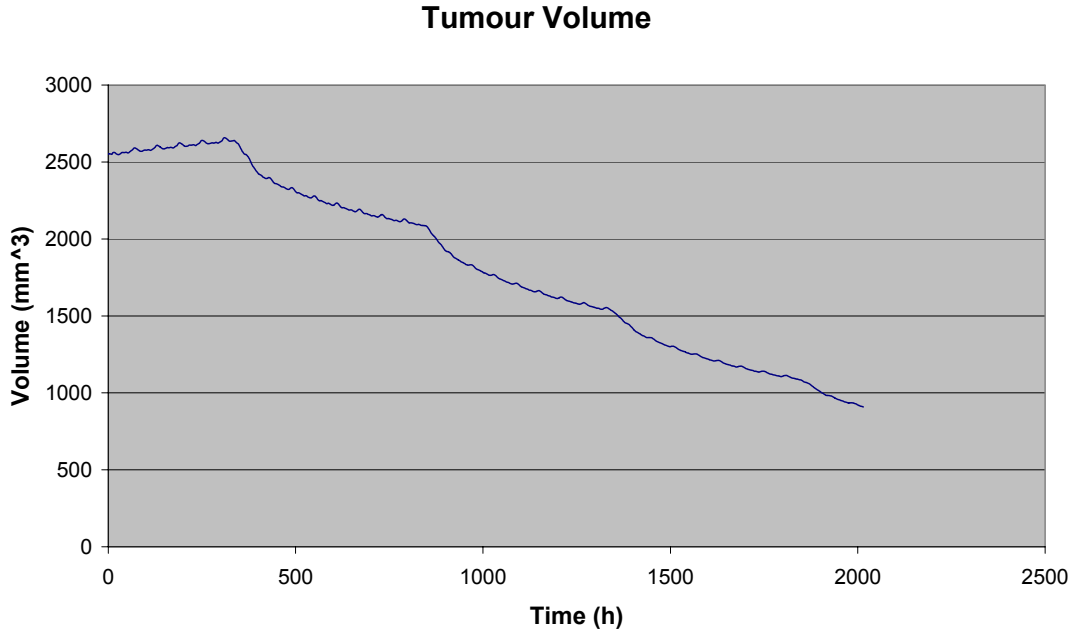

Fig. S29

*The tumour volume has been calculated from the total number of cells (N_{total}) divided by the tumour cell density 10^6cells/mm^3 i.e. $N_{tot}/10^6$ mm^3.

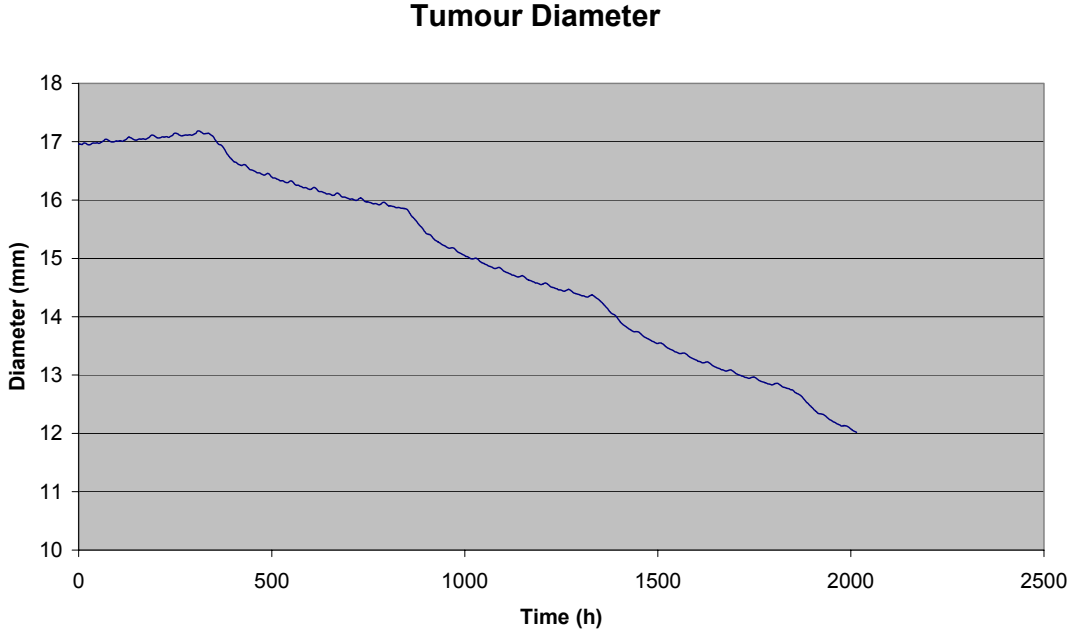

Fig. S30

*The diameter D has been calculated from tumour volume (V) based on the equation: $D = 2 * \sqrt[3]{\frac{3*V}{4*\pi}}$

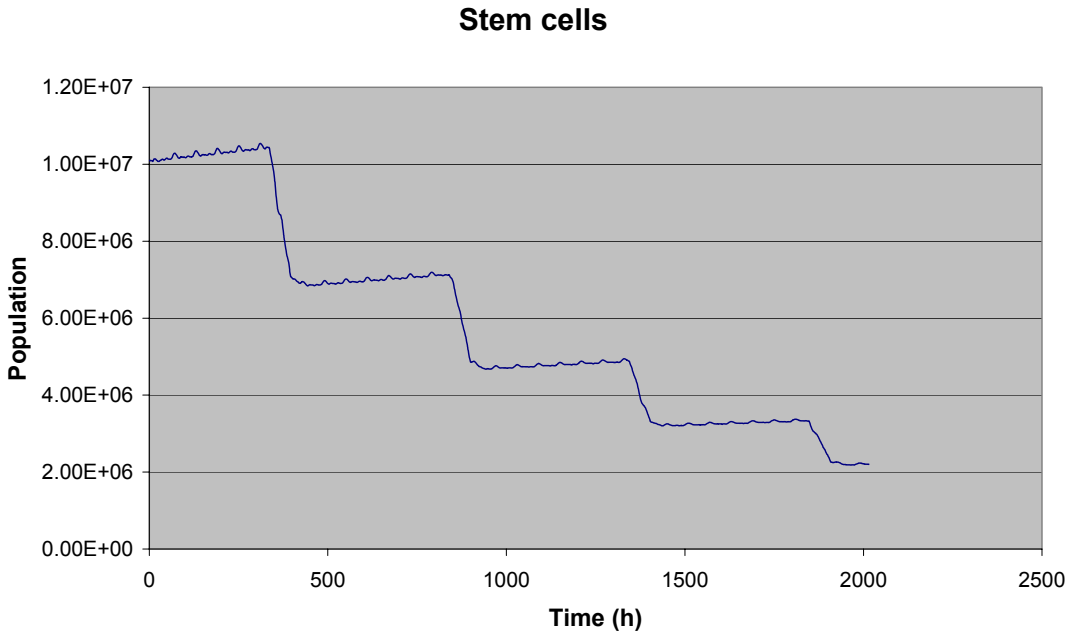

Fig. S31

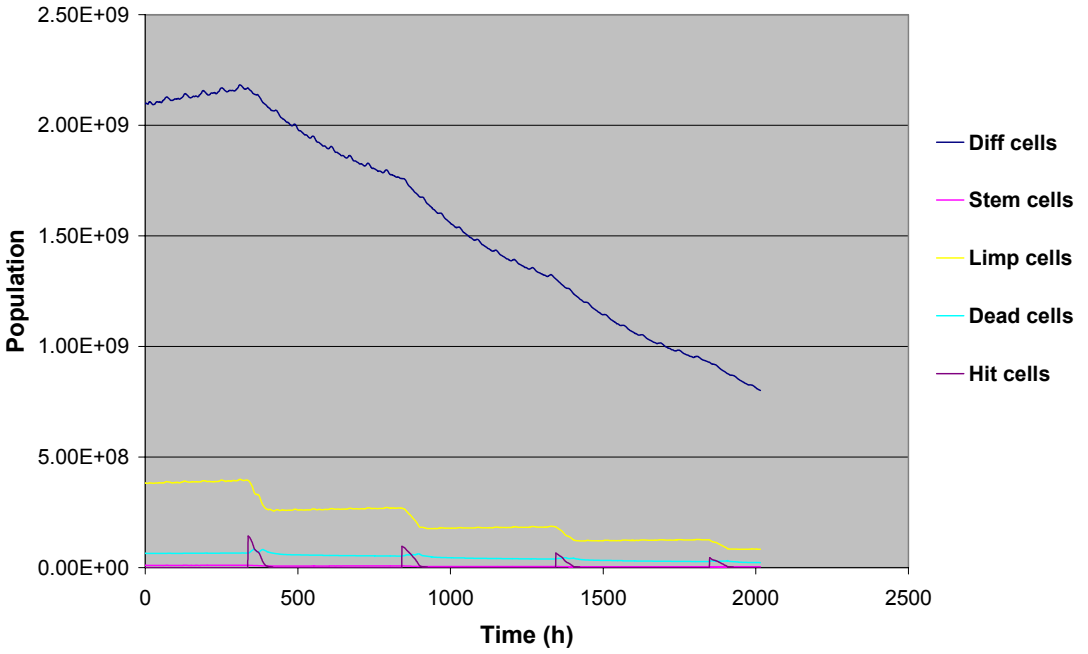

Fig. S32

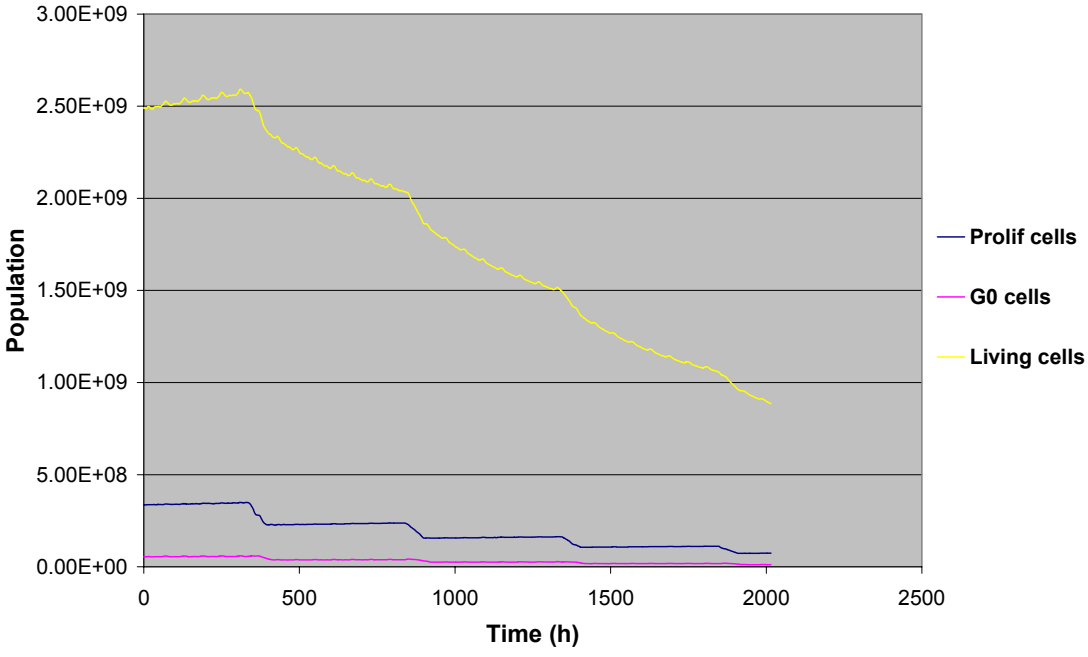

Fig. S33

5.3.2.4 Tumour visualization

Fig. S34 provides a simple three dimensional rendering of the external surface of the tumour before and after treatment (simulation prediction). It also provides a series of virtual slices of the tumour at the same time points.

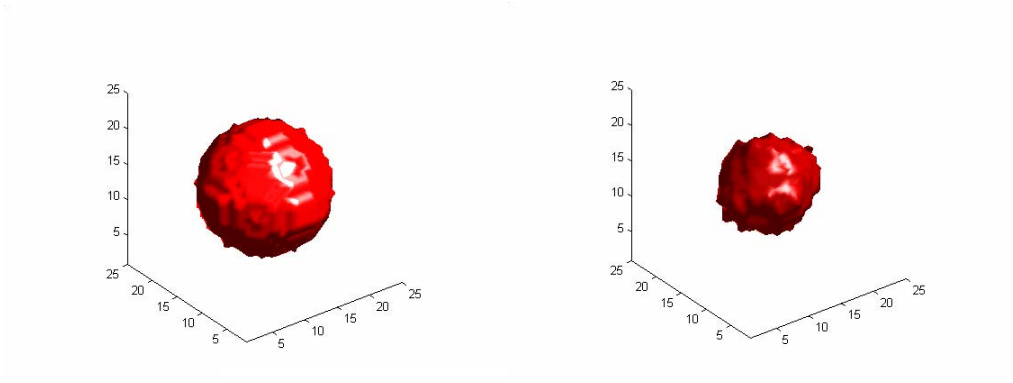

(a) Initial tumour (b) Final tumour

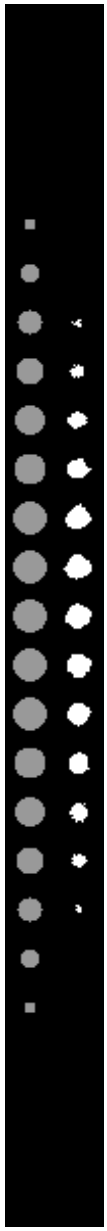

(a) (b)

Fig. S34

Similar extensive work has been done for the case of nephroblastoma treated with vincristine and dactinomycin. In order to save space we include below only the provision of a set of parameters that are able to predict tumour shrinkage for a real case of the SIOP 2001/GPOH clinical trial.

A SIOP 2001 / GPOH nephrobastoma case simulation

5.4.1 Introduction

In this section an initial step towards the clinical adaptation and validation of the nephroblastoma simulation model is presented. Two sets of MRI images have been provided, one before and one after preoperative treatment with chemotherapy. The initial images have been segmented by USAAR using a segmentation tool provided by FHG. Following appropriate image processing a three dimensional reconstruction of the tumour has been provided in a format adequate for exploitation by the simulation code. Histopathological data following treatment have also been provided.

A number of simulations have been performed by varying the values of certain input code parameters in order to achieve a combination of values able to predict the actual tumour shrinkage and at the same time to satisfy numerous biological boundary conditions. Table S25 provided such a combination of parameter values.

Table S25: Code parameters values

PARAMETER	NAME	PARAMETER VALUES
cell_cycle_duration	Cell cycle duration (h)	23.0
stem_max_g0_time	G0 phase duration (h) for stem cells	96
limp_max_g0_time	G0 phase duration (h) for limp cells	96
necrosis_time[0]	Time of necrotic cells in necrotic layer (h)	20
necrosis_time[1]	Time of necrotic cells in proliferative layer (h)	20
apoptosis_time[0]	Time of apoptotic cells in necrotic layer (h)	6
apoptosis_time[1]	Time of apoptotic cells in proliferating layer (h)	6
apoptosis_rate	Spontaneous apoptosis rate [*fraction of cell number per hour*]	0.001
diff_apoptosis_rate	Spontaneous apoptosis rate for differentiated cells [*fraction of cell number per hour*]	0.003

diff_nec_rate	Necrosis rate for differentiated cells [*fraction of cell number per hour*]	0.001
stem_g0_to_g1_percent	Fraction of dormant cancer stem cells re-entering the G1 phase per hour	0.01
limp_g0_to_g1_percent	Fraction of dormant cancer progenitor cells re-entering the G1 phase per hour	0.01
sleep_percent[0]	Fraction of cells in the necrotic layer that will enter G0 following mitosis	0.28
sleep_percent[1]	Fraction of cells in the proliferative layer that will enter G0 following a mitosis	0.28
sym_percent[0]	Fraction of the stem cells in the necrotic tumour layer that divide symmetrically.	0.42
sym_percent[1]	Fraction of the stem cells in the proliferative tumour layer that divide symmetrically	0.42
no_limp_classes	Limited mitotic potential (progenitor) cell stages	3
x_dim	Number of geometrical cells along the x axis	51
y_dim	Number of geometrical cells along the y axis	52
z_dim	Number of geometrical cells along the z axis	61
number_biological_cells	Number of cells contained within a geometrical cell of the mesh	8*1000000
margin_percent	Acceptable over-loading or under-loading of each geometrical cell	0.1
color_criterion	Minimum percentage of cells that should be dead in order to "paint" the geometrical cell necrotic	0.98
distance_factor[0]	Factor adapting cell killing probability to the necrotic layer	1.0
distance_factor[1]	Factor adapting cell killing probability to the proliferative layer	1.0
drug	Which drug or drug combination is to be simulated?	3
mode	What tumour course is to be simulated?	2
reconstruction	Will geometric reconstruction be included in the simulations?	1
vcr_adm_interval	Interval between two subsequent administrations of vincristine (h)	168
vcr_start_time	Time point of the first drug administration since initialization (h)	96

vcr_no_sessions	Number of consecutive vincristine sessions to be simulated	4
stem_vcr_cell_kill_ratio	Cell kill ratio of stem cells for a specific vincristine dose	0.3
limp_vcr_cell_kill_ratio	Cell kill ratio of limp cells for a specific vincristine dose	0.3
act_adm_interval	Interval between two subsequent administrations of actinomycin-D (h)	336
act_start_time	Time point of the first drug administration since initialization (h)	96
act_no_sessions	Number of consecutive actinomycin-D sessions to be simulated	2
stem_act_cell_kill_ratio	Cell kill ratio of stem cells for a specific vincristine dose	0.2
limp_act_cell_kill_ratio	Cell kill ratio of limp cells for a specific vincristine dose	0.2
dt_posttreatment_scan	Time interval between last treatment and post-treatment scan (h)	72

REAL CLINICAL VOLUMETRIC DATA		
Initial number of biological cells	1.22E+11	1.22E+11
Final number of biological cells	3.35E+10	3.39E+10
Shrinkage percentage	72.54	72.18

5.4.2 Results

5.4.2.1 Initialization of the simulated tumour

Convergence of the initial cell category/state relative populations was achieved 3542 virtual hours after the initiation of the tumour creation process. Table S26 presents the initial cell category/state population fractions formed for a convergence limit $\varepsilon = 10^{-7}$

Table S26

Cell categories population fractions formed for a convergence limit $\varepsilon = 10^{-7}$

Basic cell category population fractions	
Stem	0.098
Limp	0.175
Diff	0.670
Dead	0.058
Cell cycle phase population fractions	
G1	0.159
S	0.159
G2	0.071
M	0.018
G0	0.593
Limp (progenitor) population fractions	
Limp1	0.228
Limp2	0.321
Limp3	0.452
Dead cell population fractions	
apoptotic	0.197
necrotic	0.803

5.4.2.2 Free growth of the simulated tumour

In order to ensure that the selected combination of parameter values (Table S25), apart from being able to predict the actual tumour shrinkage, leads to a clinically acceptable free tumour growth tumour evolution has been simulated for some time after the baseline (Fig. S35). Fig. S36 and S37 provide the time course of the basic cell category populations.

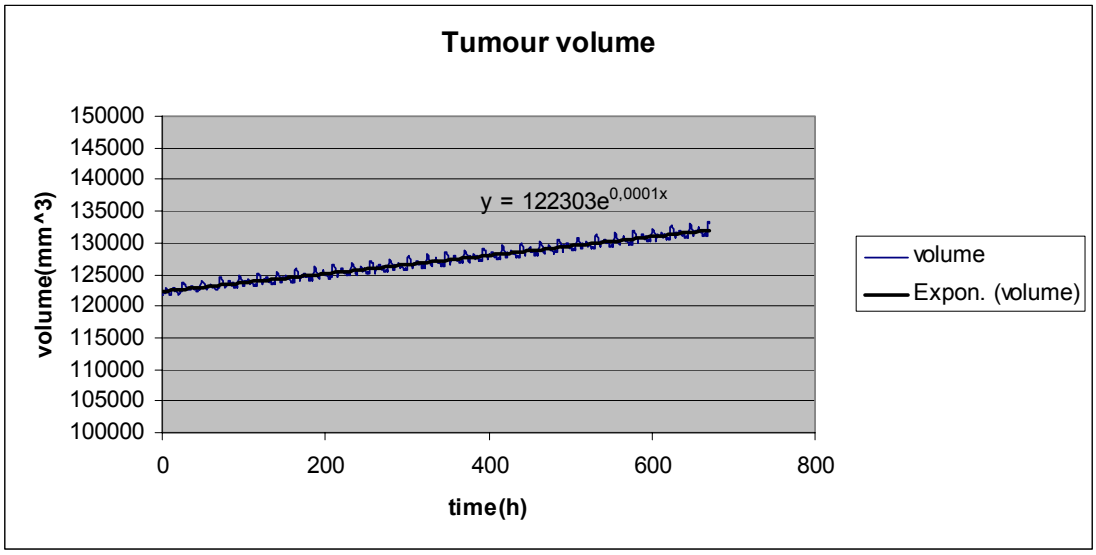

Fig. S35: Time course of the free tumour volume evolution

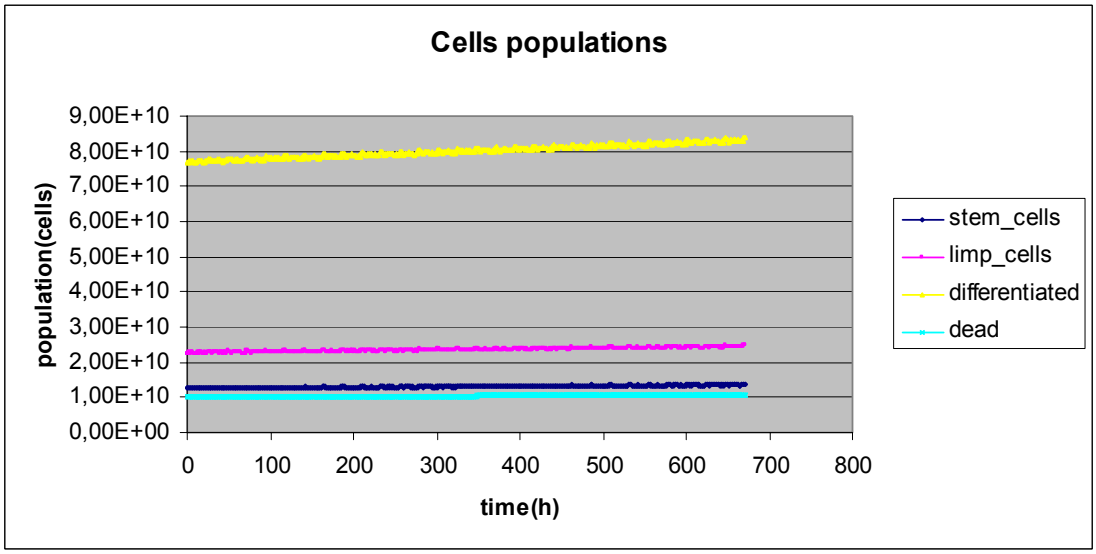

Fig. S36. Time course of the four basic cell category populations for free tumour growth

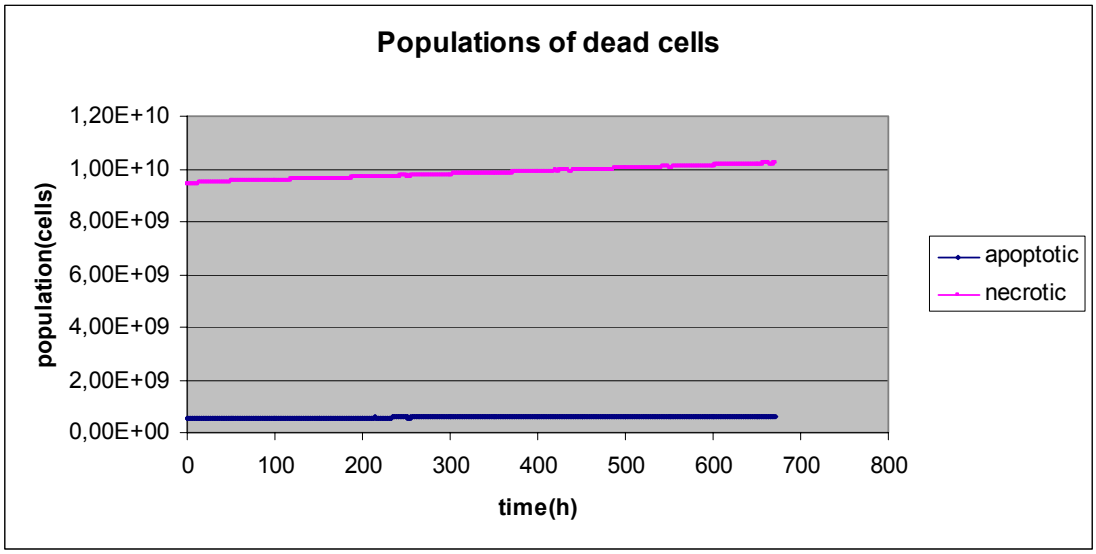

Fig. S37. Time course of the dead cell populations for free growth

All cell category/state populations increase during free growth of the tumour. This ensures that the boundary conditions regarding the monotonicity of increase of the tumour cell category/state populations is satisfied. However, in analogy with the breast cancer case the efforts for the identification of more plausible solutions which will satisfy further clinical requirements (e.g. tumour volume doublin time falling within the range corresponding to a particular tumour type etc.) will continue.

5.4.2.3 Results concerning treatment response

The simulation algorithms developed so far address the cases of preoperative chemotherapy with a combination of actinomycin-D and vincristine for unilateral stage I-III nephroblastoma tumours treated according to the SIOP 2001/GPOH clinical trial in the framework of the ACGT project (Fig. S28).

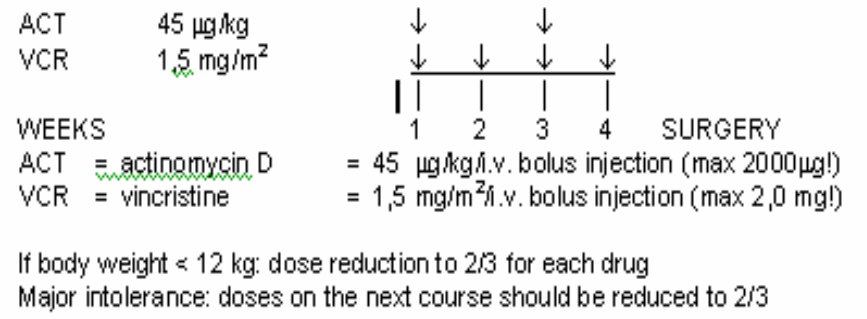

Fig. S38. The for the simulation used Wilms tumour treatment protocol

According to the clinical treatment plan applied to the particular patient considered chemotherapy started 4 days after the pre-treatment imaging data were collected. Post-treatment imaging data were collected 3 days after the last chemotherapy session. These pre- and post-treatment intervals have also been simulated. The clinical tumour was reduced by 72.54 % while the simulated tumour has shrinked by 72.18 %.

The simulation results concerning the response of the tumour to the chemotherapeutic treatment (Fig. S38) are presented in Fig.S39 – Fig. S46). Again a reasonable tumour behaviour can be easily noticed.

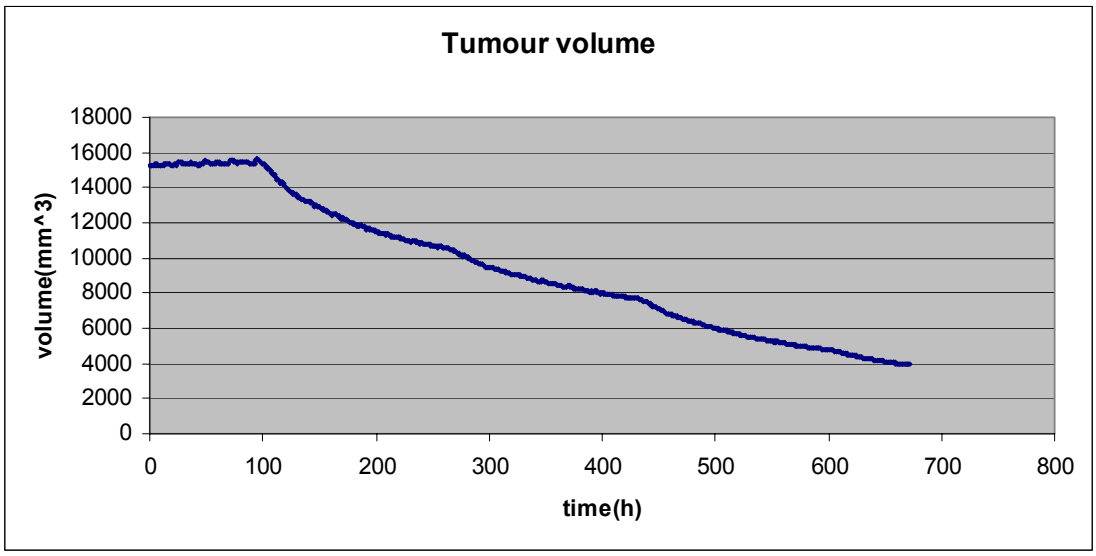

Fig. S39. Time course of the tumour volume before, during and after the chemotherapeutic treatment

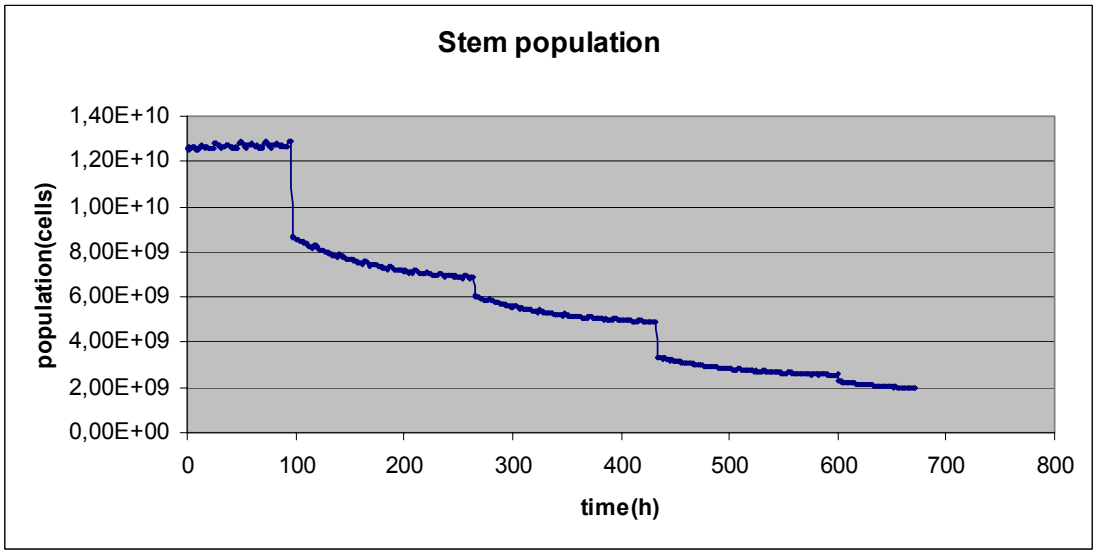

Fig. S40. Time course of the stem cell population before, during and after the chemotherapeutic treatment

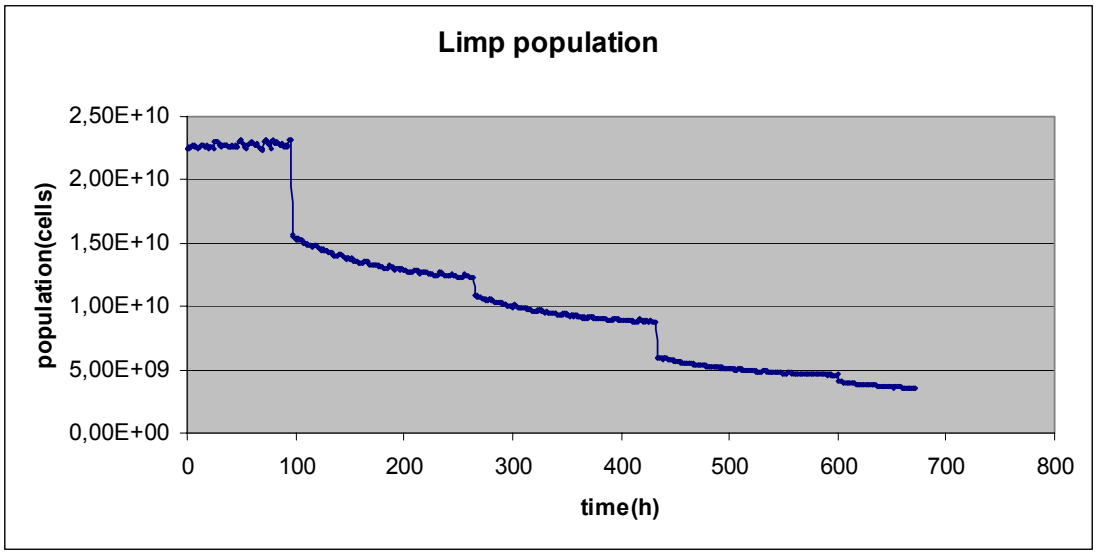

Fig. S41. Time course of the progenitor (limp) cell population before, during and after the chemotherapeutic treatment

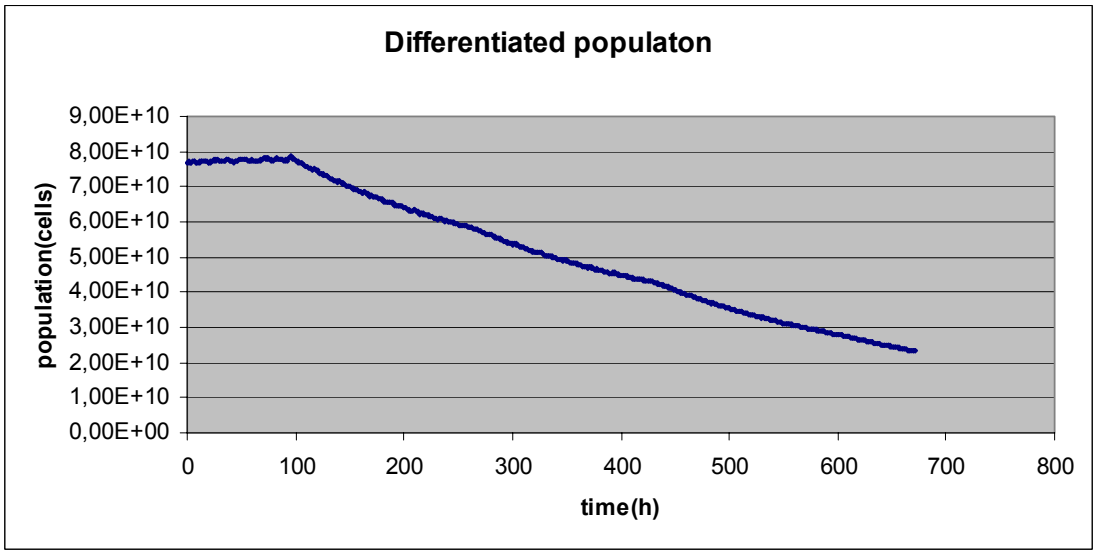

Fig. S42. Time course of the differentiated cell population before, during and after the chemotherapeutic treatment

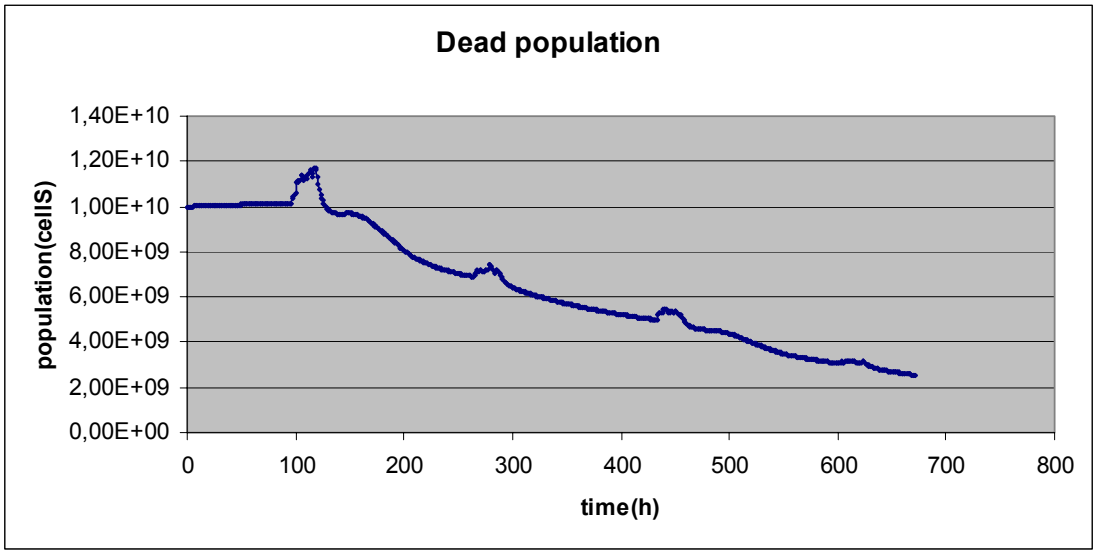

Fig. S43. Time course of the dead cell population before, during and after the chemotherapeutic treatment

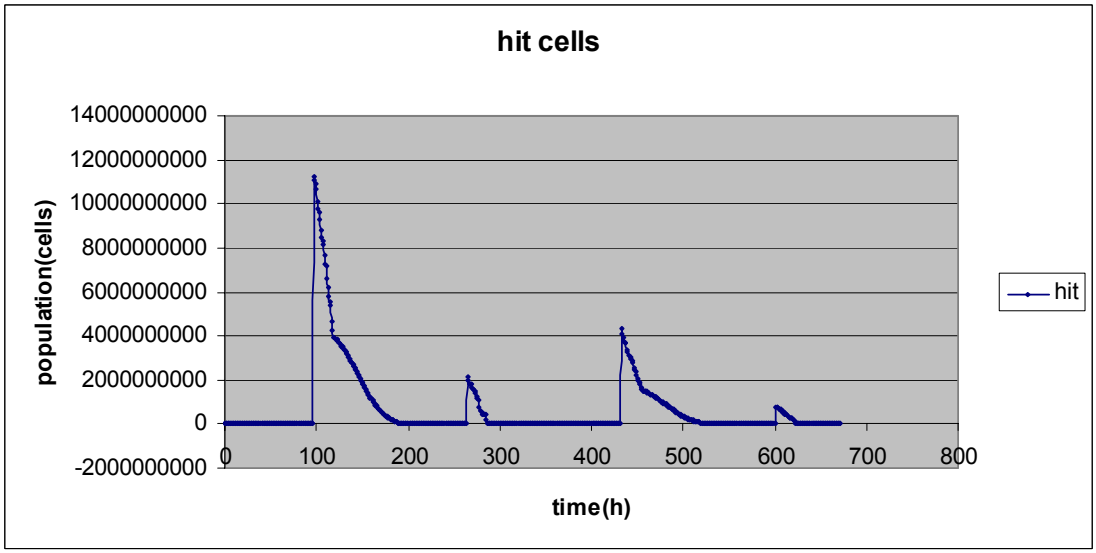

Fig. S44. Time course of the drug hit cell population before, during and after the chemotherapeutic treatment

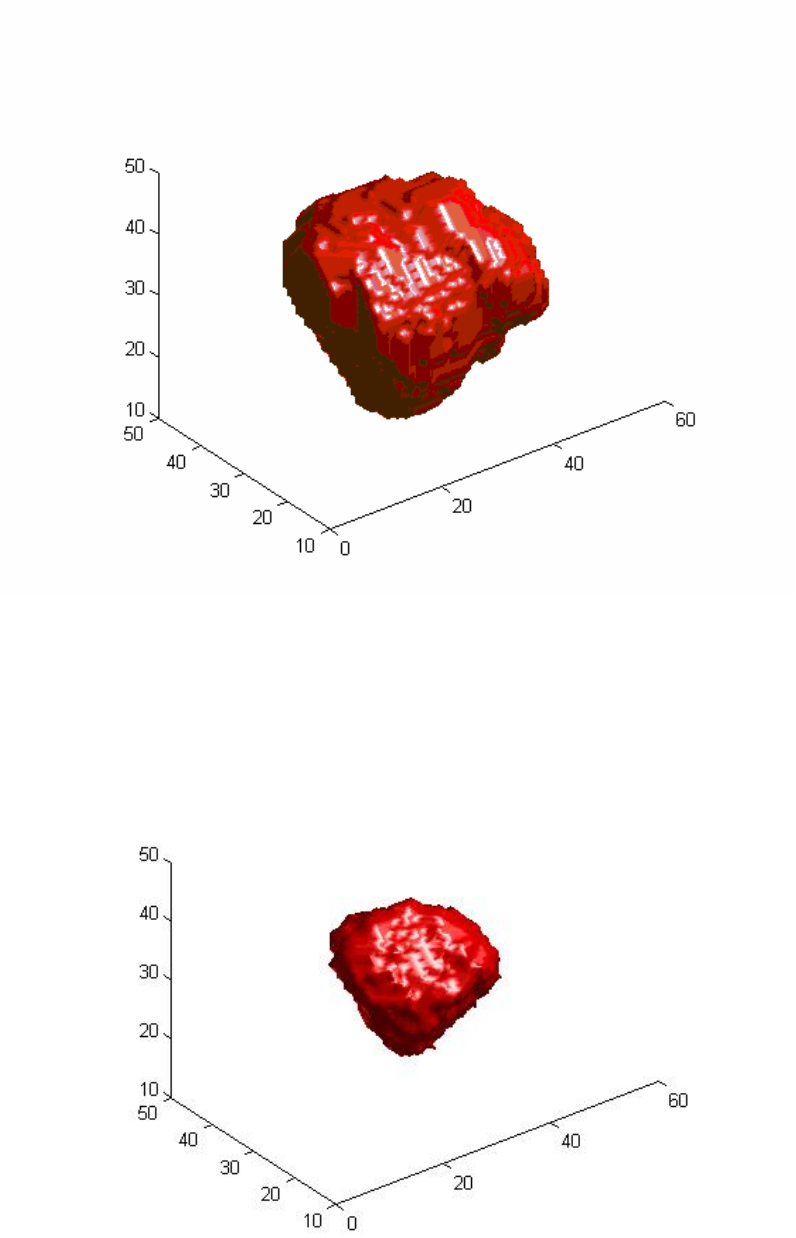

Fig. S45. 3D tumour visualization. Upper panel: tumour four days before treatment initiation, lower panel: predicted tumour three days after completion of the treatment course

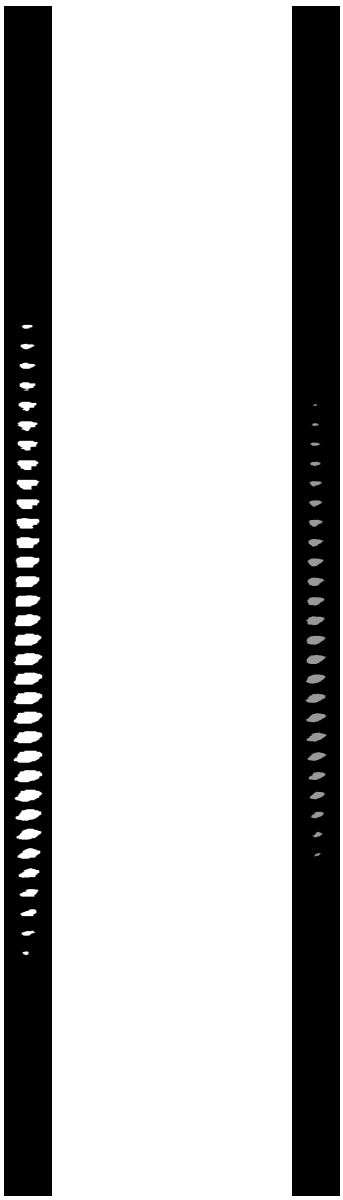

Fig. S46. 2D slices of the simulated tumour. Left panel: tumour four days before treatment initiation, right panel: tumour three days after completion of the treatment course

References

S1. G. Steel, The growth rate of tumours, in Steel Ed. "Basic Clinical Radiobiology", 2nd edition, Arnold, London, 1997. pp. 10-11, Fig. 2.3 and Fig. 2.4

S2. A. Zoubek , I. Slavc, G. Mann, G. Trittenwein, H. Gadner, Natural course of a Wilms' tumour, Lancet 1999 Jul 24, 354(9175):344

S3. N.Graf and A. Hoppe, What are the expectations of a Clinician from In Silico Oncology ? Proceedings of the 2nd International Advanced Research Workshop on In Silico Oncology, Kolympari, Chania, Greece, Sept. 25-26, 2006 pp. 36-38.

S4. A. Begg, Cell proliferation in tumours, in Steel Ed. "Basic Clinical Radiobiology", 2nd edition, Arnold, London, 1997, pp.13-16

S5. G.S.Stamatakos, D.D.Dionysiou, N.M.Graf, N.A.Sofra, C.Desmedt, A.Hoppe, N.Uzunoglu, M.Tsiknakis , The Oncosimulator: a multilevel, clinically oriented simulation system of tumor growth and organism response to therapeutic schemes. Towards the clinical evaluation of in silico oncology , Proceedings of the 29th Annual International Conference of the IEEE EMBS Cite Internationale, August 23-26, SuB07.1: 6628-6631 , Lyon, France , 2007

S6 N.Graf,C.Desmedt,F.Buffa,D.Kafetzopoulos,N.Forgo,R.Kollek,A.Hoppe,G.Stamatakos,M.Tsiknakis Post-genomic clinical trials - The perspective of ACGT, Ecancermedicalscience Vol. 2, 2008

S7. E. Ch. Georgiadi, G. S. Stamatakos, N. M. Graf, E. A. Kolokotroni, D. D. Dionysiou, A. Hoppe, N. K. Uzunoglu, "Multilevel Cancer Modeling in the Clinical Environment: Simulating the Behavior of Wilms Tumor in the Context of the SIOP 2001/GPOH Clinical Trial and the ACGT Project"accepted to be published as an 8 page full paper in Proceedings of the 8th IEEE International Conference on Bioinformatics and Bioengineering, Athens, Greece, 8-10 October 2008, *in press*

S8. E. A. Kolokotroni, G. S. Stamatakos, D. Dionysiou, E. Ch. Georgiadi, C. Desmedt, N Graf, "Translating Multiscale Cancer Models into Clinical Trials: Simulating Breast Cancer Tumor Dynamics within the Framework of the "Trial of Principle" Clinical Trial and the ACGT Project," accepted to be published as an 8 page full paper in Proceedings of the 8th IEEE International Conference on Bioinformatics and Bioengineering, Athens, Greece, 8-10 October 2008, *in press*

6 Image Processing of the Medical Data

[Chapter code: I]

In general, the term *segmentation* denotes the process of assigning sets of pixels to one or more distinct groups that are defined by the needs of the respective image processing task. Regarding medical imaging, volumetric segmentation is based on the classification of voxels to regions, which usually correspond to objects or organs in the data set. Finding criteria to decide which voxels in the volume are similar or share a common property is therefore the essential part of every segmentation technique. The result of segmentation is a classification that labels every voxel to be part of a certain region. This is referred to as *binary segmentation* since a voxel either shares a property with its neighbours or not.

For the needs of the ACGT Oncosimulator, tumours have to be segmented from MRI data sets in order to simulate tumour growth and to compare the results with the real outcome of treatment. Therefore, a segmentation tool has been developed by FHG that can be used by a physician to manually contour the tumours in every slice. Fig. I1 shows the result of such a slice-based segmentation. The contouring is done by defining a set of points placed on the borders of the tumour and by interpolating between the points using B-Spline interpolation, respectively.

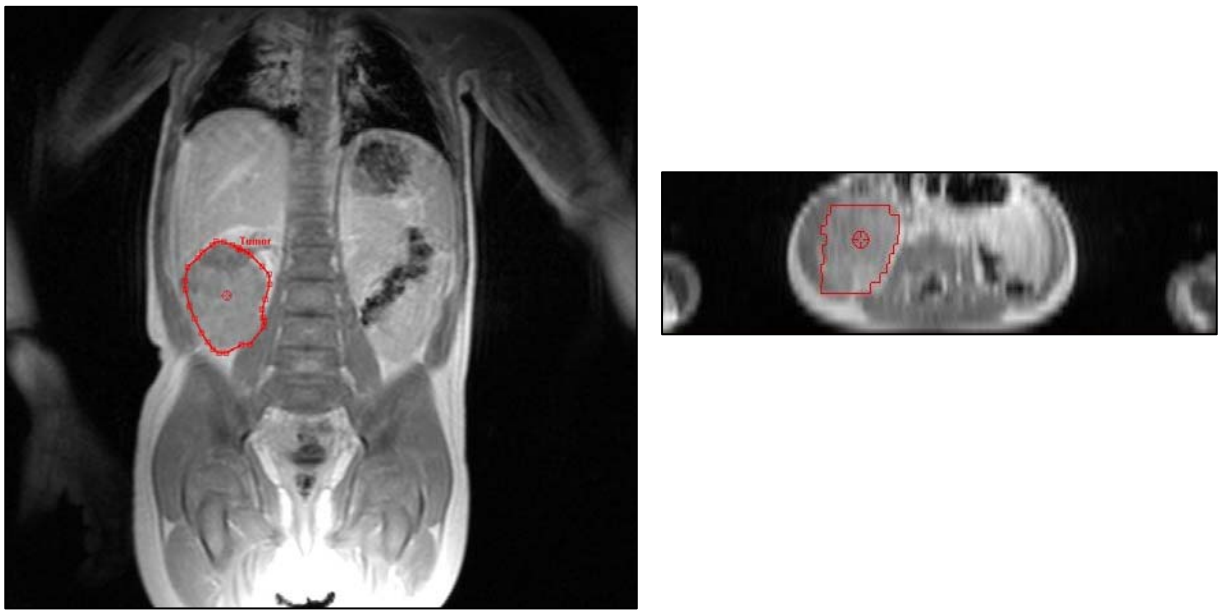

Fig I1: Contouring of tumours in MRI data sets

The results can also be viewed as a 3D rendering showing tumour and MRI volume visualization at the same time (Fig. I2).

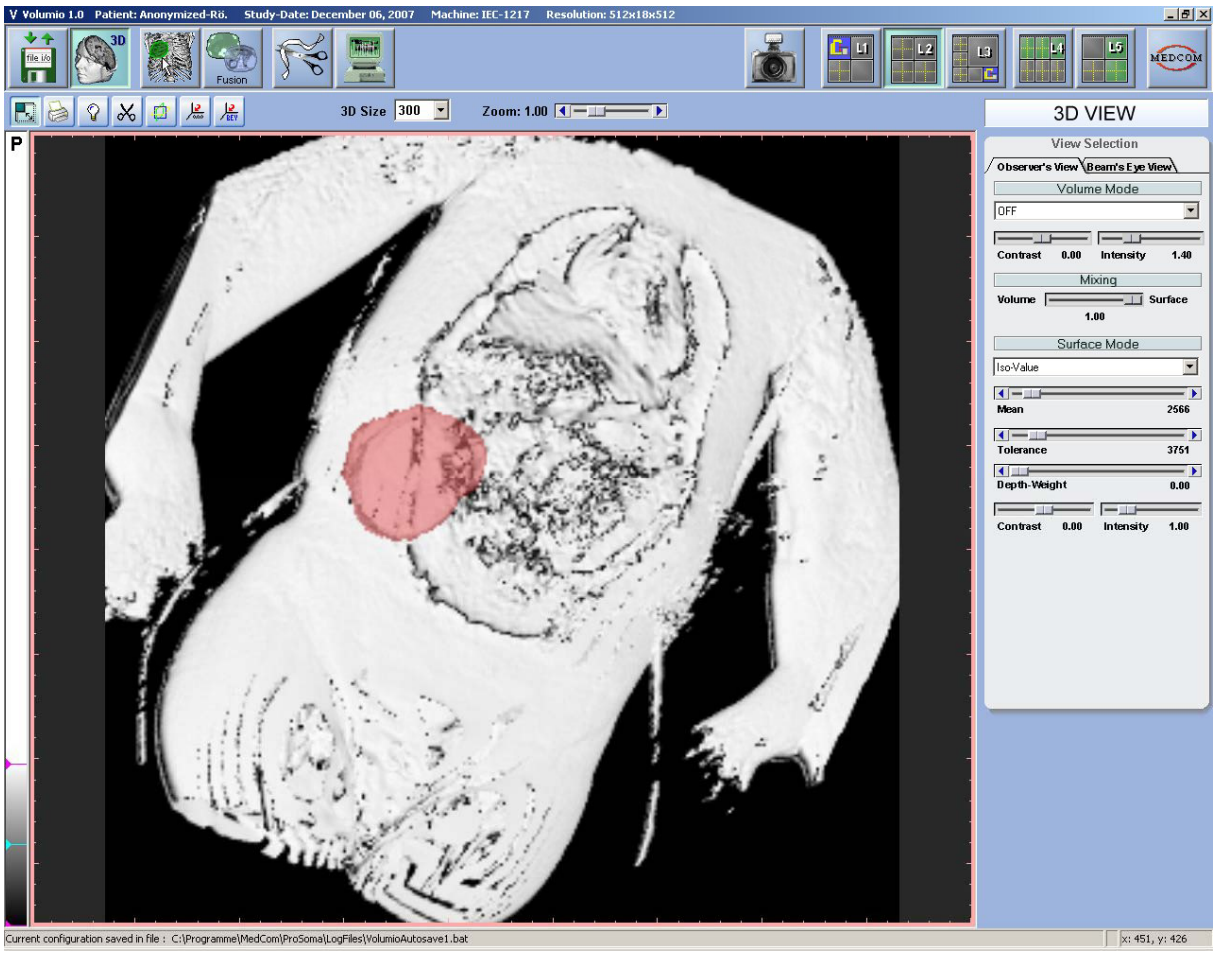

Fig.I2: 3D Visualization of tumour and thorax.

Resampling and Interpolation of Binary Segmentations

Usually voxels in MRI data sets are non-isotropic, i.e. their dimensions differ in x-, y- and z-direction. Therefore, binary labelled volumes are also non-isotropic. In order to allow for a proper simulation of tumour growth, the label volume has to be resampled. While resampling of the volume itself is not a difficult task, the resulting label should also be interpolated in order to have a smooth transition from slice to slice. Fig. I3 shows the principle of interpolating a coarse grained label to a voxel grid of higher resolution. Since we are not working on grey value data, there is not sufficient information to interpolate between the slices. Therefore, we compute a distance transform for the binary label volume using level sets [I1]. The result is a grey level volume with the zero crossings denoting the zero level set. Fig. I4 gives an overview of the approach. One can think of the zero level set as an estimate for a surrounding minimal surface of the binary label data. By finding the zero-crossing in the volume, a new label volume can be defined which represents the resampling of the original data set.

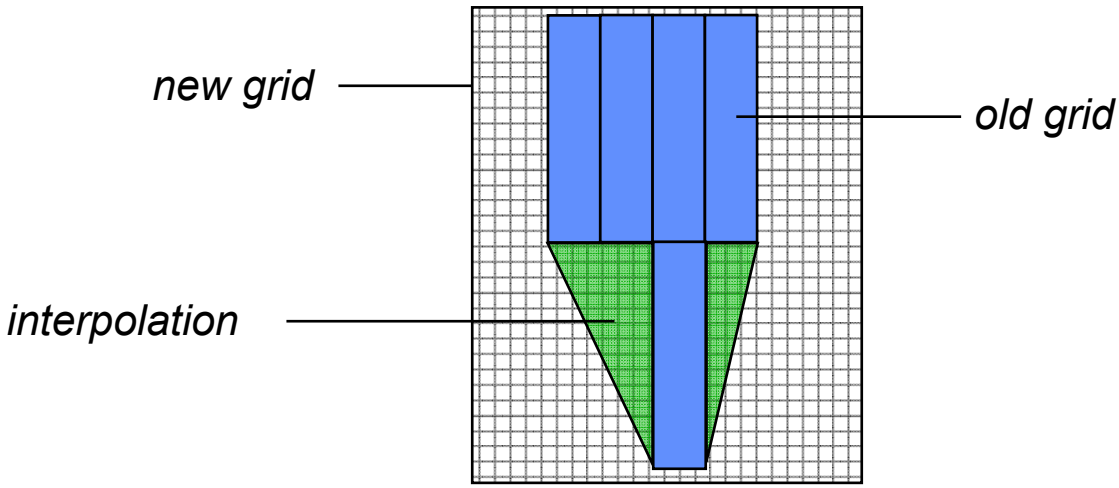

Fig. I3: Interpolation between two coarse grained slices to a voxel grid of higher resolution.

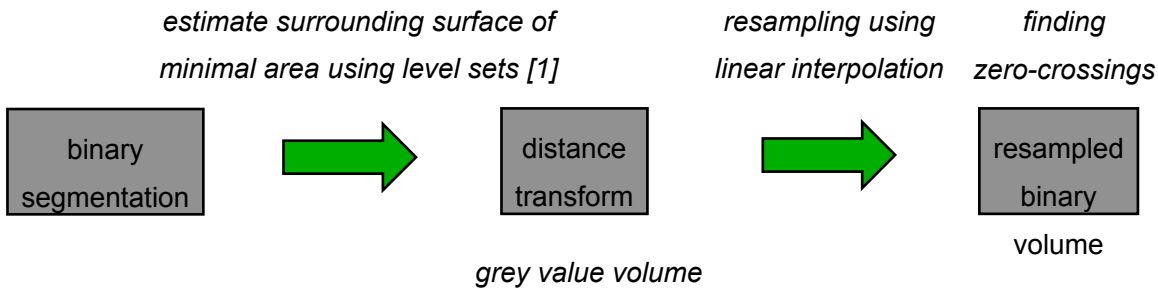

Fig.I4: Resampling of binary label volume using level sets.

Exploration of the applicability of automatic segmentation techniques to the real Oncosimulator data is also taking place.

References

I1. R. Whitaker. Reducing Aliasing Artifacts in Iso-Surfaces of Binary Volumes. IEEE Volume Visualization and Graphics Symposium, October 2000, pp.23-32.

7 The Oncosimulator Grid Execution Scenario

[Chapter code: G]

The Oncosimulator application can be used as a standalone tool but it can also benefit from the Grid environment. This chapter presents a scenario of executing the application in the ACGT grid testbed that was developed by PSNC. The scenario was demonstrated during the May 2008 ACGT Review meeting in Eindhoven.

The Grid environment created for the purposes of the ACGT project consists of the following two layers:

- basic grid infrastructure: this is based on the Globus Toolkit solution and provides common interface for remote access to computational resources
- advanced grid services : this is built with the Gridge Toolkit and provides advanced solutions for resource management, data management, grid monitoring etc.

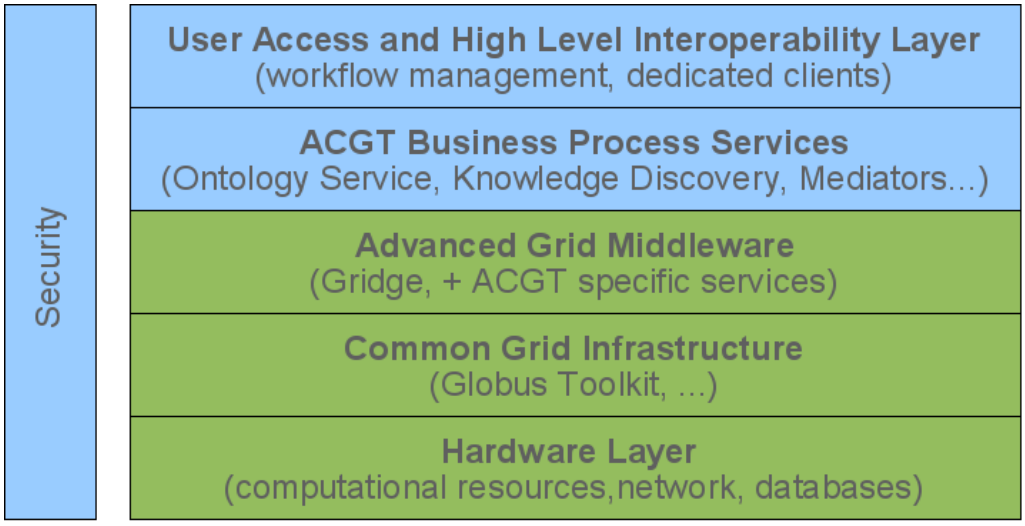

Fig.G1.Grid Layers on the ACGT architecture

The most important component of the Grid Layers used in the presented scenario in GRMS is the Gridge Resource Management System. GRMS is a very powerful tool used for managing computational resources in grid. It is able to discover automatically available resources in the grid and send incoming jobs to the best available ones at that time. The other goal of the system is to balance the load of the machines. An interesting feature of GRMS is to support workflows. It is possible to define a job as a set of tasks that can be run in a sequential or a parallel way. That attribute allows for defining a more complicated scenario of application execution with an additional flow of data.

The new feature of GRMS developed particularly for ACGT is to support parametric executions. It is possible to define a parameter of application execution as a set of values. The system is responsible for running the application multiple times with different parameters.

Another important component of the grid environment is GDMS - Gridge Data Management System. It is responsible for storing users data and providing it to all other elements of the grid in a uniform way. Clients can refer to the stored data by using logical identifier of files or

directories. More detailed information about services in grid layers can be found in deliverable D 4.1.:"Prototype and report of the ACGT GRID layer".

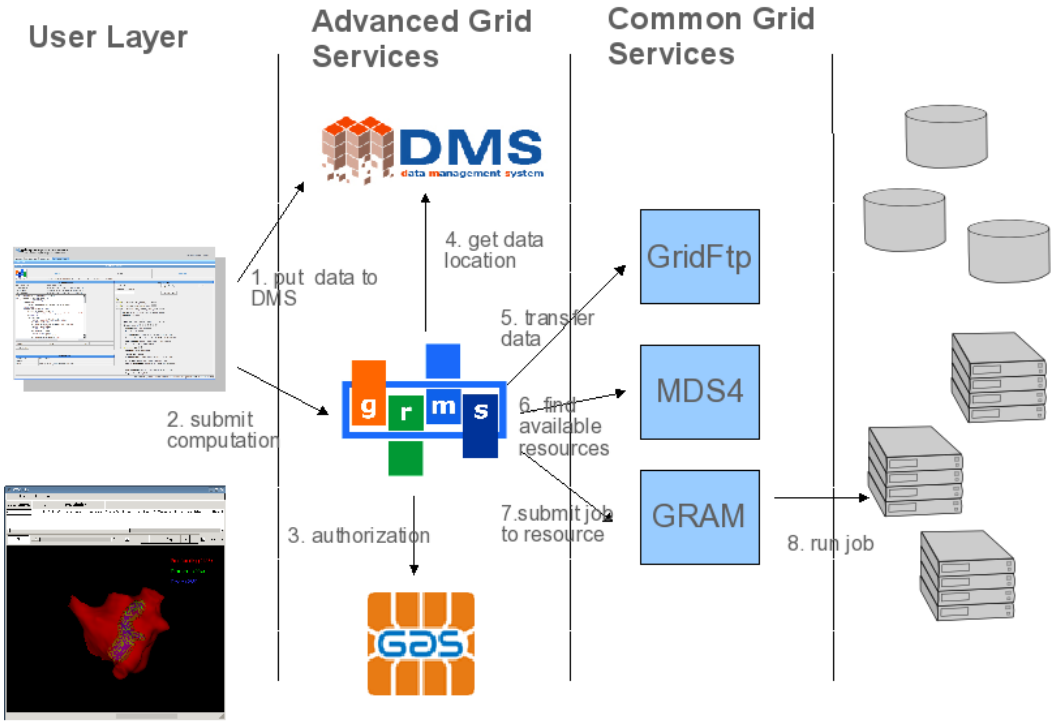

Fig.G3.Components of the grid environment

The scenario described below, concerns not only a simple submission of application, but also presents the integration with the visualization tools.

The first step of the scenario is devoted to preparation of the input data for the computation.

The clinician needs to prepare MRI sets of slices of the tumour corresponding to the tumour before treatment (e.g. with vincristine and dactinomycin).

Using specialized tools he/she also needs to draw the tumour contours on the provided anonymized/pseudonymized slices.

The user uploads all required anonymized/pseudonymized files from his/her machine to the Gridge Data Management System using web portal client. The files are then managed by DMS and can be accessed by the user or other services acting on behalf of the user.

Then by using a specialized Oncosimulator portlet the user defines the parameters of the simulation by filling proper fields of the portal form. The interesting feature of the system is its ability to define the arguments of execution in a parameter sweep manner. So with one click multiple runs can take place with parameters from a defined set with a selected step. This feature is supported on the grid resource management level.

Besides parameters, location where the output data will be stored must be provided. It is used by the Visualization System for presenting the results of computation.

After the 'submit' button is clicked a description of the job for the Gridge Resource Management System is built and then submitted to the system. In this case the job definition (XML document) is a workflow that consists of a set of tasks and dependencies between them.

Tasks description (task as a single execution of the application or script) has two parts: the first one describing execution (executable file, input parameters, environment variables, etc.), the second one comprises resource (hardware) requirements for task execution. Based on those requirements the resource management system can take a decision as to where to put the task for execution. In the executable definition references to the data management system are used.

In our scenario at first the simulation code is unpacked, compiled and executed. During the application runtime all data generated is transfered to the visualization system location provided by the user.

After the simulation has finished all the output data is also uploaded to the Data Management System.

A detailed view of the submitted workflow is presented on the following picture:

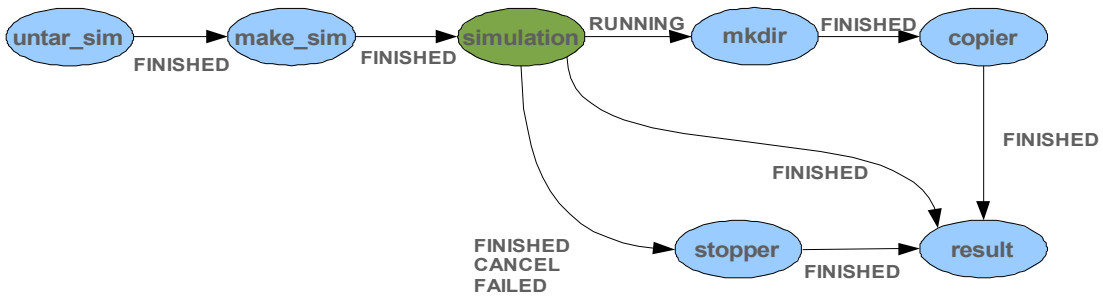

Fig.G4.Workflow submitted to GRMS

Tasks on the picture:

- untar_sim: unpacking of application code
- make_sim: compilation of the simulation code
- simulation: Oncosimulator simulation execution
- mkdir: task responsible for making directory for generated output by simulation on visualization machine
- copier: task responsible for transferring newly generated files to visualization site
- stopper: stopping the copier task as soon as the simulation stops working
- result: pack the output of the simulation and sends it to the Data Management System

After the the job is submitted GRMS takes care about the workflow management and provides additional information for monitoring purposes. The user can take advantage of this information using the portal.

After the simulation has finished all the output data is also uploaded to the FTP server of the Visualization System and stored in the Data Management System of the Grid. The user performing the simulation has access to them.

8 Cluster Execution and Parallelization of the Oncosimulator Code

[Chapter code: P]

Introduction

Execution acceleration of the Oncosimulator code has been undertaken by INRIA. The following three essential requirements for the Oncosimulator users that justify the need for the reduction of the execution time from several minutes to about ten seconds have been identified:

1. Intensive computations: a clinician has to test many parameter combinations. This implies the need to launch numerous executions concurrently.
2. High-accuracy results: the better the definition of the tumour is the better the prediction of the tumour behaviour will be. However, increasing accuracy implies multiplying the number of computations.
3. Interactivity: based on the results from a simulation execution, the user can direct the the next simulations to a more promising region of the parameter space.

Therefore, we are working on a solution using both parallel machines and multicore processors in order to considerably increase the speed of simulations [P1].

Simultaneous executions on cluster machines

The ACGT Grid infrastructure is made up of sets of cluster machines. A worthwhile strategy of the Grid use is to distribute the amount of simulations on all the available machines as is shown on Fig. P1. Such a repartition is a good answer to the first requirement. A submission web server dealing with a very early version of the simulation module has been developed on the INRIA cluster and is available at http://acgt.genouest.org. Moreover, such an implementation could also be easily developed on the ACGT Grid.

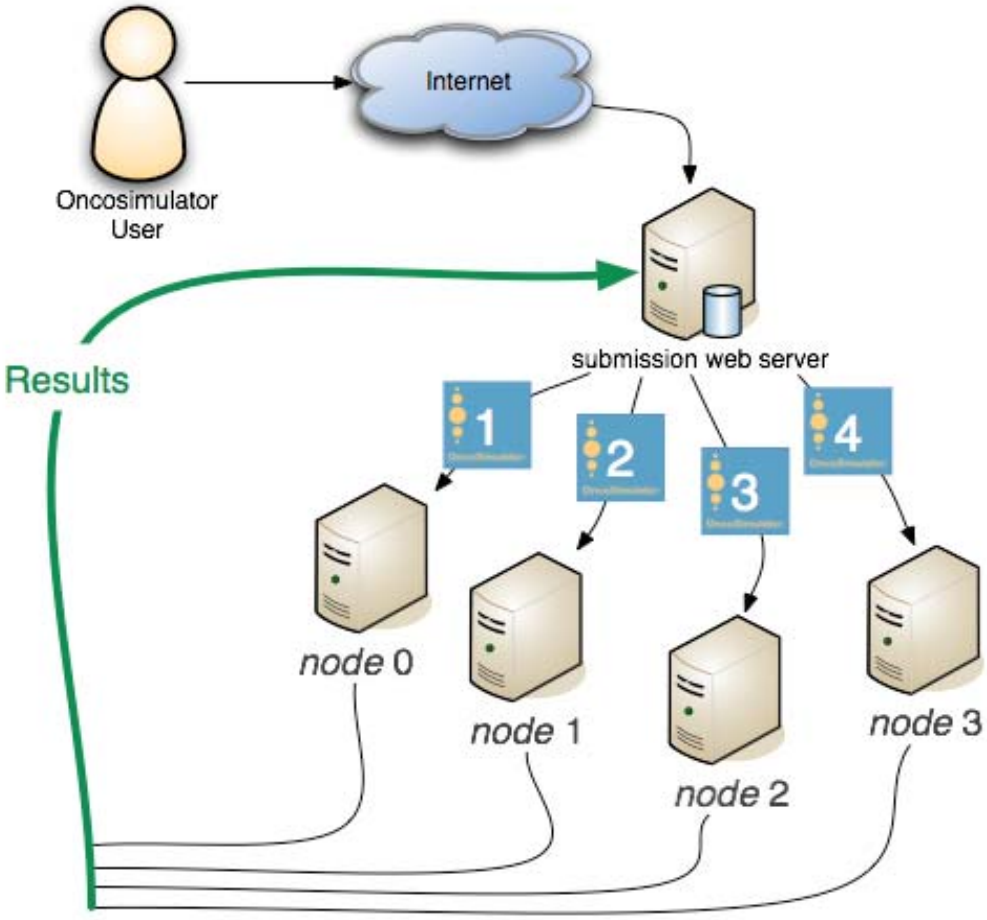

Fig.P1 Four concurrent executions of the Oncosimulator

Multithreaded parallelization of the Oncosimulator

Up to now the Oncosimulator simulation code consists of a single process. However, microprocessor development is nowadays oriented to multicore architectures (several cores on the same chip). Multicore architectures will soon represent the majority of cluster machines. In order to take the advantage of these new architectures we are developing a multithreaded version of the Oncosimulator code. A distribution of threads coming out from one single execution of the Oncosimulator and executed on a quad-core processor is introduced in Fig. P2.

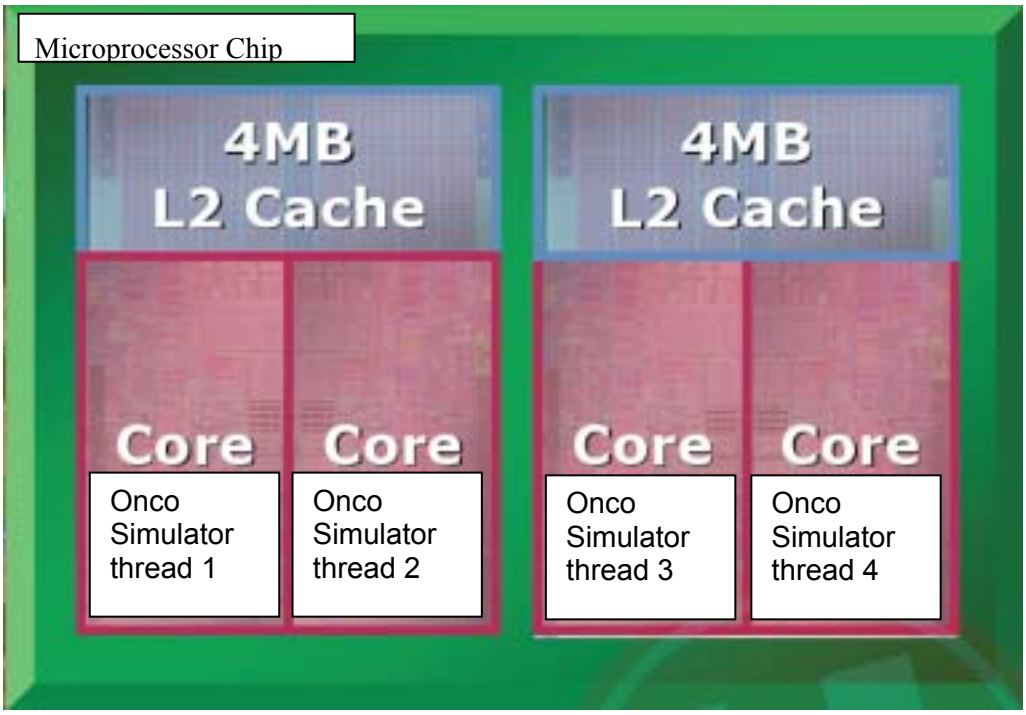

Fig. P2 An example of a quad-core architecture where four threads can be executed at the same time.

This type of parallelization is well adapted to the implementation of the Oncosimulator since the memory is shared between threads. As a consequence the execution time can be drastically reduced and therefore requirements 2 and 3 can be also satisfied.

Future deployment of the Oncosimulator

Finally, in order to answer all the user requirements, we will proceed to the merging of the above mentioned two approaches. Next we will implement the multithreaded version of the Oncosimulator in the Grid Execution Scenario.

References

P1. D. Lavenier and J. Jacques, "Parallelizing the ACGT Oncosimulator", Proceedings of the 3rd International Advanced Research Workshop on *In Silico* Oncology, Istanbul, September 23-24, 2008 *in press*

9 Interactive and Virtual Reality Visualization

[Chapter code: V]

Introduction

Interactive visualization is a powerful paradigm for the user-controlled exploration of scientific data. Visualization is most often used in situations where automated data analysis techniques fail or are non-existent. In these cases visualization algorithms are used to map scientific data to a graphical representation that allows the scientist's cognitive abilities, experience and expertise to visually detect structure and patterns. Interaction methods that influence the visualization algorithms put the scientist in the driver seat of an interactive vehicle that allows him to explore his data.

This chapter describes the facilities that have been developed for the interactive visualization of Oncosimulator results and medical images by UvA. We have designed and built a lightweight framework that allows for the interactive visualization of data over a distributed architecture. Each visualization facility is wrapped into a service that allows integration into third-party applications including desktop applications, web portals and interactive Virtual Reality devices. This architecture has been demonstrated within the framework of the Integrated Oncosimulator Demonstrator at the second ACGT Review in Eindhoven, May 2008. In this demonstration the visualization services were used in three different settings to interactively explore the results of a tumour response simulation model.

The structure of this chapter is as follows: we begin with a short explanation on why service-based interactive visualization is a necessary but challenging functionality for the ACGT project, the Oncosimulator in particular. We also provide an overview of related work on web- and grid-based distributed visualization. The visualization facilities implemented for the ACGT Oncosimulator are described in Section 9.1.2. Section 9.1.3 describes our implementation and outlines the structure of our visualization services. Next, we describe three test cases using these services. Finally, we present conclusions and details on future work.

Service-based interactive visualization

One of the objectives of the ACGT project is to provide integrated access to the project's results through a web based portal. This has the advantage that all of ACGT's services are accessible to end-users through a standard web browser. The "ACGT Main Portal" is the main user interface that invokes the services required for the definition of clinical trials, data management and the definition of data analysis workflows. The decision to use a service-based design allows co-ordinated resource sharing and problem solving in a dynamic, multi-institutional, Pan-European virtual organization, including:

- precise control over access patterns to protect, for example, privacy-sensitive data and services, and
- controlled shared access to distributed computing resources.

Interactive visualization tools are used throughout the ACGT project, both by developers during the implementation of services and workflows but also by the end-users; the clinicians that define and manage a clinical trial. The decision on a service-based design and the integration of these services into a web based portal poses a significant challenge in the development of interactive visualization services for the representation and exploration of data. The visualization services should be able to provide:

- integration - the services must be ready for integration by third-party applications, and shared web portals in particular;
- flexibility - the visualization needs in the ACGT project range from simple 2D graphs to interactively rendered 3D volumes;
- interaction - the visualization services must both provide interaction capabilities for navigation (i.e. pan, scale) as well as (re-)parameterization of visualization algorithms;
- responsiveness - a service based design over a networked distributed architecture will add latency to the response time after interaction that should be minimized;
- scalability - the services must be able to withstand increases in the number of simultaneous service requests.

Unfortunately, for *interactive* visualization these capabilities do not go well together. Methods that provide *non*-interactive visualization methods for the graphical representation of information and scientific data are abound. Most of these can easily be integrated into third party applications, web portals included, and they often provide flexible 2D and 3D visualization methods. They are, however, not interactive.

Interaction with applications that run on a distributed architecture is far from trivial. Their distributed design implies that communication needs to take place between components which, in turn, negatively influences responsiveness. Furthermore, existing paradigms for the construction of service-oriented architectures (e.g. WSRF) impose a significant amount of overhead on the performance of applications which has a negative effect on both responsiveness and scalability. This has led us to design and build a lightweight framework that allows for the implementation of third-party applications using network accessible visualization facilities.

9.1.1 Related work

We have investigated the results of research projects that address distributed visualization and assessed its utility based on the requirements described in the previous section. We found that most are restricted to the visualization of specific data types or for particular technological domains, or they are limited in their support for interaction.

A good review of research areas and technologies for the support of distributed and collaborative visualization is provided by Brodlie et al [BDG 04]. For web-based visualization projects they make a useful distinction between *Full service* technologies where the service provider executes the visualization algorithms and provides graphical data to the client, *Software delivery* where the client executes the visualization algorithms, provided by the server, and *Local operation* where visualization software is assumed to be available at the client which is triggered by the download of data from the web.

Examples of the *Local operation* paradigm are servers that compute a graphical representation (such as VRML, X3D) of the data which is then transferred to the client. The browser must support the rendering of this type of graphical data. Different plugins for VRML and X3D formats are available, but they differ in maturity and graphical capabilities. Most importantly, the VRML format lacks support for non-polygonal types of visualization and has very limited support for interaction.

In *Software delivery* scenarios, the server provides visualization code and data for representation on the client. The responsibility of rendering graphical data lies with the client which has the advantage that local graphics hardware can be effectively used. Alternatives based on Java-based plugin using Java3D [Jav] or JOGL [JOG] have the downside of having to create a "bridge" from the visualization server to the browser plugin, and vice versa. The integration of visualization algorithms into either a browser plugin or as a standalone

application often implies a substantial amount of work to support. Transparently providing a plugin installation that picks the right libraries for any given end-user platform and browser combination is possible, but cumbersome.

Probably the best known example of a *Full service* visualization service is VNC (Virtual Network Computing [VNC]). VNC allows the desktop of one machine (the server) to be displayed on a number of clients (the viewers) and features efficient image compression and input control between server and viewers. The main problem with VNC is that it is not trivial to integrate into third-party applications and that it does not perform well in 3D visualization applications. SGI VizServer [Viz] and Chromium [HHN*02] are similar in structure to VNC but designed to support to remote high performance OpenGL rendering hardware.

The Grid Visualization Kernel (GVK [HK03]) was developed within the CrossGrid project and uses *glogin* [RK04] to provide a tunnel between a running grid job and the client as well as a facility that allows X11 port forwarding. This provides an interactive connection to running grid jobs, but this method is not suitable for integration into web based applications.

Visualization and the Oncosimulator

The Oncosimulator combines tumour information obtained from medical imaging techniques (CT, MRI, PET and ultrasound) with mathematical models that predict the growth of tumours and the response to chemotherapy or radiation therapy [SDG*07], specifically for the types of tumour under consideration: nephroblastoma and breast cancer. The Oncosimulator produces spatiotemporal predictions of the composition and morphology (shape) of the tumour over the course of time. These predictions provide clinicians with valuable information on the most effective treatment out of several alternatives, as well as detailed parameters on the optimal composition of a treatment scheme, including the total treatment period, the type of drug(s), dose, and interval between treatments.

A treatment is defined by several parameters, each of which has a range of possible values and is usually influenced by other parameters. When a new clinical trial is defined, simulation models help to define the initial parameters that predict the treatment most likely to be most effective. Finding the optimal combination of parameters for a certain treatment is difficult. As no analytical method exists for finding this optimum, the ACGT Grid environment is used to perform a large number of simulations for combinations of parameters that are thought to be most successful. The architecture developed in ACGT consists of a Grid-based distributed computing and software framework. It allows *in-silico* tumour simulation models, interactive visualization methods and other data sources to be combined into an interactive visual exploration environment. This environment can be used to explore simulated predictions of tumour growth and treatment response.

The visualization needs for the Oncosimulator are varied. First: the desired visualization methods vary depending on the role of the end-user: a simulation model developer will be interested in visualization methods that help in tracing bugs, but a clinician will want to see an immediate picture on tumour response given a range of different treatment. Second: the application context in which the visualization methods are used play a role: desktop applications will have other resource capabilities than a web portal or an interactive virtual reality device.

9.1.2 Visualization of Oncosimulator data

The Oncosimulator takes a bi-level 3D volume dataset as input. The two levels in the input denote which voxels (a volumetric pixel) of the volume are parts of the tumour and which are not. The output of a simulator run is a volume (of the same dimensions as the input volume) for each hour of simulated time, containing an updated tumour region. Other Oncosimulator outputs include counts of the different cell categories used internally by the simulator. This

cell count is best represented in 2D time-versus-count plots. The volume output is represented by 3D isosurfaces or volume rendering. The main visualization methods required for the Oncosimulator are categorized as follows:

1. Predicted change in overall tumour volume:
    a. 2D line graph showing number of geometrical cells involved in the tumour, over time.
    b. 2D line graphs showing number of cells of each type in the whole simulation, over time.
2. Predicted change in overall tumour shape:
    a. Basic view: 3D rendering of the external shape of the tumour delineated by healthy tissue area or necrotic core.
    b. Animated view: 3D rendering of the change in shape of the tumour over simulated time.
    c. For comparison with after-treatment scans and segmentation: this will in general require registration of the after-treatment scan with the simulated tumour. This is non-trivial, but if done properly it offers overlaid presentation of the medical images with the simulated tumour.
3. Predicted composition of tumour:
    a. Basic view: colour-coded geometric cells (healthy, mostly proliferating, mostly necrotic).
    b. Internal view: 2D cut-through plane of a 3D rendering to reveal internal structure.

Previous work – interactive visualization on the desktop

As a first step towards the visualization of Oncosimulator results we designed and implemented a desktop visualization environment called VTKFly2. This application was implemented using the Python programming language and the Visualization Toolkit (VTK) [SML06].

VTKFly2 provides a graphical user interface in which simulation datasets can be loaded and the evolution of the simulated tumour played back. The application allows multiple, colour-coded isosurfaces extracted from the simulation output to be displayed simultaneously to show the (change in) composition of a tumour (methods 2a, 2b and 3a listed in section 9.1.2, see also Fig. V1). It can show simulation output together with volume rendered DICOM imaging data allowing visual comparison of pre-treatment and after-treatment tumour shapes (2c). An interactive cutting plane provides methods to slice through any data volume to reveal internal structure on a 2D sample plane (3b).

For the first ACGT Review meeting in Poznan in April 2007, VTKFly2 was integrated with a Grid-enabled version of the Oncosimulator. When a simulation run started, the sequential output files written by the Oncosimulator (one per hour of simulated time) are transferred to the desktop system running VTKFly2. The application detects new incoming output files and, after loading, appends these to the current visualization time line. This allows a user of VTKFly2 to inspect the simulation outcome *while* it is running on the remote system.

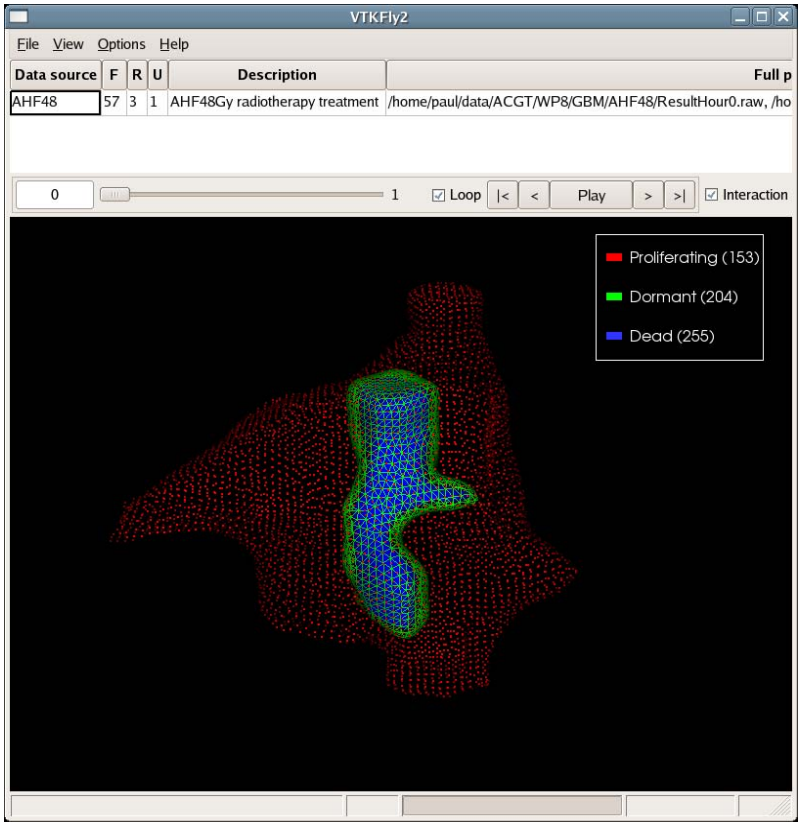

Figure V1. Screenshot of the desktop application VTKFly2 showing the results of an Oncosimulator experiment. This application supports interactive 3D visualization methods and animated playback of a live tumour simulation experiment.

Visualization as a service

Although VTKFly2 was successfully integrated with the ACGT infrastructure it was still a standalone desktop application. This limited its application within ACGT. To increase availability and flexibility we designed an architecture that provides visualization facilities through services. A service here resembles a resource that is accessible over a network and that produces one or more visualizations. The behaviour of a visualization facility is manipulated through Service Parameters that are defined and changed by the users of the service. A visualization service does not *have* to produce an image as output. Intermediate steps needed to produce that image, like isosurface extraction or the placement of glyphs, can also be provided by a service. By chaining multiple services together any desired output can be accomplished. Individual services can be distributed over multiple machines when necessary resources are not available in the same location.

Architecture overview

In its most basic form, the architecture consists of a collection of visualization services that are each accessible through the standard web protocol HTTP. Each visualization service can be seen as a regular web server from which the end-user requests one or more images using a conventional URL. The visualization service returns the output of in the form of an image or an intermediate representation suitable for processing by (an)other service(s). Changes to the visualization service state are made using HTTP requests. As the visualization service communicates with the outside world using only the HTTP protocol, integration of the service with existing applications is straightforward. The users of the

service do not necessarily have to be web-based applications, as anyone can use the visualization results in any way. An example of this could be a movie creation service that requests a sequence of images and turns these into a single movie file.

9.1.3 Visualization service design

Our service design does not require the installation of plugins in the browser. The design supports any kind of imaging output produced by the visualization algorithms and so is not limited by what is implemented on the browser side. The visualization services includes support for interactive 2D and 3D renderings in a regular web browser with the only prerequisite that the browser supports Javascript. The architecture of this solution is presented next.

9.1.4 Service implementation

Each visualization service is implemented as a tiny application that consists of two parts: one part performs the actual visualization and rendering, the other part handles service requests via HTTP. Most visualization functionality is implemented using the classes provided by the Visualization Toolkit (VTK) and other libraries. Graphical rendering to images is performed through hardware-accelerated OpenGL libraries where available. To handle service requests, the application contains a minimal web server capable of servicing HTTP GET and POST requests [FGM99]. A tightly integrated system like this has multiple advantages over an architecture consisting of a regular visualization application coupled with a "full blown" web server, like Apache or Lighttpd. In that case, some form of communication would have to be implemented between the two processes, resulting in overhead which negatively influences responsiveness and scalability. By merging both components into a single application we ensure the web server has direct access to the visualization output thereby greatly reducing overhead. Furthermore, incoming service requests can directly be applied to the visualization service without any intermediate processing or process communication induced by a web server.

Images sent from a visualization service to the browser are encoded in PNG format. For reduced image size and transmission time JPEG would have been an alternative choice. However, the compression algorithm used in JPEG is not lossless which may result in undesirable compression artefacts visible in the images.

9.1.5 Interaction with visualization services

We classify interaction with visualization in two categories: parameterization and navigation. Parameterization of scientific visualization services is done through HTTP, as described in the previous sections. Navigation is the type of interaction that allows the user to change the view on a visualization, i.e. panning, rotation and scaling. To accomplish this type of interaction we use a form of AJAX (Asynchronous Javascript) programming. Whenever the user interacts with a 3D views, Javascript code in the HTML page sends updated view parameters to the instance of the visualization service that provides the image. The new view parameters are distributed by the service to the instances on the server to provide synchronized 3D views. After sending the updated parameters, the Javascript code in the HTML page invalidates all 3D view images which causes the browser to fetch updates images from the visualization instances. This method provides synchronized interactive 3D views in a web browser.

Test cases

We have applied our visualization architecture to four test-cases:

9.1.6 Test-case 1: The ACGT Portal

Integration with the ACGT portal is illustrated through a working prototype, shown in Fig. V2. This figure shows a screenshot of a web browser in which the output of two visualization services are visible. Each service shows a different simulation dataset but at the same time step. The left dataset corresponds to untreated tumour growth, while the right one shows the results of treatment with the drug epirubicin.

Isosurfacing has been applied to the simulation output to extract the tumour shape. The use of clipping and colour coding reveals differing numbers of cells on the inside of the simulated tumour. The user changes simulation time steps and location of the clipping plane using the buttons underneath the views. The user can manipulate the 3D views to pan, scale and rotate the tumour with the mouse. The two 3D views are kept synchronized on the server during interaction. For synchronization we use a tuple space model, similar to the LINDA system [Gel95].

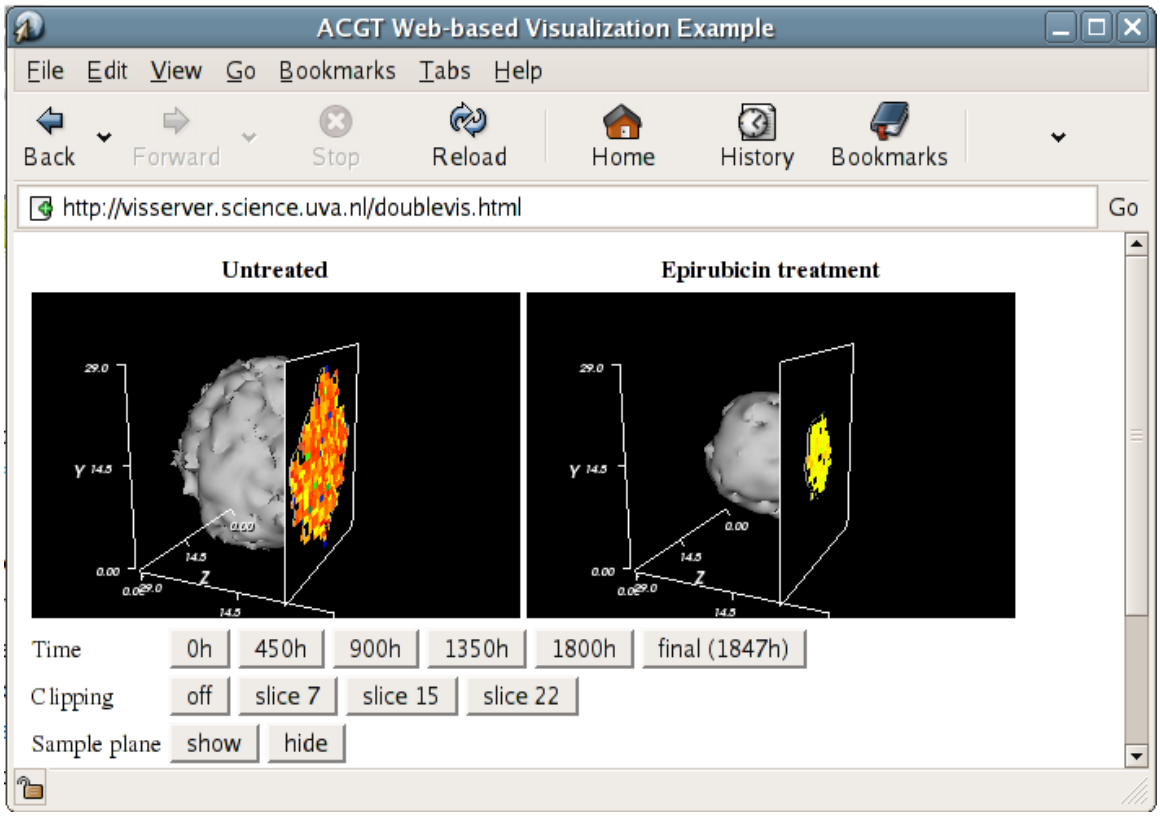

Fig. V2. Visual comparison of two simulation datasets in a web portal. The left dataset corresponds to untreated tumour growth, the right shows the results of treatment with the drug epirubicin. The 3D views are interactive: the view can be panned, rotated and scaled interactively using the mouse.

9.1.7 Test-case 2: The RecipeSheet

The RecipeSheet allows parameter spaces to be interactively navigated in an intuitive way by providing ways for different scenarios to be compared and easily altered. It will show output for multiple scenarios so that the user can compare explore alternative treatment scenarios simultaneously. For this it provides special GUI components and interaction methods. The RecipeSheet is described in more detail elsewhere in this document.

To support interactive exploration of treatment scenarios with the RecipeSheet, a Grid portlet has been created within ACGT with which simulator parameters can be set and one or more simulator jobs can be started. The portlet allows ranges of parameters to be specified, so that it can be used to start simulator runs that cover (part of) the parameter space of the Oncosimulator. When each of the simulator runs completes, its output is transferred from the Grid node that executed the run to the visualization server. When the output is fully transferred, the server adds the output to a list of available runs. In the list the parameters used for each run are stored. This list can be queried by users of the visualization service to discover which sets are available for use with the visualization services.

Fig. V3 shows the visualization services integrated with the RecipeSheet. The four views of the simulation output are not generated by the RecipeSheet. They are not even regular images. Instead, each image is an embedded web browser component that retrieves HTML pages from our visualization services. The four 3D views in these pages are interactive and synchronized, as described in Test-case 1. When a user changes any of the parameter values used for defining the current scenario, the RecipeSheet sends the updated values to the visualization service and reloads the image. The RecipeSheet does not know (and does not have to know) anything about how these visualizations are produced by the service, as the RecipeSheet is merely the service user. It only needs to know how to communicate with the service, what visualization elements the service provides and what parameters are available to influence these elements.

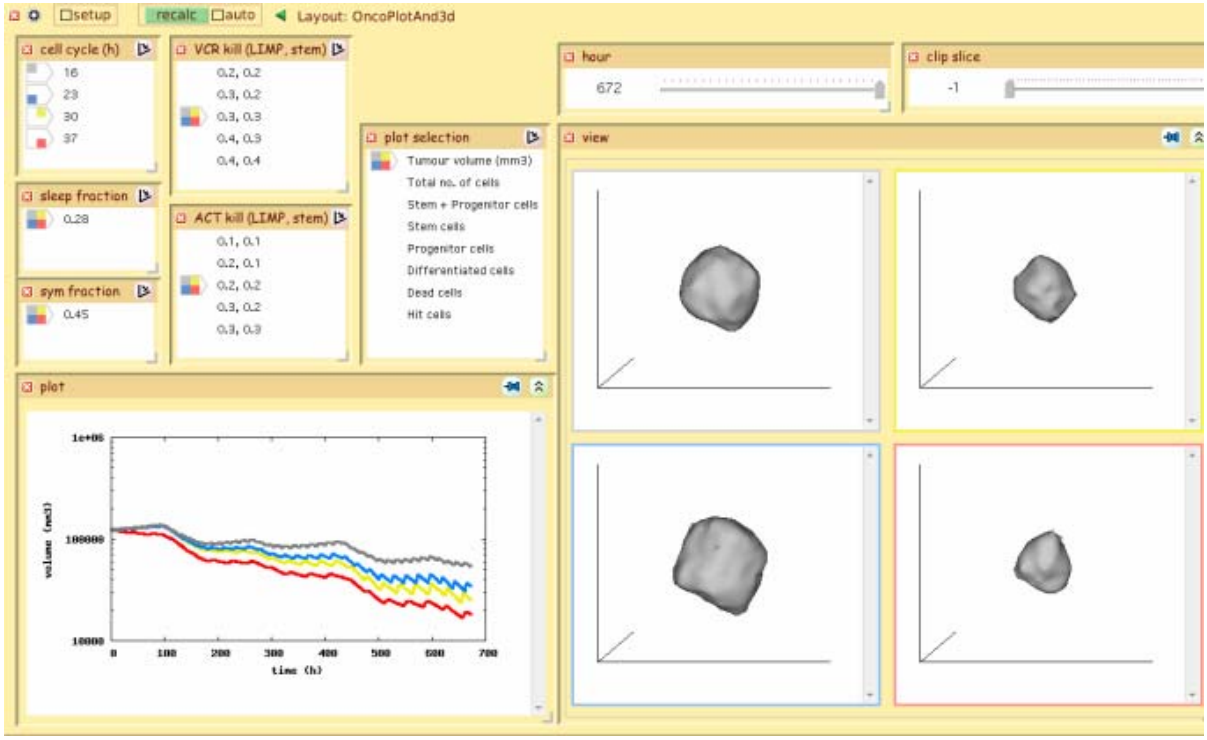

Fig. V3. Screenshot of the visualization services used in the RecipeSheet. The 2D graph in the lower left and the four 3D views on the right are generated by visualization services.

9.1.8 Test-case 3: The Personal Space Station

We have constructed a third test-case for our visualization services in the shape of an application for a personal Virtual Reality device called the Personal Space Station (PSS, see also Fig. V4). The PSS supports stereoscopic 3D rendering on a mirror display and optical

hand and object tracking to create an environment where the user can "reach in and touch their data". The optical tracking system tracks the user's head so that the orientation of the projected image can be altered to generate a motion parallax effect. This effect is an important depth cue used by the visual system to get a sense of distance and size of a 3D object. Object tracking adds the ability for a user to change the orientation and location of a 3D visualization by changing the orientation and location of a handheld object.

The combination of stereoscopic rendering together with the intuitive interaction methods provided by hand and head tracking creates the illusion that objects appear to float in front of the user. This provides the viewer with an almost instantaneous understanding of the morphology of 3D objects. Within the ACGT project, this type of visualization can provide information on the shape of a simulated tumour obtained from an Oncosimulator experiment within the context of the medical images obtained from the patient. Especially in cases where tumour resection will take place after chemotherapy or radiation therapy, the decision on when to terminate treatment often depends on the shape and size of the tumour with respect to the surrounding organs. An example of this type of visualization is shown in Fig. V5.

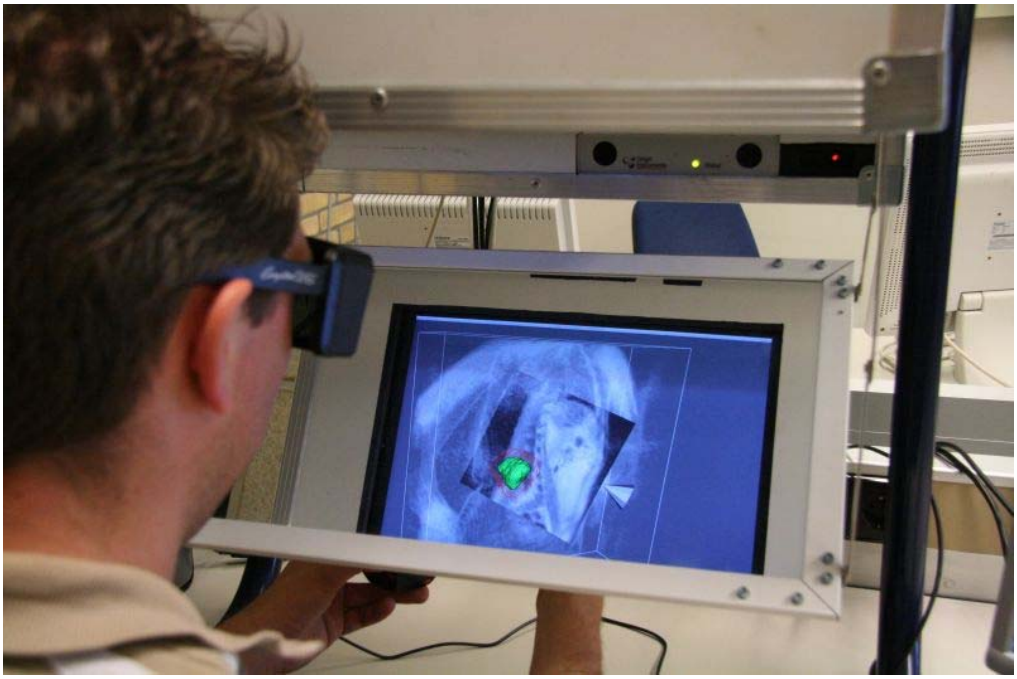

Figure V4. . Interactive visualization of Oncosimulator data on a Virtual Reality device called the Personal Space Station (PSS). The system combines stereoscopic rendering with head and hand tracking to give the illusion that objects appear to float in front of the user.

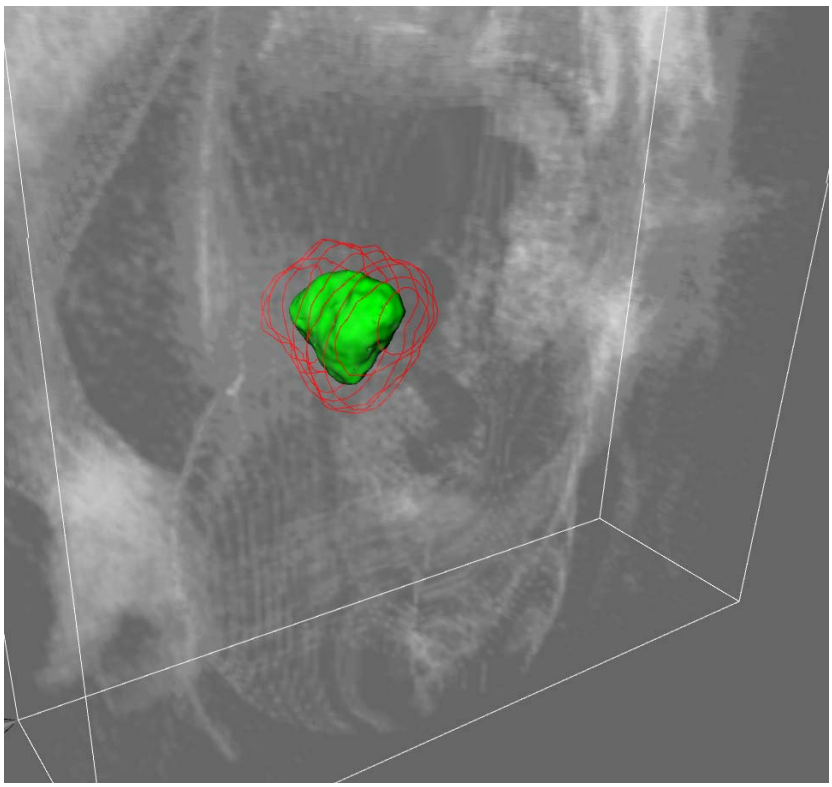

Fig.V5 . Simultaneous visualization of patient imaging data (white), pre-treatment tumour contours (red) and simulated post-treatment tumour (green).

Conclusions and future work

In this chapter we have described the architecture developed for the interactive visualization of Oncosimulator data. The "visualization as a service" paradigm is a powerful and flexible way of allowing visualizations to be used by different parties. Our architecture allows interactive 3D visualizations from third party applications such as web portals, desktop applications and Virtual Reality devices.

The performance of the architectures can currently only be described in qualitative terms. We have had good results with use of our services in local and regional settings. Applications that are widely distributed have shown significant decreases in responsiveness of the visualization services. We are currently in the process of acquiring quantitative performance measurements.

The current implementation of our architecture uses the hardware resources from a limited number of workstations. To provide a scalable solution that can be used by multiple users from different locations, a collection of resources would need to be created. Unfortunately, this will be hampered by the fact that grid-accessible computing resources do not support interactive access in most cases.

References

V1 or [BDG_04] BRODLIE K., DUCE D., GALLOP J., WALTON J., WOOD J.: Distributed and collaborative visualization. Computer Graphics Forum 23 (2004), 223–251.

V2 or [FGM_99] FIELDING R., GETTYS J., MOGUL J., FRYSTYK H., MASINTER L., LEACH P., BERNERS-LEE T.: Hypertext transfer protocol – http/1.1. http://www.faqs.org/rfcs/rfc2616.html.

V3 or [Gel85] GELERNTER D.: Generative communication in linda. ACM Transactions on Programming Languages and Systems 7 (January 1985), 80–112.

V4 or [GNU] Gnuplot. http://www.gnuplot.info.

V5 or [HHN_02] HUMPHREYS G., HOUSTON M., NG Y., FRANK R., AHERN S., KIRCHNER P., KLOSOWSKI J.: Chromium: A stream processing framework for interactive graphics on clusters. In ACM SIGGRAPH (2002).

V6 or [HK03] HEINZLREITER P., KRANZLMÜLLER D.: Visualization services on the grid: The Grid Visualization Kernel. Parallel Processing Letters 13 (June 2003), 135–148.

V7 or [Jav] Sun Developer Network, Java 3D API. http://java.sun.com/javase/technologies/desktop/java3d.

V8 or [JOG] Java.net, The JOGL API Project. http://jogl.dev.java.net/.

V9 or [LH06] LUNZER A., HORNBÆK K.: RecipeSheet: Creating, Combining and Controlling Information Processors. In Proceedings of the 19th annual ACM symposium on user interface software and technology (UIST 2006) October 2006), pp. 145–153.

V10 or [RK04] ROSMANITH H., KRANZLMULLER D.: glogin - a multifunctional, interactive tunnel into the grid. In Fifth IEEE/ACM International Workshop on Grid Computing (November 2004), pp. 260–265.

V11 or [SDG_07] STAMATAKOS G., DIONYSIOU D., GRAF N., SOFRA N., DESMEDT C., HOPPE A., UZUNOGLU N., TSIKNAKIS M.: The "oncosimulator": a multilevel, clinically oriented simulation system of tumor growth and organism response to therapeutic schemes. towards the clinical evaluation of in silico oncology. Engineering in Medicine and Biology Society, 2007. EMBS 2007. 29th Annual International Conference of the IEEE (August 2007), 6628 – 6631.

V12 or [SML06] SCHROEDER W., MARTIN K., LORENSEN B.: The Visualization Toolkit An Object-Oriented Approach To 3D Graphics, 4 ed. Kitware, Inc., December 2006.

V13 or [TKP_06] TSIKNAKIS M., KAFETZOPOULOS D., POTAMIAS G., MARIAS C., ANALYTI A., MANGANAS A.: Building a European Biomedical Grid on Cancer: The ACGT Integrated Project. In Proceedings of HealthGRID 06 Conference (2006), pp. 247–258.

V14 or [Viz] SGI VizServer. http://www.sgi.com/software/vizserver/.

V15 or [VNC] RealVNC Limited. http://www.realvnc.com/.

V16 or [WSS_07] WEGENER D., SENGSTAG T., SFAKIANAKIS S., RUPING S., ASSI A.: GridR: An R-Based Grid-Enabled Tool for Data Analysis in ACGT Clinico-Genomics Trials. In IEEE International Conference on e-Science and Grid Computing (December 2007), pp. 228–235.

10 Subjunctive Interfaces for the Oncosimulator

[Chapter code: J]

Introduction

In this chapter we describe the facilities that have been developed by UHok for helping users to explore and compare the results and visualisations generated by the Oncosimulator for alternative data sets and/or parameter settings.

The structure of the chapter is as follows: First we explain why we consider it so important to be able to compare alternative results from the Oncosimulator. We then introduce the concept of subjunctive interfaces – interfaces that specifically support the comparison of alternatives – and the RecipeSheet, a spreadsheet-like environment for building subjunctive interfaces for particular applications. We describe how the RecipeSheet was used to create a simple interface, demonstrated at the ACGT annual review in May 2008, suited to the kind of parameter-space exploration needed for the initial stages of validating the Oncosimulator. We then describe the mechanisms at work in that interface, in particular those for communicating with the visualisation services. We finish with a look towards the future.

Comparison of alternatives is key to Oncosimulator use

Part of the vision driving the development of the Oncosimulator is the idea that one day a doctor will be able to upload a detailed description of a patient and his or her tumour, then simulate the application of various alternative treatments and thus obtain a prediction as to the relative effectiveness of those alternatives. This prediction could then be used as a factor in deciding which treatment the patient will receive. This requires support for *a treating physician to simulate how alternative standardised treatments would work for a given patient*.

Prior to such deployment, the Oncosimulator could be used in developing the range of standardised treatments that a doctor would be submitting for comparison. For example, if thorough simulation over a range of commonly encountered tumour sizes and compositions establishes that administering a given chemical agent once a week or twice a week (at the same overall intensity but lower short-term toxicity) makes no difference to the expected reduction in tumour volume, it might be decided that there is no reason to include the higher-toxicity plan in the treatments on offer. So here the requirement would be to allow *a research clinician to explore alternative treatment regimes to ascertain their relative merits and disadvantages.*

However, before either of these applications of the Oncosimulator can become a reality it is necessary to validate and provide quantitative levels of confidence in the predictions of the simulation software itself. Part of this validation procedure will be rigorous examination of the performance of the simulator under different conditions: checking whether each parameter to the model, individually and in relevant combinations with others, has the expected influence on the simulation outcome. In this case we must allow *a simulation developer to explore the behaviour of the simulation in the face of alternative parameter settings.*

These situations of use illustrate that for doctors, for research clinicians, and even for the Oncosimulator developers themselves, being able to define and run alternative simulations and compare their results is a fundamental requirement. This is what led to the decision that for the front-end of the ACGT Oncosimulator we would investigate the use of so-called subjunctive interface techniques.

What is a subjunctive interface?

A subjunctive interface [Lunzer 99; Lunzer & Hornbæk 08] is a style of application user interface that makes it easy for a user to set up multiple execution scenarios based on alternative values for the application's inputs, and then to view and manipulate those scenarios in parallel. The three key features of an application with a subjunctive interface are as follows:

Multiple scenarios can co-exist. At any given time the application can support multiple scenarios, whether created by explicit request of a user or automatically by the application. The scenarios typically deal with mutually incompatible application states. For example, when asked to choose a single value for some application input, a user who is equally interested in several alternative values may request the creation of a separate scenario to cater for each value.

The user can view scenarios side by side. The application displays all currently existing scenarios side by side, in a way that helps the user to compare them while still being able to examine each scenario individually.

The user can adjust scenarios in parallel. The user can make changes to many scenarios at the same time, for example by adjusting an input that is shared across scenarios, and can see immediately how this affects the outcome of each one.

These three features are supported by provision of input widgets (e.g., text-input fields, menus) that are enhanced to let the user make multiple alternative selections, and result-display widgets (e.g., line plots, textual lists, arbitrary graphical displays) that are enhanced to allow multiple alternative results to be seen simultaneously. Both the input and result widgets must also support some form of value markup, typically based on assigning a distinct colour to each scenario, to help the user understand which input values have given rise to which results.

In recent years the construction of subjunctive interfaces for new applications has been simplified by the development of the RecipeSheet [Lunzer & Hornbæk 06], an end user programming environment in the tradition of the spreadsheet but with subjunctive-interface features built in at the base level. Like a standard spreadsheet, values appearing within cells on the sheet can either be entered directly by the user or derived by calculation on the basis of values in other cells. What makes the RecipeSheet special is that cells in which the user enters values can hold multiple alternative values that can be used to set up alternative scenarios, and the cells showing derived values (which can include graphics or rendered HTML, rather than just numbers or text strings) can show the corresponding alternative results. Thus RecipeSheet cells have the behaviours necessary to act as the input and result widgets of a subjunctive interface.

A simple subjunctive interface for Oncosimulator validation

At the time of writing, simulator code is available for predicting the temporal behaviour of an arbitrarily shaped tumour under conditions of free growth or chemotherapeutic treatment with a range of agents and freely specifiable doses and administration timing. However, the cell life-cycle model embodied by the simulator includes a number of parameters for which it is unclear what value would reflect accurately the situation of the *in vivo* tumour being modelled. Some parameters, such as the duration of the overall cell cycle, seem prone to variation across patients and tumours; others, such as the probability that a cell within the proliferative region of a tumour will divide symmetrically, might be amenable to fixing at a single value for all tumours in all patients.

The clinical validation of the Oncosimulator proceeds by a process of exploring the dependence of the simulator outcome on variation in such parameters, and in particular trying to find parameter settings such that the outcome conforms as closely as possible to the observed outcomes in a cohort of patients who have already been treated. We have developed and are now testing a RecipeSheet-based interface for carrying out this exploration.

Fig. J1 shows the RecipeSheet demonstrated at ACGT's annual review in May 2008. This sheet provides an interface for generating and viewing visualisations based on a repository of pre-computed simulation results. These results all correspond to the tumour and treatment data of a single anonymised patient, and the exhaustive combination of small sets of values on each of seven simulation parameters.

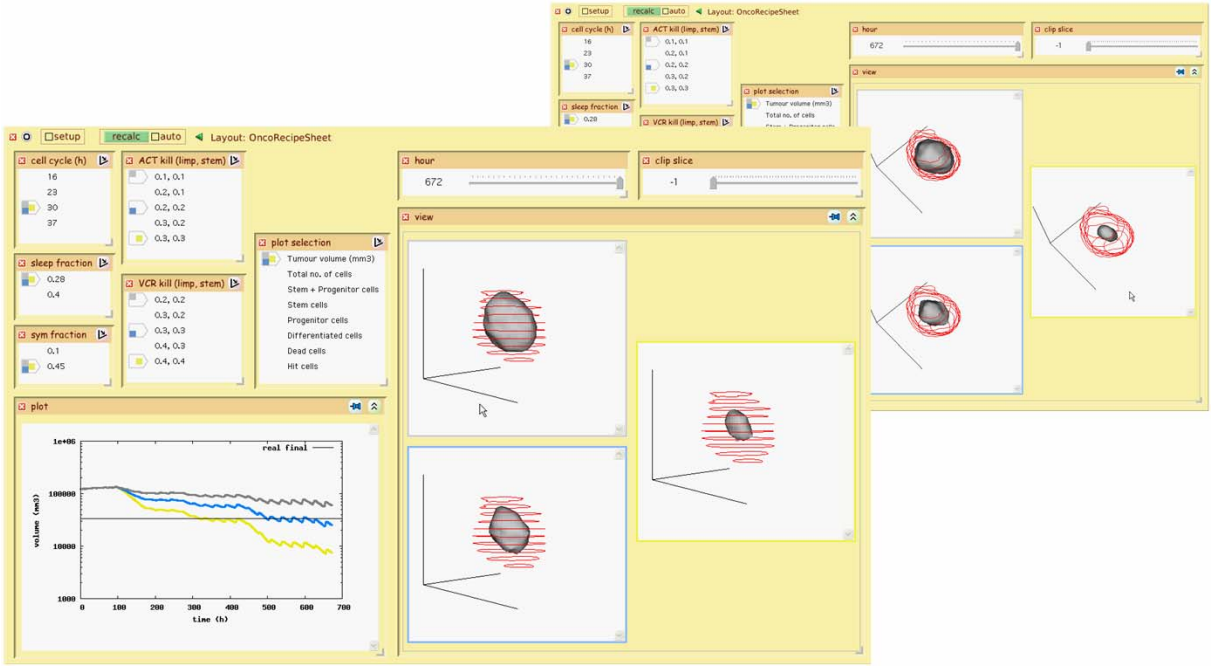

Fig.J1 : The RecipeSheet shown at the ACGT review in May 2008, also showing (in the background) the result of synchronised manipulation of the 3D graphical view

The main features of this sheet are as follows:

The five input cells at top left (see Fig. J2 for an enlarged view of this region) allow the user to select the values for the seven simulation parameters that were varied in creating the pre-computed results. Note that the "ACT kill" and "VCR kill" cells set two parameter values each: one pertaining to LIMP cells, the other to stem cells.

In the cell labelled "plot selection" the user chooses from a set of cell-count or tumour-volume measures that are recorded by the simulator at each time step. The corresponding time-based plot appears in the cell at bottom left.

The large cell on the right is for showing a 3D visualisation of the simulated tumour, on which are superimposed the contours of the tumour as delineated by segmentation of the patient's original DICOM images. In the figure this cell is showing three views, corresponding to three scenarios. Above this cell the input cells "hour" and "clip slice" allow the user to select, using sliders, which time point to view, and on which x-value plane (if any) the visualisation should show a slice through the tumour.

All of the input cells, including the sliders, allow the user to select multiple alternative values and hence alternative evaluation scenarios. In Fig. J1 the user has selected three alternative values in each of the kill-ratio cells, correlating the selections between the cells to create three scenarios in total (i.e., the smallest value in "ACT kill" is selected in the same scenario as the smallest value in "VCR kill", and so on). These scenarios, which are automatically given the colours grey, blue and yellow respectively, thus correspond to low, medium and high sensitivity of the tumour to treatment. The two visualisations – the plots of tumour volume against time, and the 3D visualisation of the predicted tumour shape at the end of treatment – show that the simulator indeed predicts greater shrinkage when the tumour is more sensitive.

The 3D visualisation supports direct-manipulation interaction. By clicking and dragging with the mouse, the user can rotate a view about horizontal and vertical axes. When there are multiple scenarios, and hence multiple views, their orientations are synchronised such that rotating any one view causes the others to rotate the same amount. The result of such manipulation is seen in the background of Fig. J1

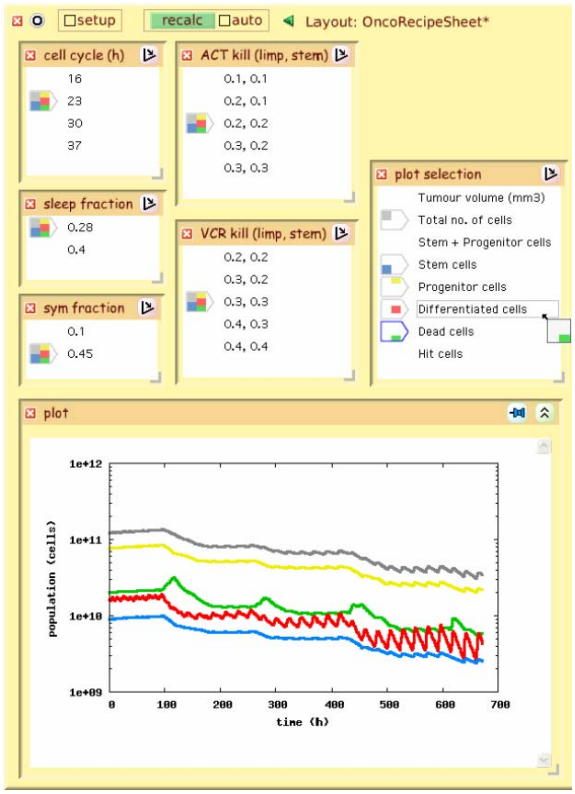

Fig. J2 The above RecipeSheet being used to explore the variation over time of the counts of five categories of biological cell

Fig. J2 shows a detail of the same sheet, with multiple scenarios set up to compare not the results from different simulation runs but the time-based plots for five types of cell count from a single run. The top (grey) line represents the total number of cells; below are the counts for four individual cell categories. By seeing the counts plotted in parallel the user can quickly understand, for example, that the periodic oscillation that appears in the total cell count and seems to grow over time arises almost entirely from the count of differentiated cells – here drawn in the fourth scenario, and therefore coloured red.

Implementation Details

Here we describe the construction and behind-the-scenes mechanisms of the sheet demonstrated above.

10.1.1 The cell and recipe setup

Instead of the inter-cell formulas supported by standard spreadsheets, on the RecipeSheet relationships between cells are defined in terms of multi-input, multi-output procedures that are referred to as recipes ([Lunzer & Hornbæk 06] contains a general description of the properties of recipes). Here we first describe the particular recipes used for the initial Oncosimulator demonstration, and then the mechanisms we have developed to support more flexible construction of such sheets in the future.

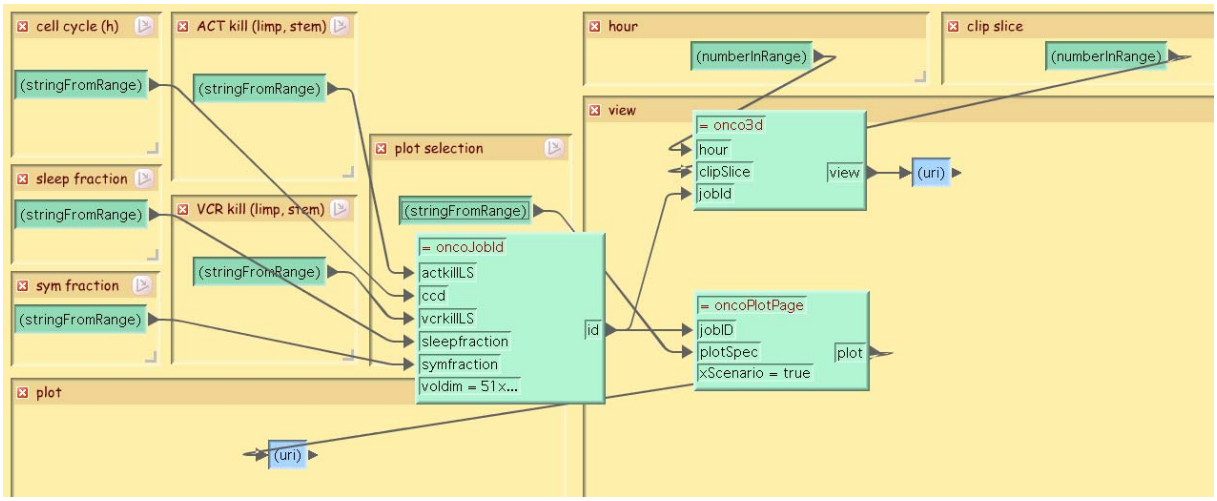

Fig. J3 The "setup" view of the RecipeSheet, showing the Oncosimulator-specific recipes and their respective connections

Fig. J3 shows a (partly clipped) view of the Oncosimulator RecipeSheet in setup mode, which reveals how its cells are connected by recipes. The three recipes used on this sheet are all written in Smalltalk (indeed, the entire RecipeSheet system is implemented on the Squeak Smalltalk environment), and perform the following functions:

oncoJobId takes a total of six inputs, corresponding to Oncosimulator parameters, and uses them to look up the job identifier of the corresponding simulator run. On this sheet five of the inputs are taken from cells, while the sixth – the input *voldim*, representing the simulation-volume dimensions – is left to take its default value (as fixed in the declaration of the oncoJobId recipe).

onco3d takes a job identifier, an hour, and a slice-plane coordinate (or -1 for no slice), and generates a value *view* that is the REST-style URI for requesting from the visualisation server a page containing the desired 3D visualisation. The Smalltalk code for this recipe (with some minor optimisations removed, to improve readability) is as follows:

```
port := 7000 + topRecipe evalScenario.  "separate port for each scenario"
baseUri := 'http://tara.science.uva.nl:', port asString, '/'.

view := baseUri,
        'viewonly.html?diagnosis=1&preop=0',
        '&dataset=', jobId,
        '&time=', (hour // 24) asString,
```

```
        '&clipping=', clipSlice asString.
```

Notice that the *view* value is calculated simply as a string. However, because the recipe declares *view* to be of type URI, the cell set up to display this value consists of a Web-browser that accepts the value as a target URI.

Notice also that this recipe only contains the logic for creating a single view, corresponding to a single scenario. When there are multiple scenarios the recipe is invoked multiple times, and the results from these invocations are laid out within the result cell. This is the responsibility of the RecipeSheet, not of the individual recipe.

oncoPlotPage again takes the job identifier; its other main input is a string specifying the name of a data measure to plot (e.g., "Stem cells"). This recipe has considerably more to do than the previous one – namely:

- looking up the name of the data file corresponding to the specified measure (e.g., stem_cells.dat);
- creating the commands to instruct Gnuplot to build the appropriate plot – with appropriate axis types and labels, any reference value that should be plotted (e.g., the known volume of the tumour after treatment), and the right line colour according to the colours used by the RecipeSheet for each scenario;
- sending the Gnuplot command stream as the data within an HTTP POST to one of the dedicated ports of the visualisation server, then returning a URI for reading the generated plot image from that same port.

Unlike onco3d, oncoPlotPage is registered as a "cross-scenario" recipe, meaning that its code is written to accept each input as a scenario-ordered list of values. This is how the recipe can assemble the Gnuplot commands to create a single graph with multiple colour-coded lines.

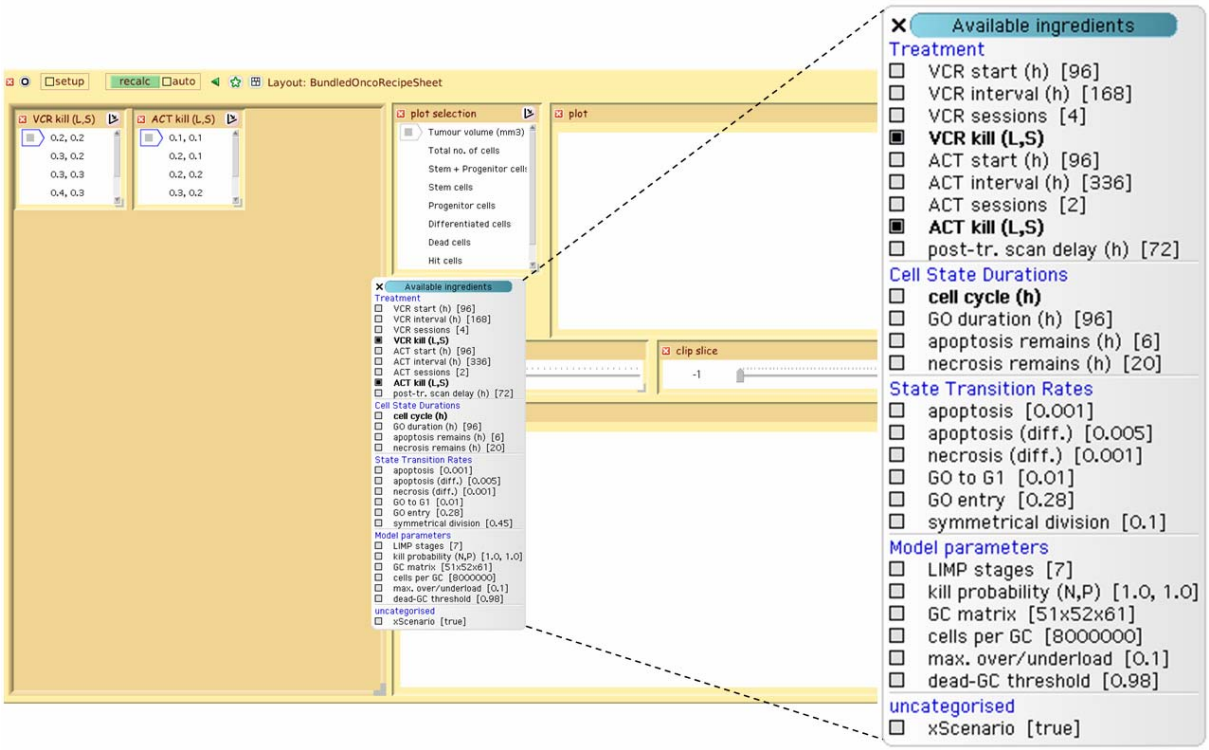

Fig. J4 An alternative RecipeSheet layout that allows the user to choose, from a pop-up menu, which recipe inputs should have their own input cells

One of the obvious limitations of the setup shown up to this point is that it addresses only a limited range of parameters, fed by a fixed set of input cells. Fig. J4 shows mechanisms that have been developed recently to let the user choose dynamically which parameters are to be made available for adjustment.

The main novel feature shown in Fig. J4 is the large brown region set up on the left of the sheet. This is an automatic cell-layout region, in which cells created by the user are laid out in rows, and their placement adjusted automatically if the user resizes or reorders any cells. The range of cells available is determined by the variable declarations of the recipes on the sheet. This sheet includes an expanded version of the oncoJobId recipe, that declares 25 Oncosimulator parameters. The user chooses from the pop-up menu for a result cell; the figure shows the menu for the "plot" cell. Where a parameter name is followed by a value in square brackets, this is the default value that will be supplied to the recipe if no cell is set up. The entries in bold text are those for which there is no default value: the user cannot use the recipes on this sheet without setting up cells for at least those parameters.

In order to avoid the sheet's setup-mode view degrading into a spaghetti-like muddle of connections between large numbers of inputs and respective recipes, we have also developed a mechanism whereby recipes can take their inputs from appropriately named cells without requiring an explicit wired connection. We are currently testing these new mechanisms, and plan to make them available to the Oncosimulator developers shortly.

10.1.2 Synchronised control of interactive visualisations

As described in the Interactive Visualisation chapter of this document, some of the visualisations are designed to support synchronised viewing of multiple instances. Within the RecipeSheet this is used for visualisations such as the cell containing 3D views in Fig..

The method for synchronising views in this case is, as described in the visualisation chapter, server-driven. The visualisation server guarantees that the visualisations delivered through designated ranges of HTTP ports will be mutually synchronised (e.g., one set might be the ports 7001 to 7012; another 7021 to 7032). The RecipeSheet negotiates with the server to reserve a port range to use for the alternative views used in a single cell.

Each visualisation view is a fully functional Web browser (an instance of the .NET WebBrowser class, with facilities equivalent to those of Microsoft's Internet Explorer), and therefore supports AJAX-style interactive Web pages. When a user interacts with a view, such as by clicking and dragging to rotate an image, JavaScript code in the page communicates with the server to update the page contents. The server simultaneously updates the pages that are being served on any synchronised ports. The RecipeSheet, detecting that user interaction has taken place on one view, automatically forces the sibling views to refresh their contents.

In contrast to this server-driven approach we have also explored a client-driven method, based on the use of VNC (Virtual Network Computing). Fig. J5 shows a RecipeSheet with four VNC-based views, each displaying the live state of a dedicated virtual Linux desktop running on the server. In this case each desktop holds a single application window – an instance of the University of Amsterdam's VTKFly visualisation environment – into which has been loaded the simulation results corresponding to one scenario defined by the input-cell selections. The setup of the desktops, and the launching of VTKFly on the appropriate dataset on each desktop, is performed by invoking Bash shell scripts on the server through secure remote invocation.

In this case, inter-view synchronisation is achieved by using a custom VNC client, implemented in Smalltalk that captures every user interaction event (from the mouse or keyboard) and echoes it to all the sibling views. Thus, for example, if the user clicks on the "Play" button in any view, a click at the same location will be sent to all views. Clearly this will only lead to meaningful synchronisation if all interface elements (such as the Play button) are guaranteed to appear at the same location in every view.

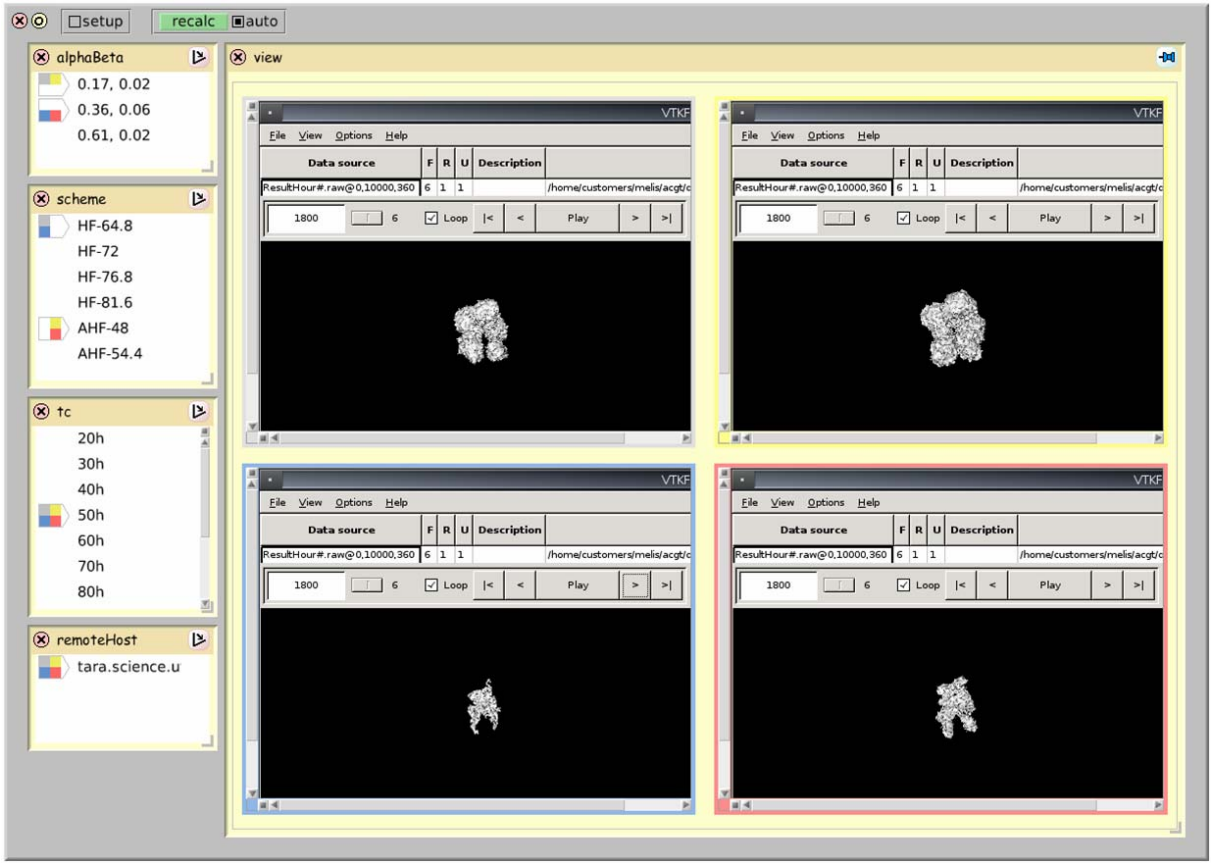

Fig. J5 A RecipeSheet with VNC-based synchronization between views; the data seen here is from a simulation of the radiotherapeutic treatment of glioblastoma multiforme

We now provide a brief comparison of these synchronisation methods: the server-based approach based on AJAX, and client-based approach based on VNC.

Interaction responsiveness: An AJAX-style Web page contains JavaScript code, executed within the client computer, that can deliver highly responsive, complex interactions such as (where appropriate) selection from cascading menus. By contrast, a VNC client must send to the server every individual event (e.g., each incremental change in mouse location while dragging), and wait for the server to reply with the corresponding view updates. Given a high-speed, low-latency connection, such as when the client and server are on the same LAN, this might not be a problem; in general if a system responds within 200 milliseconds its users are likely to perceive the feedback as instantaneous [Card et al. 83]. But as the server communication delay increases, the frequent communications required for VNC-based interaction can soon make it frustratingly sluggish.

Synchronisation semantics: The VNC approach has the advantage of universality: any tool that can appear on a graphical desktop can potentially be used, without modification, in a synchronised way across multiple desktops. However, as noted above, the simple event-echoing approach that makes this possible will only work if the views all contain, at all times, the same interaction objects at exactly the same locations. This constrains the kinds of interaction that can be supported with this approach: for example, if two views contain renderings of an object at different scales or seen from different orientations, a mouse click at a given screen location on one view might hit a different object in the other view and cause

surprisingly different responses. By contrast, although the AJAX approach requires that the visualisations be designed explicitly with synchronisation in mind, this gives the visualisation designer the opportunity to implement operations at a higher level of granularity than individual mouse events. For example, an operation such as "rotate by 15 degrees around the x axis" can be applied unambiguously to all graphical views.

Server role: In the AJAX approach adopted in this project, the server is responsible for carrying out all synchronised updates. Doing so requires that it keep a record of the groups of visualisations that are to be synchronised, which in turn requires the client to request the views in such a way that such groups will be formed. The VNC approach not only removes the need for such negotiated group construction, but can work for tools that have no synchronisation features and could be running on entirely independent servers.

This comparison illustrates just a few of the tradeoffs between these two methods. For now we believe that using AJAX is the most suitable approach for the Oncosimulator, but we will continue to consider and evaluate other options.

Conclusions and future work

This chapter has described how we are using the RecipeSheet to build interfaces that support exploration of alternative results in the Oncosimulator. The first context for pursuing such explorations is in validating the behaviour of the simulation code, by confirming that the simulation results are affected as expected by changes in parameter settings. At a later stage, exploration will be needed when attempting to tune the simulator such that its predictions closely match the true results seen in a cohort of patients who have already received treatment. Later still, once the reliability of the simulator has been demonstrated, we expect result-space exploration to be valuable when comparing the likely efficacy of a range of treatment options. At all stages we will be observing the usability of the RecipeSheet in this domain, and looking for ways to improve its design.

One of the known challenges ahead is the implementation of mechanisms that will allow the RecipeSheet to be used for requesting additional Oncosimulator runs based on new parameter settings, as opposed to the present situation of only being able to browse results from runs that were requested through a separate portal. The teams within WP8 will collaborate to make this possible.

References

J1 or [Card et al. 83] Card, S. K., Moran, T. P., and Newell, A. *The Psychology of Human Computer Interaction*, Lawrence Erlbaum, Hillsdale. 1983.

J2 or [Lunzer 99] A. Lunzer. Choice and comparison where the user wants them: Subjunctive interfaces for computer-supported exploration. *Proceedings of the IFIP TC. 13 International Conference on Human-Computer Interaction (INTERACT '99)*, 474-482. IOS Press, 1999.

J3 or [Lunzer & Hornbæk 06] A. Lunzer and K. Hornbæk. RecipeSheet: Creating, Combining and Controlling Information Processors. *Proceedings of the 19th Annual ACM Symposium on User interface Software and Technology (UIST '06)*, Montreux, Switzerland, Oct 2006, 145-153. ACM Press, 2006.

J4 or [Lunzer & Hornbæk 08] A. Lunzer and K. Hornbæk. Subjunctive interfaces: Extending applications to support parallel setup, viewing and control of alternative scenarios. *ACM Transactions on Computer-Human Interaction* **14**(4), January 2008.

J5 or [Stamatakos et al. 06] Georgios S Stamatakos, Vassilis P Antipas, and Nikolaos K Uzunoglu. A spatiotemporal, patient individualized simulation model of solid tumor response

to chemotherapy in vivo: the paradigm of glioblastoma multiforme treated by temozolomide. *IEEE Trans Biomed Eng.* **53**(8):1467-77. August 2006

11 The Oncosimulator Component Collaboration Diagram

[Chapter code: D]

In the following (Fig. D1) a diagram of the Oncosimulator component collaboration is presented.

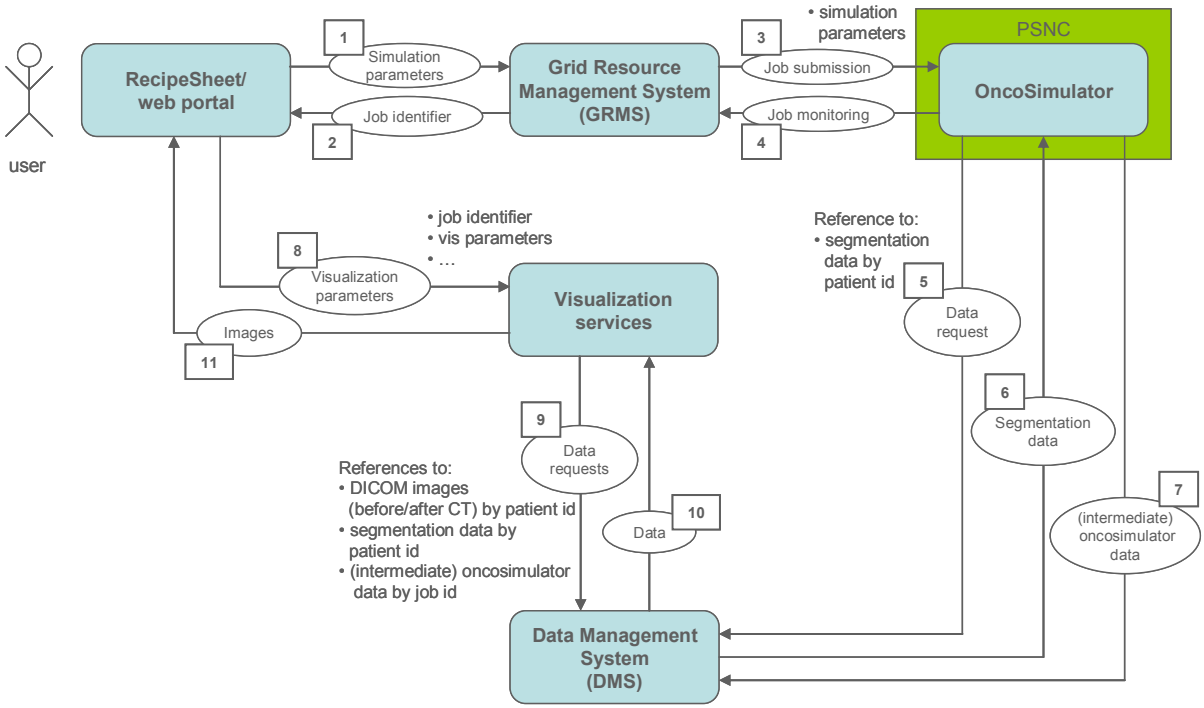

Fig. D1 Collaboration diagram illustrating the components used in the integrated Oncosimulator scenario that was demonstrated at the Eindhoven review, May 2008.

In this diagram:

- rounded boxes represent the different components in the demonstration;
- arrows represent interactions between components;
- ellipsoids on the arrows represent the semantics of the interaction (there may be multiple interactions between components but with a different meaning - each is represented by a different arrow). Where necessary, the parameters included in the interaction are itemized next to the ellipsoid.
- square numbered boxes represent the typical order of interactions between components over the course of an experiment, as described next:

Steps 1 to 7 take place once per instance of the Oncosimulator. Note that the Recipesheet may request multiple instances of the Oncosimulator, each with different simulation parameters:

1. The Recipesheet requests the GRMS to run an Oncosimulator instance with a particular set of simulation parameters.

2. The *Grid Resource Management System* (GRMS) returns a job identifier to the Recipesheet. The Recipesheet uses this identifier in its interactions with other services pertaining to this job.
3. The GRMS spawns a version of the Oncosimulator, in this diagram on a system in *Poznań Supercomputing and Networking Center* (PSNC), with the specified parameter values.
4. The GRMS monitors the state of the simulation (in queue, running, finished).
5. Once the Oncosimulator starts, it asks the *Data Management System* (DMS) for the initial tumour data (segmentation data derived from a patient's before-treatment DICOM images).
6. The DMS supplies the segmentation data.
7. During execution, the Oncosimulator stores intermediate data on the DMS.

Steps 8 to 11 are repeated while the user is using the Recipesheet:

8. The Recipesheet requests the Visualization service for a graphical representation. The data is referred to by job identifier. The visualization parameters specify the desired representation.
9. The Visualization service asks the DMS for the data it needs to comply with this request; DICOM image data (referred to by patient id), segmentation data (referred to by patient id) and/or Oncosimulator (referred to by job id).
10. The DMS supplies the requested data.
11. The images produced by the Visualization service are provided to the Recipesheet.

This diagram disregards any handling of "exceptions", i.e.: How is a job terminated? When and how should intermediate files be deleted? What should the Visualization service do if the Recipesheet asks for a representation of data of a job that has not yet produced any data? The proper handling of these exceptions is left to a later stage.

12 Comments on the Initial Steps Towards the Clinical Adaptation and Validation of the Oncosimulator

[Chapter code: A]

An outline of an initial step towards the clinical adaptation and validation of the Oncosimulator system has been presented. Anonymized real data before and after chemotherapeutic treatment for the case of the SIOP 2001/GPOH nephroblastoma and TOP breast cancer clinical trials constitute the basis for the clinical adaptation and validation process. Functioning of the initial Oncosimulator platform including both basic science and technology modules was demonstrated during the Eindhoven ACGT annual review (May 27-28, 2008). Using the real medical data referring to nephroblastoma and breast cancer in conjunction with plausible values for the model parameters (based on available literature) a reasonable prediction of the actual tumour volume shrinkage was made possible through the simulation module. Obviously as more and more sets of medical data are exploited the reliability of the model "tuning" is expected to increase. It should also be stressed that the large number of biological boundary conditions (e.g. monotonic increase of all tumour cell categories for an imageable freely growing tumour) dramatically limits the number of possible solutions (i.e. sets of parameter values that are able to predict real tumour shrinkage following treatment). This is very important since such limitations drastically facilitate the approach to *the* solution best representing clinical reality for each given medical data case. Extensive exploitation of the potential of the technology modules in conjunction with the simulation model is expected to dramatically accelerate the clinical adaptation and validation procedure. Furthermore the future "implantation" of the Oncosimulator into the overall ACGT architecture is expected to considerably facilitate a more direct medical data feeding of the system by the clinical trials environment. In the next WP8 deliverables progress towards these directions will be reported.

13 A Future Extension of the Model (Immune Reaction Modelling)

[Chapter code: F]

IEO in collaboration with ICCS and USAAR has started exploring the feasibility of the eventual inclusion of an additional module into the Oncosimulator dealing with the immune system (IS) responses to the tumour and possibly with the effect of immunotherapies in the final stage of the ACGT lifetime.

Although no clinical validation for this more qualitative module has been planned, its aim would be to deepen the understanding of such phenomena and of the follow-up period after the end of chemotherapy when as in the initial stages of tumorgenesis an important role might be played by the immune surveillance, alone or enforced by a suitable immunotherapy (either active or passive).

The Oncosimulator might be particularly fit to this task since it provides a satisfactory way to model spatial dynamic phenomena such as the ones taking place during the interaction of IS with a solid tumour. This might be particularly valuable in the field of tumour immunology, where the literature concerning spatio-temporal aspects is in its first phase of development (see Chaplain & Matzavinos 2006, and references therein).

In a preliminary analysis a shell based simulation schema has been envisaged. At each simulation step time t, a series of conformal shells of geometric cells covering all proliferating and quiescent zones may be identified.

A further component of death probability due to the interaction with the infiltrated effectors and other IS cells, coming both from the surface and through the blood vessels might be introduced. Due to the limited ability of various kind of cells of IS in infiltrating tumours, this additional component for death should involve a limited amount of the more external conformal shells.

Thus, a small vascular tumour subject to the interaction with the immune system might be simulated by imposing a decreasing profile of this additive component of the death probability.

On the contrary, for bigger tumours, the existing modules concerning chemotherapy might be suitably adapted in order to simulate the spreading of the effectors internally to the tumour. In fact the computational mechanism embedded in the Oncosimulator to reproduce the spread of chemotherapeutic agents and their consumption should be somehow reused to reproduce the spreading of effectors of IS.

Moreover the possibility of modulating the parameters related to the mechanisms of drug consumption should be included. This would allow reproducing fundamental mechanisms of active immunotherapies where the ability of tumour cell killing is amplified thanks to the action of the antitumour vaccines.

A major but feasible modification in Oncosimulator simulation module would thus be the introduction of a new equivalence class specific to tumour-IS interactions and immunotherapy: the class of cells killed by the effectors.

Two inter-linked specific feature of immune system effectors should be taken into account: their reproductive ability and the dependence of their reproduction rate on the local density of cells. However, to implement this important feature one might suitably adapt those main modules of the Oncosimulator that are dealing with the proliferation of tumour cells themselves. As a consequence, geometric cells would be the 'habitat' of two proliferating and interacting populations: the tumour cells and the immune system cells. However, only tumour cells would determine the laws of splitting of the geometric cells.

Another important factor that may influence the tumour-immune system interaction outcome of therapy is the delay between tumour growth and immune proliferation. This point might be simulated for small tumours by rendering the above mentioned modulation of death probability dependent on the past history of the tumour burden, whereas for larger tumours by rendering the local proliferation dependent on the past history of the local tumour burden (at the geometrical cell level).

Following the implementation of these modifications in the Oncosimulator it would be of interest to investigate if the densities of infiltrated IS cells into large tumours follow patterns characterized by decrease or spatially oscillatory patterns. Moreover, in non-solid tumours there is a corpus of experimental data, supported by mathematical models, indicating that both damped and sustained oscillations are possible (Kennedy 1970; Kuzsnetsov & Al. 1994, Kirschner D. and Panetta 1998, d'Onofrio 2006). At the best of our knowledge, there have been no specific experimental studies to assess if in solid tumors there may also appear some forms of oscillations. Simple theoretical models seem to indicate than mechanistic sources of these oscillations might be both the intrinsic nonlinear nature of the interaction between the neoplasms and the immune system and also the above mentioned delayed stimulatory effect of the tumour burden on the IS cells proliferation (d'Onofrio 2006). However, there is a large corpus of studies reporting spontaneous regressions of both primary tumours and metastases, often followed by regrowth of the neoplasms (Ikuta & Al. 2002; Abdelrazeq 2007 and references therein). Thus, we are envisaging to use the TIS module in order to perform numerical experiments in order to assess involvement of the interplay of T-IS in these regression phenomena and more generally in the onset of oscillation patterns (e.g. super imposed to a growth pattern).

Another set of simulations that we are designing have the aim to assess the relevance of the way of scheduling immunotherapies. In fact, for some anti-tumour therapies, as the anti-angiogenic therapy, the way of delivering the active agents may influence the degree of effectiveness of the treatment. As far as immunotherapy of non-solid tumours is concerned some theoretical studies (d'Onofrio 2005) seem to indicate that the scheduling is not relevant, but in a spatio-temporal framework, such as that required for solid tumours the temporal patterns of the treatment delivery might be relevant. Since to the best of our knowledge the medical literature does not provide clear experimental answers about this point, we would like to theoretically start assessing whether this issue might be relevant or not in the framework of immune therapies of solid tumours. Thus, we are envisaging some preliminary experiments that might be easily implemented in the Oncosimulator. In particular, continuous infusion vs boli-based passive immuno-therapies on small tumours might be simulated by different temporal patterns of change of death probabilities. These simulations, for small tumours, would not require significant modifications of the code of the Oncosimulator.

Finally, the module we are designing will also be able to deal with special cases of immunotherapy: the virotherapy, where oncolytic viruses diffuse in a tumour, infect its

cells and kill them. In turn the infected cells would elicit an immune response, that would mitigate the oncolytic effect (Tao and Gao, 2005). In particular, in the case of small tumours, this therapy might roughly be simulated without changes in the actual structure of the software, by simply modulating the death probability.

As a support for the design of the above described integrative modules and the planning of numerical experiments we are developing some basic mathematical models, based on Lotka-Volterra like representations of interactions between the various cellular populations. In particular we are extending the families of models of tumour-IS interaction and passive immunotherapies proposed in (d'Onofrio 2005; d'Onofrio 2006) in order to assess the possibility of onset of sustained oscillations in the presence of delays, by considering various patterns of influence of past tumour burden on the proliferation of IS cells. Other modifications we are studying refer to the inclusion of active therapies. The aim of the development of such theoretical models is to determine some biologically meaningful key parameters that influence the effectives of the therapies, and/or the natural history of the interplay between the neoplasm and the IS.

Bibliography

F1. Abdelrazeq A.S. 2007 : Spontaneous regression of colorectal cancer: a review of cases from 1900 to 2005. Int. J. Colorectal Dis. 7 727-736

F2. Chaplain M. and Matzavinos A. 2006 Mathematical Modelling of spatio-Temporal Phenomena, in: Friedman A. (Ed.) *Tumour Immunology. In: Tutorials in Mathematical Biosciences: Cell Cycle,Proliferation and Cancer* Springer Verlag, Hiedlberg-New York

F3. d'Onofrio A. 2005. A general framework for modeling tumor-immune system competition and immunotherapy: analysis and medical inferences. Physica D 208, 220-235

F4. d'Onofrio A. 2006 Mathematical Models and Methods in Applied Sciences Vol. 16, No. 8 1375–1401

F5. Shin-ichi Ikuta, Chikao Miki, Eiji Ookura, Hitoshi Tonouchi, and Masato Kusunoki 2002 Spontaneous Regression of a Metastatic Liver Tumor: Report of a Case. Surg Today 32 844–848

F6. Tao Y. and Guo Q. 2005. The competitive dynamics between tumor cells, a replication-competent virus and an immune response. J. Math. Biol. 51, 37–74

F7. Kennedy B. J. 1970. Cyclic leukocyte oscillations in chronic myelogenous leukemia during hydroxyurea therapy, Blood 35 751–760.

F8. Kirschner D. and Panetta J. C. 1998. Modeling immunotherapy of the tumor — Immune interaction, J. Math. Biol. 37 235–252

F9. Kuznetsov, I. A. Makalkin, M. A. Taylor and A. S. Perelson 1994, Nonlinear dynamics of immunogenic tumors: Parameter estimation and global bifurcation analysis, Bull. Math. Biol. 56 295–321

14 Conclusion

In this deliverable the initial version of the Oncosimulator, integrating both basic science and technology modules, has been outlined. A description of the clinical requirements and the types of medical data exploited has been provided. An outline of the major improvements, refinements, extensions and numerical checks and explorations of the simulation model, originally described in deliverable D8.2, has been presented. A rather detailed description of the technology modules has also been included. The technology modules refer to the image processing of the medical data, the grid execution scenario, the cluster execution and parallelization of the simulation code, the interactive and virtual reality visualization, the subjunctive interfaces for the system and the Oncosimulator component collaboration diagram. A brief outline of a possible future extension of the system which would address the immune system reaction has also been made. The favourable outcome of a first step towards the clinical adaptation and validation of the Oncosimulator has been presented and discussed. Provision of additional medical data (e.g. antigen scenario data) for new cases that will take place shortly is expected to considerably enhance the system's potential. The successful performance of the combined Oncosimulator platform as demonstrated during the Eindhoven annual ACGT review is seen as a strongly encouraging step towards the clinical translation of the integrated system, being the first of its kind worldwide.

Appendix 1 - Abbreviations and acronyms

ACGT	*Advancing Clinico-genomic Trials on Cancer*
AJAX	*Asynchronous JavaScript And XML*
CRF	*Case report form*
DICOM	*Digital Imaging and Communications in Medicine*
FhG	*Fraunhofer Gesellschaft*
GPOH	*Gesellschaft für Pädiatrische Onkologie und Hämatologie*
HTTP	*Hypertext Transfer Protocol*
ICCS	*Institute of Communication and Computer Systems- National Technical University of Athens*
IJB	*Institut Jules Bordet*
IS	*Immune System*
MRI	*Magnetic Resonance Imaging*
NTUA	*National Technical University of Athens*
PET	*Positron emission tomography*
RECIST	*Response Evaluation Criteria in Solid Tumors*
REST	*Representational State Transfer*
SIOP	*Société Internationale d'Oncologie Pédiatrique*
SOA	*Service Oriented Architecture*
TOP	*Trial of Principle*
URI	*Uniform Resource Identifier*
UvA	*University of Amsterdam*
USAAR	*University hospital of Saarland*
VNC	*Virtual Network Computing*